AN ABSTRACT OF THE THESIS OF

Courtney van Stolk for the degree of Master of Science in Geography presented on June 5, 2019.

Title: Evaluation of Compartmentalized Aquifers in the Walla Walla Subbasin of Oregon Using Isotopic and Geochemical Tracers

Abstract approved:

_____

Michael E. Campana

The Walla Walla Subbasin (WWSB) in Oregon is underlain by formations of the extensive Columbia River Basalt Group (CRBG) which have been deformed by post-Miocene folding and faulting. Extensive irrigation with groundwater from these basalt groups, as well as sedimentary aquifers and surface water diversions from the Walla Walla River, has enabled the WWSB to become a productive agricultural region despite its semi-arid climate. Over the past 10 years water levels in the basalt aquifer have declined to the point where some senior groundwater right holders cannot access their full water allocation. Effective water management depends on an understanding of the flow and recharge pathways in this complex groundwater system.

This research uses spatial analysis of geochemical characteristics of groundwater samples to test the hypothesis that local faults create barriers to flow and isolate

compartments of groundwater. For this study 31 wells were sampled for analysis of oxygen isotopes, hydrogen isotopes, pH, temperature, and conductivity. At a subset of 18 of those wells, samples were collected for a more extensive array of tests which also included carbon-14, tritium, and ten major ions. These parameters provide information to evaluate the range and distribution of groundwater age, evidence of modern recharge, and the progression of chemical reactions along hypothesized flow paths. Results of these laboratory analyses were compared with a literature review of fault geology and hydrogeology in the CRBG, results of interference pumping tests of basalt wells in the WWSB, and known physical characteristics of the wells sampled.

This information was used to test three conceptual models of groundwater flow through the basalt aquifers. The first conceptual model was based on groundwater movement in unfaulted, sloping CRBG terrain where water infiltrates in upland recharge zones where the basalt is exposed, and moves laterally through the sloping interflow zones of the aquifer to wells. The second conceptual model describes local recharge in the vicinity of a well flowing slowly downward through the aquifer until the depth at which is became hydraulically connected to the well. The third model added faults into the model as lateral barriers to flow and vertical conduits to recharge.

Comparisons of the monovalent/divalent cation ratios, stable isotope values, and principal component models with well depth, well surface level elevation, and well locations provide insights that conflict with the first two conceptual models and supported the third model. Further comparisons of these parameters with geologic characteristics of these faults from the literature through the lens of the third conceptual model provide a basis for estimating fault hydrogeologic characteristics in the WWSB.

©Copyright by Courtney van Stolk

June 5, 2019

Creative Commons License

Evaluation of Compartmentalized Aquifers in the Walla Walla Subbasin of Oregon Using Isotopic and Geochemical Tracers

by
Courtney van Stolk

A THESIS

submitted to

Oregon State University

in partial fulfillment of
the requirements for the
degree of

Master of Science

Presented June 5, 2019
Commencement June 2019

Master of Science thesis of Courtney van Stolk presented on June 5, 2019

APPROVED:

Major Professor, representing Geography

Dean of the College of Earth, Ocean, and Atmospheric Sciences

---

Dean of the Graduate School

I understand that my thesis will become part of the permanent collection of Oregon State University libraries. My signature below authorizes release of my thesis to any reader upon request.

Courtney van Stolk, Author

ACKNOWLEDGEMENTS

The author expresses sincere appreciation to the residents of the Walla Walla Subbasin who allowed me access to their land and wells for this study. Jen Woody and the staff at the Oregon Water Resources Department (OWRD) provided invaluable guidance and access to information, as well as access to their time, funding, and resources that supported the collection of samples for this project. Hank Johnson and the staff at the Portland office of the US Geological Survey were exceedingly generous with their knowledge, training for sampling techniques, support, and funding that enabled the laboratory analysis of the samples for this project.

Sincere thanks to my committee members Dr. Michael E. Campana, Dr. Julia Jones, and Dr. Catalina Segura for their guidance and encouragement. The College of Earth, Oceanic, and Atmospheric Sciences financially supported my studies at Oregon State through an assistantship for which I am grateful.

I'm so grateful to my family, friends, and fellow graduate students whose community kept me sane and my spirits up during while I was working on this degree!

TABLE OF CONTENTS

Introduction 1
Background 4
Geology of the Walla Walla Subbasin 4
Hydrology of the WWSB 11
Hydrogeology of the Columbia River Basalts in the WWSB 12
Ion Chemistry and Evolution in the WWSB 16
Carbon-14 17
Tritium 20
Stable Isotopes 21
Literature Review for Well Records and Lithology 22
History of Groundwater Use and Management of the Walla Walla Subbasin 23
Methods 26
Sample Collection Methods 26
Laboratory Analysis Methods 30
Compilation of Physical Well Properties for Analysis 30
Statistical Methods: Principal Component Analysis 31
Statistical Analysis: Clustering Analysis of Limited Suite of Parameters 32
Results 33
Field-Measured Parameters: Temperature, pH, and Specific Conductance 33
Geochemistry 33
Stable Isotopes 34
Radioactive Isotopes 36
Principal Component Analysis 36
Spatial Analysis of PCA 40

TABLE OF CONTENTS, continued

Clustering Analysis of Limited Suite of Parameters 41
Comparison of Interference Tests and Chemical Data 41
Discussion 43
Field-Measured Parameters: Temperature, pH, and Specific Conductivity 43
Geochemistry 45
Stable Isotopes 47
Radioactive Isotopes 50
Principal Component Analyses 51
Spatial Analysis of Principal Component Analysis 54
Clustering Analysis of Limited Suite of Parameters 55
Comparison of Interference Tests with Chemical and Isotopic Data 58
Conclusion 58
References 62
Appendix A: Tables of Analytical Results 66
Appendix B: Well Physical Characteristics 70
Appendix C: Figures 74

LIST OF FIGURES

Figure Page

1. Location of the Walla Walla Subbasin……..……..2

2. Diagram identifying fault zone features…….....8

3. Named faults in the WWSB…….....9

4. Illustration of basalt flow structures and their permeability ...…….13

5. Conceptual scheme for fault-related fluid flow……...…….……15

6. Map of wells sampled for this summer in the summer of 2018.……27

7. Relationship between d18O and d2H, with stratigraphy…….....35

8a. Map of ion PC2 individual values at wells compared to interpolated potentiometric surface and faults……..…….....40

8b. Distance from fault along flow path versus ion PC2 score……..40

9. Map of pumping interference test results……...42

10. Difference between measured water temperature and expected geothermal gradient……40

11. Tritium concentration versus percent modern carbon…….50

12. Graph of d2H versus ^{14}C……..51

13. Mapped conclusions for fault properties.…….....58

LIST OF TABLES

Table Page

1. Wells sampled in the summer of 2018…….....29
2. Ion principal component analysis coordinates…….34
3. Principle component individual coordinates……38
4. Comparison of PCA group interpretations……..39
5. Comparison of OWRD and SCMC clustering…….57

APPENDICES

Appendix A: Tables of Analytical Results Page

A1. Field-measured parameters...66

A2. Major ions, in mg/L.....67

A3. Secondary ion analytes, in mg/L.....67

A4. Radioactive isotope results.....68

A5. Stable isotope results, in permil.....69

Appendix B: Well Physical Characteristics Page

B1. Table of well stratigraphy and construction.....70

B2. Long-term hydrographs for sampled wells.....73

Appendix C: Figures

Figure Page

C1. CRBG stratigraphy.....74

C2. Geology of the Walla Walla Basin and Subbasin.....75

C3. 1985 interpolated potentiometric surface for the Wanapum basalt.....76

C4. 1985 interpolated potentiometric surface for the Grande Ronde Basalt.....77

C5. Sampled wells with stratigraphy from OWRD database...78

C6. Map of observed ranges of pH values.....79

C7. Map of observed ranges of specific conductivity values.....80

C8. Stiff diagrams for groundwater samples.....81

C9: Map of cation ratio values.....82

C10. Relationship between land surface elevation and cation ratio.....82

C11. Relationship between well depth and cation ratio.....83

C12. Relationship between well bottom elevation and cation ratio.....83

Appendix C, continued

Figure Page

C13. Relationship between d18O and land surface elevation…….……...83

C14. Relationship between d18O and well bottom elevation…..……..84

C15. Relationship between d18O and well depth……..84

C16. Graph of modern precipitation and groundwater stable isotope values……85

C17. Mapped ranges of deuterium excess values……..86

C18. PCA biplot of ion PC1 versus ion PC2…….……87

C19. Variable coordinates of ion parameters in PC1 and PC2……..87

C20. Map of individual coordinate values for ion PC1…….88

C21. Map of individual coordinate values for ion PC2…….89

C22a. PCA biplot of non-ion PC1 vs non-ion PC2……...90

C22b. PCA biplot of non-ion PC2 vs non-ion PC3……...90

C23. Variable coordinates from PCA of non-ion parameters……91

C24. Individual non-ion coordinates for PC1……92

C25. Individual coordinates for non-ion PC2……93

C26a. Map of spatial clusters of d2H values…….....94

C26b. Spatially constrained multivariate clustering box plots for d2H…….94

C27a. Map of spatial cluster s of d2H and d18O values……95

C27b. Graph of spatial clusters and d2H versus d18O……..95

C28. Map of 12-cluster SCMC analysis of d2H and d18O……...96

C29. Map of OWRD water level elevation groups…….……...97

Appendix C, continued

Figure Page

C30a. Boxplots of d2H by interference test group…….....97
C30b. Boxplots of pH by intereference test group…….....98
C30c. Boxplots of well bottom elevation by interference test group…….…...98
C30d. Boxplots of specific conductivity by interference test group…….……99
C30e. Boxplots of temperature by interference test group…….……...99

Introduction

The massive Columbia River Basalt flows of northern Oregon and central Washington are a defining geologic feature of both states. They cover approximately 164,000 square kilometers (Riedel 1998), which is roughly equivalent in the size to the state of Georgia. These basalts, emplaced between 17 and 6 million years ago, are up to three kilometers thick in the center of the Columbia River Plateau and have an estimated volume of 174,000 cubic kilometers (Reidel 1998). The basalt flows are collectively referred to as the Columbia River Basalt Group (CRBG), and as a whole the aquifer is called the Columbia Plateau Regional Aquifer System (CPRAS). The large lateral extent of each ancient lava flow is not only objectively impressive but also gives aquifers in the interflow zones of the basalt a unique hydrogeologic character based on the high lateral transmissivity of the interflow zones and the low vertical conductivity of the lava flows themselves (Tolan et al. 2009). However, these layers have been folded and faulted in the southern and southeastern Yakima Fold belt region of the Columbia River Plateau by post-Miocene tectonic forces (Riedel et al. 2002). The roughly 4,600 square kilometer Walla Walla Subbasin of Oregon (WWSB) is located on the southern edge of the Columbia River Plateau within the Yakima Fold Belt region. The WWSB is surrounded by the Blue Mountains, the Horse Heaven Hills, and the Washington border. A map of the study area's geographical setting is presented in Figure 1.

In the course of this thesis, I have been working alongside hydrogeologists at the Oregon Water Resources Department (OWRD) who are conducting a period of intensive groundwater data collection to better characterize the CRBG aquifers in the WWSB. The OWRD will use this improved understanding of the flow system to characterize the scope of the groundwater decline in the basin (see hydrograph in Appendix B) and propose opportunities for sustainable water

management. Historical and preliminary studies (Riedel et al 2002, Packard et al 1996, Newcomb 1965, Newcomb 1951) indicate that the basalt groundwater system may be compartmentalized by faults, as shown by patterns of groundwater elevation and long-term trends.

My research supports OWRD's characterization of the CRBG hydrogeologic framework by using spatial analysis of geochemical characteristics of groundwater samples to test the hypothesis that some local faults create barriers to flow and isolate compartments of groundwater. For this study I collected samples from 31 wells for analyses of oxygen isotopes, hydrogen isotopes, pH, temperature, and electrical conductivity. At a subset of 18 of those wells I collected samples for a more extensive array of tests which also included carbon-14, tritium, and ten major ions. These parameters provide information to explore three specific research questions:

1. What are the range and distribution of groundwater age accessed by these wells, as indicated by carbon-14 analyses?
2. Where is there evidence of modern recharge, as shown by the stable isotopic signatures and tritium concentrations?
3. What can the relationships between pH, temperature, conductivity, and concentrations of dissolved ions indicate about the relative length of the water flow path through the basalt aquifers?

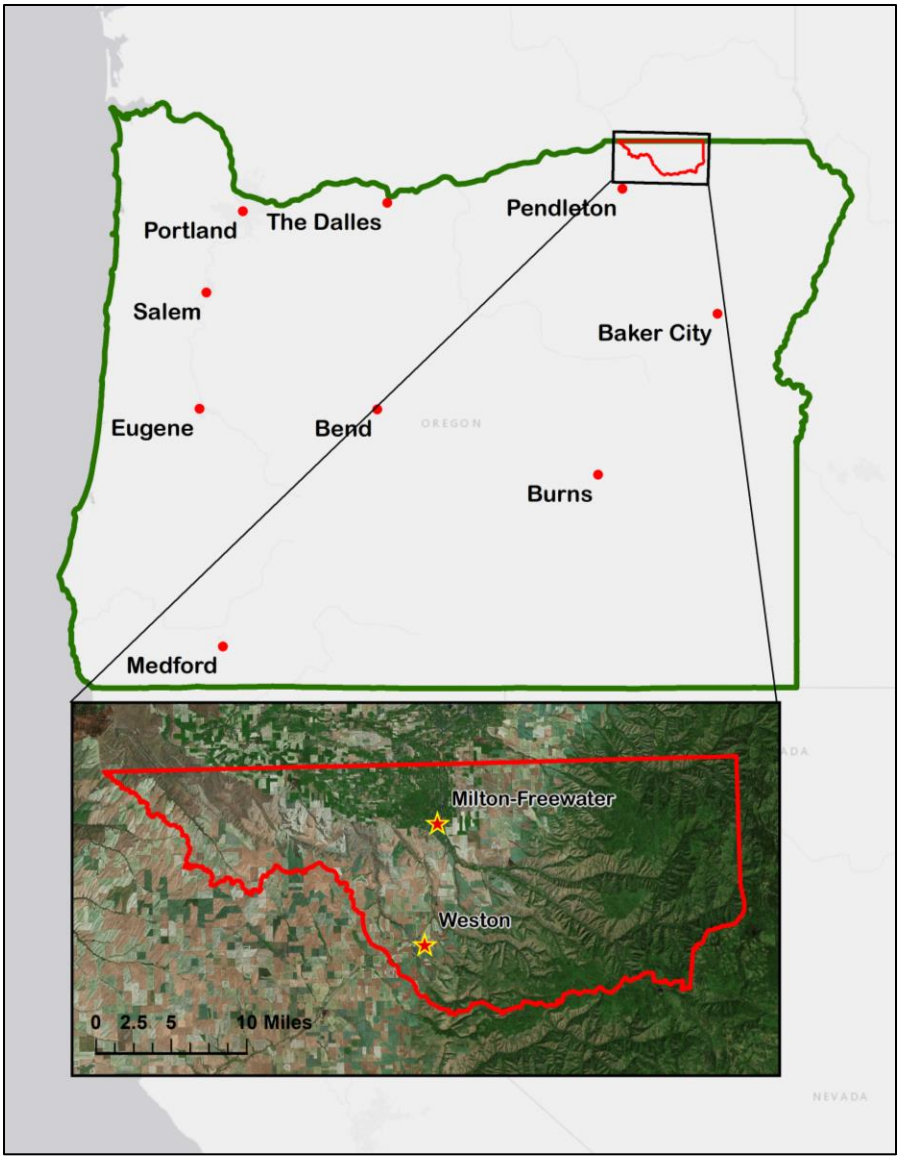

Figure 1: Location of the Walla Walla Subbasin (outlined in red) in the context of the state of Oregon (outlined in green) and selected cities.

Based on literature review, I identified several specific phenomena to test the hypotheses of variable degrees of hydraulic connectivity across faults. I describe them in more detail in the relevant background sections which follow this introduction.

Firstly, relatively less permeable faults perpendicular to the dominant flow direction would "dam" the groundwater flow, and force water from deeper flow paths to rise closer to the surface. In this situation, water in upgradient wells would have a higher temperature and more evolved characteristics compared to a nearby downgradient well of similar depth. (Newcomb 1966)

Secondly, throughout the Columbia Plateau concentrations of calcium and magnesium ions tend to decrease away from outcrop areas toward the center of the plateau, as well as with increasing depth. As those concentrations decrease, the concentrations of sodium, silicon dioxide, sulfate, and potassium increase (Steinkampf et al 1996). I hypothesize that exceptions to this trend in wells near faults could indicate disruption in this process of ion exchange along flow paths and indicate abrupt changes in the recharge pattern. For example, I hypothesize a shift from from long flow paths from higher elevation recharge areas associated with unfaulted regions to shorter flow paths based on anomalous vertical transmissivity associated with fault damage zones.

Background

Geology of the Walla Walla Subbasin

The Walla Walla Subbasin study area encompasses roughly 4,600 square kilometers in northeastern Oregon along the Oregon-Washington Border. It is geologically bounded by the Horse Heaven anticline in the southwest and the Blue Mountains to the southeast, and geographically bounded by the Washington-Oregon border to the north. The entire Walla Walla basin continues north into Washington with no significant change in geology, but this study and the WWSB stop at the border for regulatory reasons. The geology of the WWSB study area is dominated by Miocene basalts of the Columbia River Basalt Group (CRBG). The CRBG erupted in the Cascade back-arc setting between 17 and 6 million years ago from groups of dikes close to the boundary between the Precambrian craton and the Mesozoic accreted terranes that occur to

the west of it (Tolan et al 2009). However, around 96% of the volume of the CRBG was emplaced between 17 to 14.5 million years ago (Riedel 1998). The flood basalts, covering 164,000 km^2 and with an estimated volume of 174,000 km^3, filled the basin between the Cascade Mountains and the Rocky Mountains to a depth of up to 3 km (Riedel 1998). The resultant area is also referred to as the Columbia Plateau.

Three formations of the CRBG exist in the study area; from oldest to youngest, they are the Grande Ronde basalt, the Wanapum Basalt, and the Saddle Mountains basalt (see figure C1 in Appendix C). The Wanapum basalt is exposed in the southwestern area of the WWSB, the Saddle Mountain basalt is exposed south of Milton-Freewater, and both the Wanapum and Grande Ronde formations are exposed in the southeastern part of the study area in the Blue Mountains. Figure C2 in Appendix C illustrates these outcrops in the WWSB and also in the larger Walla Walla basin. In the lower-elevation north-central area of the WWSB the basalt formations are covered by Quaternary alluvial sediments. The Saddle Mountains basalt formation is present under the alluvial sediments on the northern side of the fault zones (Madin and Geitgey 2015). In the study area, the units present include the Umatilla Member of the Saddle Mountains Formation, the Frenchman Springs member of the Wanapum Basalt Formation, and the Sentinel Bluffs, Winter Water, and Downy Gulch members of the Grande Ronde Basalt (Keinle 1979).

In the lowland areas of the WWSB, and in most of the Walla Walla basin, the basalt formations are covered by Plio-Pleistocene sedimentary units, extensive deposits of upper Pleistocene glaciofluvial deposits, and quaternary and Holocene alluvium. These units contain a wide variety of grain sizes, sorting patterns, and thicknesses including fanglomerate, loess, river deposits, torrential flood deposits, and slack-water deposits (Kienle et al 1979).

The basalt formations of the CRBG dip to the northeast and to the northwest in the WWSB because of the Horse Heaven Anticline and the Blue Mountains respectively. The northwest-southeast trending Horse Heaven anticline was created after the CRBG had been emplaced, and so deformed the overlying formations. It is the largest anticlinal feature in the southern part of the Yakima Fold Belt section of the Columbia River Plateau. Within the Walla Walla Basin, this Horse Heaven Hills Anticline has an amplitude of approximately 400 m and is asymmetrical. The south flank has a slope of 0.5 to 1 degree, while the northern flank has a slope of 3 to 5 degrees and is interrupted by the Wallula fault zone (Kienle et al 1979).

The Blue Mountains were a structural high point before the emplacement of the CRBG formations and form a boundary at the edge of the CRBG. The down-warping of the crust and basalt formations under their own weight is especially apparent here, where layers of basalt that were emplaced horizontally are shown to be sloped to the northwest in outcrops.

The study area is situated at the confluence of two linear fault zones in the CRBG. The Wallula fault zone on the northeastern slope of the Horse Heaven Hills defines the southwestern section of the study area. The Hite fault zone occurs on the northeastern slope of the Blue Mountains, which border the study area to the southeast. The Wallula fault zone strikes northwest between Milton-Freewater, Oregon and Kennewick, Washington. It consists of multiple normal or reverse faults that dip vertically or very close to vertically to the southwest or northeast (Personius et al 2017). Structural relief across the Wallula structure has been estimated to be 250 m with a maximum of 300 m (Coppersmith et al. 2014). Strike-slip movement along the fault has been bounded at a maximum of 5.5km by an offset in the Ice Harbor volcanic dikes which intruded through the fault zone (Hutter 1997). The Wallula fault zone is seismically actively, most recently in July 1936. The earthquake created narrow fissures and scarps in the overlying

sediments that trended parallel to the strike of the Wallula fault zone, damaged houses, and temporarily increased the flow at certain wells and springs along the fault zone (Brown 1937).

The northeast-southwest trending Hite fault zone extends from northern edge of the Umatilla National forest in southeastern Washington to the southeastern corner of Umatilla County in Oregon. Faults within the zone have been mapped as normal, left-lateral strike-slip, or right-lateral strike-slip, but more recently their movement has been categorized as left-lateral oblique (down to the northwest) (Personius and Lidke 2003). The amount of lateral offset on the main Hite fault is unknown, but at least 100 m of offset in the Grande Ronde basalt has been observed (Kienle et al 1979). Road cuts and natural exposures of the Hite fault near Mill Creek, on Indian Ridge, and north of Tollgate Chalet expose a zone 80 to 200 m wide of crushed, brecciated, and sheared basalt (Kienle et al 1979). For the purpose of this study I focus on the Wallula fault zone's impact on groundwater, as this fault zone has more overlap with developed wells and irrigated land than the Hite fault zone which outcrops mainly in the forested, less developed parts of the Blue Mountains. The exception to this assumption is the wells in Weston, where the Hite and Wallula fault zones intersect.

The width of fault zones, as defined as zones of shatter breccia and gouge, in the CRBG are variable. Zones can be fewer than 1 m wide or greater than 150 m wide. This width depends on the magnitude of fault displacement, type of fault (high- or low-angle), and the types of CRBG structures transected by the fault (i.e. flow top, entablature, colonnade, flow bottom). The fault zone often widens as it passes through the weaker CRBG structures such as the flow tops and bottoms. Fault zone shatter breccias frequently show substantial degrees of both alteration into clay and secondary mineralization of silica, zeolite, calcite, or pyrite. These two types of

secondary lithologies create a resistant cement that is often stronger than the unaltered host rock (Tolan et al 2009). Figure 2 illustrates these features.

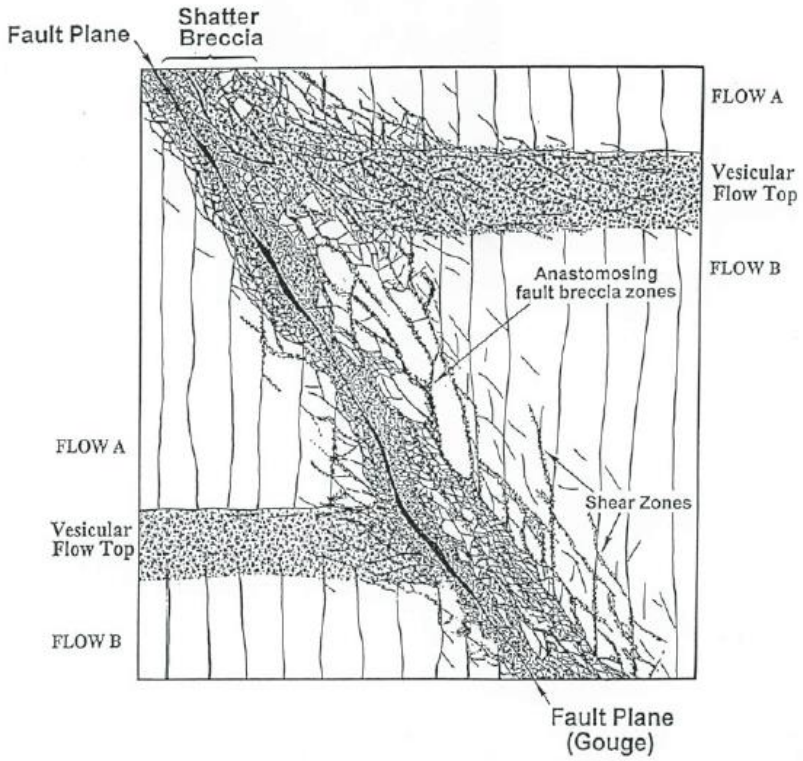

Figure 2: from Tolan et al 2009: Diagram identifying fault zone features commonly found in the CRBG

A selection of these named faults of interested this study because of their locations in between groups of wells. These faults are the Wallula fault, Umapine fault, Barrett fault, Bade fault, Milton-Freewater fault, Ryan Creek fault, Pine Creek fault, Bowlus Hill fault, Thorn Hollow fault, and Peterson Ridge fault. These faults are illustrated in Figure 3 below.

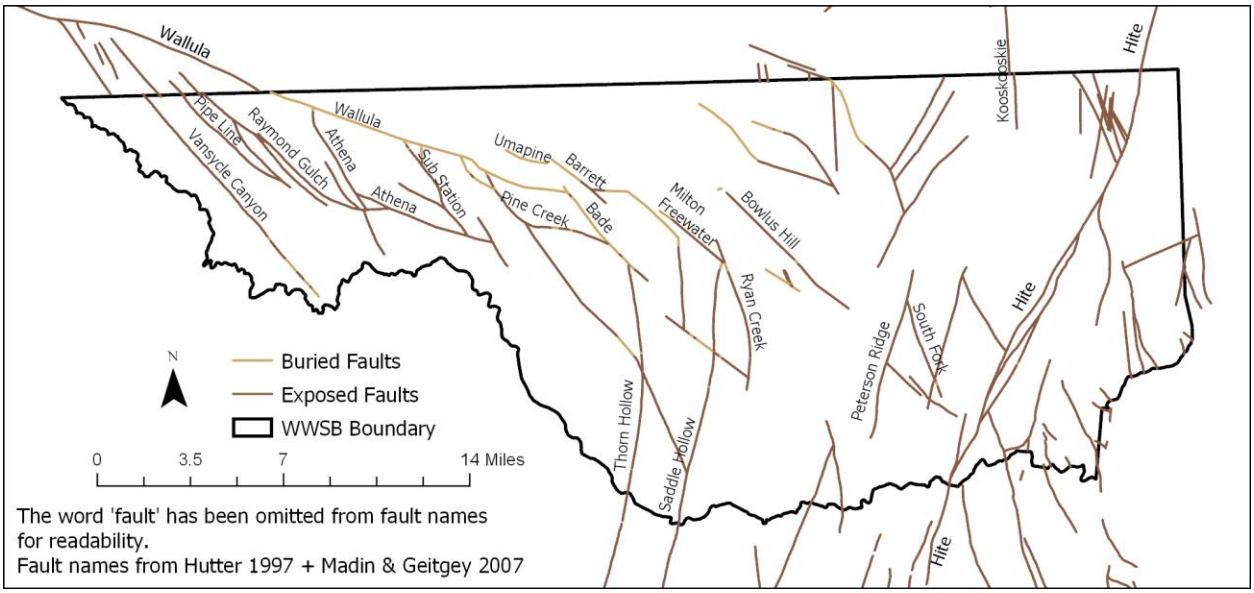

Figure 3: named faults in the WWSB, from Madin and Geitgey 2007

The Pine Creek fault offsets the contact between the Gingko and Sand Hollow units of the Frenchman Springs member of the Wanapum basalt formation approximately 30 m down to the north at the western end of the fault, and at the eastern end of the Pine Creek Fault it offsets the contact between the Sentinel Gap and Sand Hollow flows of the Frenchman Springs member of the Wanapum basalt formation by a maximum of 60 m down to the north (Hutter 1997). Is has been interpreted as a Riedel shear to the main Wallula fault zone based on its geometry and similarity of trends of apparent motion. The Bade fault's location was inferred from the mismatch of the Frenchman Springs member across Dry Creek valley, but flow contacts are not well enough constrained on either side of the fault to estimate offset (Kienle et al 1979). The Barrett fault was inferred from a prominent topographic lineament visible in 1979, and offsets clastic dikes within the sedimentary Touchet beds by 2 cm to 0.5 meters down to the north (Kienle et al 1979). The Milton-Freewater fault was inferred from a scarp-like bluff along the southwest edge of the town (Hutter 1997). Well data suggests that this fault acts as a groundwater barrier (Newcomb 1965).

The unnamed east-west trending fault directly east of the Barrett fault and west of the Milton-Freewater fault, whose western end terminates in the Barrett fault, is referred to as the Barrett-County Road fault for the purposes of this study. This buried fault was identified with scarps visible in the sedimentary layers. Although its strike is similar to the main Wallula fault, aeromagnetic geophysical surveys did not record a similar linear anomaly at this location. This does not rule out fault movement along these scarps, instead indicating that the vertical component of this fault segment is too small to be detected magnetically. Wallula fault segments further to the west with 200m or more of measured vertical displacement at outcrops were detectable in the aeromagnetic survey (Hutter 1997).

The Thorn Hollow fault south of Milton-Freewater is part of the Hite fault system. It is 43 km long and is defined by linear streams, saddles, notches, ridges, and exposed fault planes, and has been interpreted as a dextral strike-slip fault based on near-horizontal striae at its southern extent (Kienle et al 1979). The Peterson Ridge fault, while shorter at only 24 km, also expresses right-lateral slip. Kienle et al. characterized it as primarily a strike-slip fault. Vertical offset was observed at the fault but was inconsistent; at Little Cottonwood Canyon the fault seemed to have moved east-side-down by about 20 m, but in the Umatilla drainage the movement appeared to be west-side-down.

Offset on the nearby Ryan Creek fault is down to the east by about 30m, as indicated by a vertical offset in Grande Ronde formations. The Ryan Creek fault is most remarkable for its behavior during the 1936 Milton-Freewater Earthquake at its junction with Dry Creek. A spring there, which had flowed at 230 L/min before the earthquake, increased to 11,400 L/min at the time of the earthquake, diminished to 3,800 L/min one month later, and by 1960 flowed at 4L/min. This flow anomaly suggests a partial draining of an aquifer by fault movement during

the earthquake either tilting of the strata up-gradient of the fault or dilatancy within the fault gauge that allowed increased flow permeability (Kienle et al 1979).

The 42 km long Saddle Hollow fault is also a north-northeast striking strike-slip fault within the Hite group. It is notable for obviously being a groundwater barrier because of the number of springs and seeps expressed along its length, indicating upward groundwater movement through the fault. Apparent movement is primarily dextral strike-slip with approximately 25 m of east-side-down vertical movement (Kienle et al 1979).

The Thorn Hollow fault is roughly parallel to the Saddle Hollow fault to its east, and has a similar length. It is expressed as a series of linear streams, saddles, and notches, most notably Thorn Hollow Valley and Dry Creek which have been excavated following the course of the fault. South of the Umatilla river this fault also shows signs of being a groundwater barrier, exhibiting spring, seeps, and moisture-loving vegetation. Vertical offset on this fault suggest west-side-down movement. Road cuts along Highway 11 show this fault zone to be 20m in width and contain crushed and altered basalt gouge, as well as fractured gouge filled with secondary mineralization (Kienle et al 1979).

Hydrology of the WWSB

The majority of precipitation in the WWSB forms as winter precipitation in the highlands of the Blue Mountains, where it is stored as snow and flows down through the Upper and Lower Forks of the Walla Walla River into the lowlands. The developed areas in the lowlands received on average between ten and twenty inches a year of precipitation between 1981 and 2010, while the uplands received between thirty and sixty-five inches per year (OSU PRISM, 2014). Once the surface water reaches the lower elevations its natural flow is modified by extensive diversion for irrigation of orchards and other crops around Milton-Freewater. While the north and south forks

of the Walla Walla River flow out of the Blue Mountains year-round, the streams flowing out of the Horse Heaven Hills on the western side of the basin are often nonperrenial. The potential evapotranspiration in the lowlands is 28 inches per year, but it is limited by precipitation to roughly 10.5 inches per year. More water is available for groundwater recharge and stream runoff in the higher elevation areas of the Blue Mountains, where precipitation is higher and potential evapotranspiration is lower (Golder Associates, Inc. 2007).

The relationship between surface water and shallow groundwater has changed since the development of the study area for agriculture. The Walla Walla River and other smaller creeks flowing off of the Horse Heaven Hills once meandered across the Milton-Freewater area. The valley bottom is filled with sediments deposited since the Miocene. Gravel layers in these sedimentary deposits act as an aquifer and create an interface between shallow groundwater and surface water systems (Newcomb 1965).

Hydrogeology of the Columbia River Basalts in the WWSB

The basalt hydrogeology in the study area is generally defined by the stratigraphy and extent of the flood basalt flows which underly it. The lavas which cooled to form the basalt were fluid and erupted in massive quantities over relatively flat extant topography, and thus have significant individual lateral extents. Individual flows average about 30 m thick but can be as much as 100 m thick, and can cover as much as 15,000 km^2 (Riedel 1998). The position of water bearing layers was determined by the smaller-scale structures of flows within the larger mapped formations. These flows range in thickness from two to fifty meters in the Walla Walla Basin, with an average around nine meters where exposed flows have been measured along the South Fork Walla Walla (Newcomb 1965). Each individual flow is identifiable by the sequence of three parts: a permeable flow bottom that incorporates some of the underlying material, a

massive and less permeable flow interior that may contain some vertical joints or colonnades from its cooling process, and a permeable flow top. The combination of one event's flow top and the following lava flow's flow bottom is referred to as an "interflow zone".

These interflow zones form the primary aquifer layers in the CRBG, and are generally between one and three meters thick. (Newcomb 1965) Because of the large areal extent of the lava flows, their interflow zones have substantial lateral conductivity (10^{4} to 10^{-6} feet per day) and connectivity. However, the less permeable flow interiors cause the vertical element of hydraulic conductivity between interflow zones to be significantly lower, between 10^{-3} and 10^{-9} feet per day. Figure 4 illustrates an idealized cross-section showing flow interior and interflow zone transmissivities.

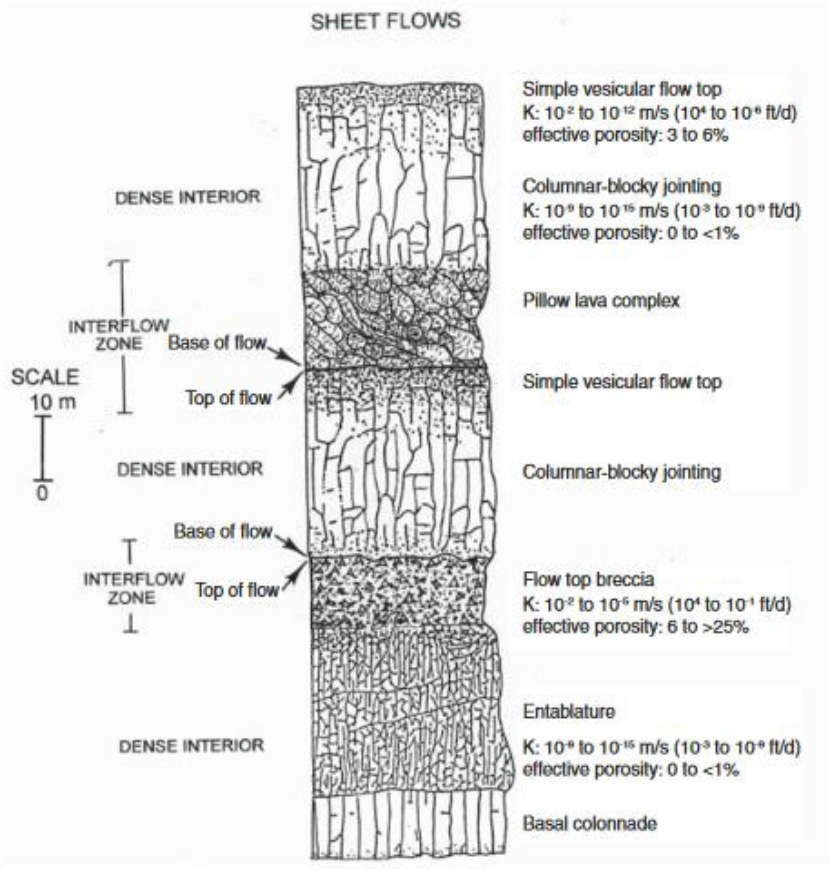

Figure 4: Illustration of basalt flow structures and their permeability (Figure from Tolan et al. 2009)

Several studies have been performed to assess the potentiometric surface and flow directions in the Saddle Mountains, Wanapum, and Grande Ronde basalt formations. One comprehensive study of potentiometric surface height in the CRBG was published by Lane and Whiteman in 1988 based on data collect in 1985. They used water level measurements from 1,105 wells with screens open to single formations to estimate these surfaces for the Saddle Mountain, Wanapum, and Grande Ronde formations. Their map shows that the potentiometric surface of the Wanapum formation aquifers roughly follows the surface topography with curved parallel lines convex to the north indicating flow from the higher elevations towards a central lower-elevation area near the Washington border. Their map of the Grande Ronde formation's potentiometric surface shows that this layer was less influenced by the topography of the Horse Heaven Hills, instead showing a gradient towards the northwest and flowing away from the Blue Mountains. The authors did not have sufficient data to map the potentiometric surface of the Saddle Mountains basalt in the WWSB study area. Their maps of water levels in the Wanapum and Grande Ronde formations, cropped to focus on the WWSB, are presented as figures C3 and C4 in Appendix C.

Faults create a permeability anomaly in the rock formations that they divide. They can serve as zones of increased or decreased permeability, and possibly connect offset permeable zones of the host rock. In structural geology, faults zones are separated into two structural units. The fault core is located at the center of the fault zone, and as the area of most intense strain it accommodates the majority of the displacement along the fault. The second structure is the damage zone, which surrounds the fault core and accommodates a lesser amount of strain by fractures, jointing, and minor secondary faults. The primary method by which faulting reduces permeability along the plane of movement is by the fault movement pulverizing the rock in the

fault core into a wider range of fine grain sizes which can pack together into a less permeable structure in the fault core.

Conversely, the deformation in the damage zone can increase permeability relative to the fault core and host rock through the opening of fractures and joints (Bense et al 2013). Total fault permeability depends on the interactions of these two structural processes. A fault with a large damage zone and small fault core could function as a conduit both perpendicular to and parallel to the dip direction of the fault, while conversely a fault with a small damage zone and extensive deformation in a fault core might be a barrier in both directions. A fault with an even ratio of fault core to damage zone could function as a conduit in the direction parallel to the dip direction because of the permeability of the damage zone, but as a barrier in the perpendicular flow direction because of the less permeable fault core (Caine et al 1996). These alternatives are illustrated in Figure 5.

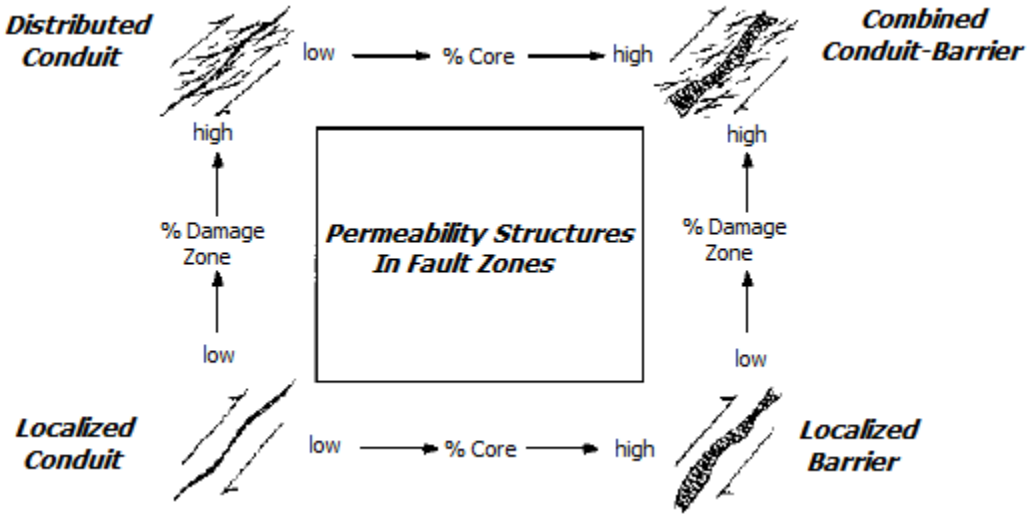

Figure 5: Conceptual scheme for fault-related fluid flow, modified from Caine et al. 1996

Thus, faults can compartmentalize groundwater by three possible mechanisms: separation by low-permeability fault gouge, secondary mineral precipitation in the fault plane, or by offsetting of permeable interflow zones against low-permeability flow interiors (Golder Associates, Inc. 2007). Studies including a component of investigation of faults and hydrogeology have been conducted in the vicinity of the study area. For example, Packard et al. published the result of a related study in the Washington side of the Horse Heaven Hills in 1996. The Horse Heaven Hills are centered on an anticline which the Columbia River has eroded through at the Wallula Gap, and so are present on both the Washington and Oregon sides. The authors found that large fault zones were generally associated with steep hydraulic gradients and infer that they are also zones of low horizontal-hydraulic conductivity. However, this is different from what we observe along developed portions of the Wallula fault zone near Milton-Freewater, where some sections show no hydraulic gradient across the fault zone as currently mapped.

Compartmentalization because of faulting in the Walla Walla Basin has been documented in Walla Walla, Washington, eight miles north of Milton-Freewater. In their 2007 report, Golder Associates, Inc. divided the aquifers in the area into five “blocks” based on a network analysis of wells’ response to pumping at other wells.

Ion Chemistry and Evolution in the WWSB

Groundwater’s major ion chemistry in the Columbia River Basalt aquifers is influenced by three chemical processes: ion exchange, silicate hydrolysis, and the precipitation of clay minerals. These create a gradient in chemical composition along flow paths. Recharge into the aquifer, once it has passed through the soil zone, is predominantly of a calcium-magnesium-bicarbonate type. Ion-exchange and precipitation reactions replace magnesium and calcium in the groundwater with sodium. At the same time silicate hydrolysis and dissolution increases the

dissolved silica, fluoride, and chloride concentrations as well as the pH of the water. On average, the pH can increase from around 7 to around 10. Furthermore, clay minerals can precipitate with longer groundwater residence times along the flow paths, which removes quantities of calcium, magnesium, potassium, iron, carbonate, and silica with the creation of smectite clays, zeolites, calcite, and silica (Vlassopoulos et al 2009). The lines of equal concentration values for the major ions have been found to approximately parallel the potentiometric contours in each unit (Steinkampf et al 1996).

This gradient was observed in the Walla Walla area in the 2007 report by Golder Associates, Inc. who recorded an east-to-west gradient of groundwater quality. They found that groundwater in the easternmost city wells was a calcium-magnesium bicarbonate water type typical of recharge to the basalt system, while further west the groundwater was a sodium-bicarbonate type suggestive of longer flow paths and greater subsurface residence times within the basalt aquifer system.

Carbon-14

The radioactive isotope carbon-14 (^{14}C) is used to date samples that are up to 40,000 years old. ^{14}C dating can be complicated in aquifers that contain inorganic carbon, such as limestone or carbonate-cemented sandstone (IAEA 2013). Carbon-14 data in the CRBG is likely to be successful because the basalt contains minimal amounts of inorganic carbon (Newcomb 1965). Cosmogenic ^{14}C is created in the upper atmosphere, but can be brought by atmospheric circulation where it is entrained in precipitation. Once removed from the atmospheric system, the age of the carbon in the water can be dated using ^{14}C's half-life, during which it decays to ^{14}N plus a beta particle (IAEA 2013). Several studies have evaluated ^{14}C in the CRBG in Washington state. For

example, Douglas et al. 2007 found that conventional radiocarbon groundwater ages in the Palouse Basin range from 4,400 to 26,400 years before present.

In their 2010 study, Brown et al. took ^{14}C and stable isotope measurements from sixty-eight wells across the CRBG. They found two distinct groups of samples. The first was of samples interpreted as modern recharge that had elevated tritium (2.8 to 14.4 tritium units), high $\delta^{18}O$ values (-16.9 to -13.5 permil), and 100% modern carbon. The second groups which they interpreted as paleogroundwaters contained samples with tritium less than 0.8 tritium units, low $\delta^{18}O$ values (-18.9 to -16.7 permil), and ^{14}C ages ranging from 6,000 to 33,000 years.

Groundwater dating using ^{14}C is more complex than would be suggested by the simple application of its decay reaction equation. The carbon used for dating is not integral to the water molecule as in the case of stable isotopes, but is in solution and can be affected by chemical reactions. There are two primary unknowns in its interpretation: the initial concentration of ^{14}C in the atmosphere compared to modern ^{14}C at the time that the water entered the groundwater system, and the interaction of the water with reactions that alter the amounts of ^{12}C, ^{13}C and ^{14}C in the groundwater. Thermonuclear testing raised the concentration of ^{14}C in the atmosphere to twice the amount as it was in 1950 (the "zero year" for carbon dating). Thus, water that entered the groundwater during the period of bomb testing could have a ^{14}C value of 200 percent modern carbon (pmC). Conversely, the burning of fossil fuels increases the amount of ^{13}C in the atmosphere, diluting the ^{14}C signature so that modern water samples can have apparently decayed ^{14}C values of as low as 75pmC. These relationships can be corrected by comparing the ^{14}C values to calibration curves taken from tree ring samples dating as far back as 7,000 years (Kazemi 2006).

There are also factors that alter ^{14}C in the atmosphere on older timescales. Studies have suggested that the production of ^{14}C by cosmic rays in the atmosphere deviated from the estimated average long-term production rate at periods between 8,500-9,500 years before present and 27,000-32,000 years before present where it was roughly double the average, and during the period between 12,000 and 16,000 years before present where the production rate was lower by a factor of approximately 1.5 (Kazemi 2006). As previous studies in the CRBG have shown ^{14}C values as old as 33,000 years (Brown et al. 2010, Douglas et al. 2006), it is possible that these periods of altered ^{14}C input to the global precipitation system could have an effect on the correlation between radiocarbon age and calendar age of samples.

In addition to differences in atmospheric inputs to ^{14}C in precipitation, geochemical processes can create sources or sinks of ^{14}C once water containing it has percolated into the subsurface. These can include dissolution of carbonate rocks (which can dilute ^{14}C activity or remove it from the system by precipitation of calcite), and the addition of "dead" carbon from sulfate reduction or methanogenesis (Kazemi 2006). The geologic composition of the WWSB simplifies this aspect of ^{14}C analysis because it contains few carbonate rocks that would significantly affect ^{14}C concentrations due to reactions in the subsurface, and it contains few other sources of organic carbon which could dilute the carbon signature with carbon lacking ^{14}C activity (Riedel 2002). There are multiple models which seek to correct ^{14}C age based on other chemical characteristics to decipher the possible impact of geochemical processes on the water. However, for this thesis I did not correct the ^{14}C ages for geochemical processes because of the favorable conditions of the local geology. NETPATH modelling of groundwater in the Hanford and Palouse Slope areas of the CRBG showed that modeled and observed ^{14}C ages differed by less than 1% in basalt aquifers (Brown et al 2010, Douglas et al 2005).

Based on a conceptual model of the roughly north-dipping interflow zones of the CRBG with recharge primarily occurring the upland area of the Blue Mountains, I would expect that ^{14}C ages would increase with distance away from the recharge zone along the flow path. However, I hypothesize that if faults provide an anomalous zone of vertical hydraulic conductivity, the ^{14}C ages would be reduced down-gradient of the fault.

Tritium

Tritium is a hydrogen atom with two neutrons and one proton in its nucleus, and is a unique signature of the nuclear bomb tests in the 1950s and early 1960s. It has a half-life of 12.43 years, and concentrations are expressed using "tritium units" which correspond to the number of tritium atoms per 10^{18} atoms of hydrogen (Clark and Fritz 1997). The atmospheric signal of tritium has diminished since the end of above-ground nuclear testing in 1964, and has recently faded to pre-1950 background levels. The presence of tritium in a groundwater sample indicates that the sampled aquifer contains water that has recharged since the 1950s (Jasechko 2018). For example, Douglas et al.'s 2005 study in the Lewiston Basin of Idaho found that tritium was present in ground water samples taken from basalt wells near the Snake River which also happened to have low percentages of modern carbon as shown by carbon-14 values. The authors consider this pattern of parameter values to indicate that parts of the aquifer near the river were receiving modern recharge, while wells with no tritium occurred further from the rivers and did not receive recharge from them.

It is also possible for a water sample with an older ^{14}C value to also have a detectable amount of tritium. This is achieved by the mixing of parcels of water along a flow path, for example where a poorly cased well or a fault has channeled modern recharge from overburden aquifers directly

into deeper layers of the aquifer, providing a shortcut through formation that otherwise have low vertical hydraulic conductivity.

Stable Isotopes

Variation in sources of groundwater recharge could be a factor distinguishing groundwater compartments. If isotope ratios of groundwater samples deviate from the ratios that characterize local precipitation, then either a fractionization process has affected the ratios or the recharge was not from a local modern source. The stable isotopes of oxygen and hydrogen found in water can be used to in some cases to evaluate the original elevation of recharge (Kendall and McDonnell 1998). The ^{18}O and ^{2}H ratios are more negative with higher elevation as the isotopic composition is "distilled" as heavier isotopes are gradually rained out of the air masses. Several studies have successfully used O and H stable isotopes to differentiate groundwater compositions in basalt members of the CRBG (Larson et al. 2000, Taylor and Gazis 2014).

Additionally, combinations of ^{14}C and stable isotope analyses have been used in the CRBG to confirm the stable isotopic signature of groundwater that was recharged during the past ice age, when massive ice sheets sequestered heavier isotopes from the global water cycle (Brown et al 2010, Hearn et. al 1989). Pleistocene-recharged groundwaters are isotopically lighter than Holocene and modern groundwater (Kazemi 2006). Circulation models of the Pleistocene and Holocene climate of the region, as well as paleo-ecological studies, have indicated that during the last glacial maximum around 20,000 years ago the region was significantly colder and drier than the present. Regional precipitation decreased by up to 28 inches per year and the mean annual temperature was estimated to be 4 to 8 degrees Celsius colder than the modern mean annual temperature. This resulted in precipitation depleted in both ^{2}H and ^{18}O (Brown et al. 2010).

In their 1989 study of stable and radioactive isotopes in groundwater at the Hanford site, Hearn et al. found this trend of lighter oxygen and hydrogen isotope ratios since the ice age to be confirmed by a directly proportional relationship between increasing 18O content and increasing ground-water conductivity (which indicates a more "evolved" and older groundwater due to progressive ion dissolution). This study found that of the three main CRBG layers, the Saddle Mountain layer appear to have the most Pleistocene recharge, while the Wanapum and Grande Ronde aquifers were interpreted to represent much older pre-Pleistocene groundwater that was recharged under very different climatic conditions. Groundwater in the Grande Ronde aquifer is enriched in ^{18}O compared to water in the Wanapum. The oldest, most evolved Grande Ronde groundwater sample was enriched by ^{18}O by 8 to 9 permil relative to the youngest and least evolved Saddle Mountain groundwater sample. The authors suggest a vertical interchange of water between the formations in the Pasco Basin, as indicated by a gradation of chemistry between the Wanapum and Grande Ronde formations (Hearn et al 1989).The flow patterns in the Pasco Basin may be different than the flow patterns in the WWSB, as it is the lowest part of the CRBG in the Columbia Plateau and a local sink. The WWSB is located at a higher elevation in the WWSB and further towards the margins of the basalt flows, and so flow direction is less likely to be redirected upwards.

Literature Review for Well Records and Lithology

Geographic information on the faults and geology of the study area was acquired from the data set originated in the work published as Madin and Geitgey (2007) and informed by previous studies such as Newcomb (1965) and Steinkampf (1989). Madin and Geitgey's geologic map synthesis and geospatial dataset included faults mapped as exposures at the surface, as well as faults that are assumed to be buried based on pre-development surveys and observations of fault

scarps in the overlying sediment. I acquired the coordinates for the all field- located wells drilled into the basalt in the study area from OWRD. I accessed well logs and lithology interpretations for the sampled wells for this study through OWRD's internal database. If the wells were classified as "Columbia River Basalt Group, undifferentiated" in the OWRD database, I referred to the web portal for the USGS CPRAS 3D model of the CRBG geologic setting to estimate the stratigraphy (Burns 2011). I looked up well stratigraphy in that web portal using the latitude and longitude of the wells, and compared the modeled elevation of the top of each formation to the well's log information for depth and seal. Stratigraphy for each well is included as a table in Appendix B. Figure C5 in Appendix C illustrates OWRD confirmed stratigraphy when available for wells, without the model-provided results for CRBG.Undifferentiated wells.

A hydrograph showing historical winter water levels in the 32 wells sampled as part of this project is presented in as figure B2 in Appendix B.

History of Groundwater Use and Management of the Walla Walla Subbasin

Agriculture, public supply, domestic users, and industries in the Walla Walla Subbasin of Oregon depend on ground water drawn from wells in sedimentary and Columbia River Basalt Group (CRBG) aquifers to supplement seasonally available surface water resources. Over the past 70 years water levels in the basalt aquifer have declined up to 200 feet to the point where some senior groundwater right holders cannot access their full water allocation. In 2016, the Oregon Water Resources Department (OWRD) conducted a basin rule change process to prevent new groundwater allocation and require measurement of water pumped using basalt groundwater rights (OAR 690-350-507(30)).

Groundwater has been withdrawn from the basalt aquifers of the Walla Walla Subbasin (WWSB) of Oregon, near the municipalities of Milton-Freewater and Weston since the 1930s. Previously,

flowing artesian wells had been used for domestic use and stock watering, but introduction of the deep-well turbine pump and improved drilling methods allowed for the access to water from the basalt aquifers for municipal supply and industrial use. The canning industry was the primary industrial withdrawal. Between the 1940s and the 1950s farmers started to use groundwater from basalt aquifers for irrigation, although the sedimentary aquifer was the predominant source of irrigation water at that time. Application rates in the area ranged from 3 gallons per minute (gpm) per acre for sugar beets to 10 gpm per acre for alfalfa, and annual withdrawal from the basalt aquifer in 1958 was estimated to be 5,600 acre-feet (Newcomb 1965). Already in the 1950s and 1960s drawdown in the basalt aquifer was observed in wells near College Place, Washington (Newcomb 1965).

While this thesis does not address policy recommendations, an introduction to the regulatory context of this study gives a sense of the justification and need for this work. Beginning in 2016, the OWRD initiated public meetings in the WWSB to discuss the declining water levels and potential long-term management solutions. Some basalt wells are declining up to 4 feet per year, indicating that the aquifer withdrawal exceeds recharge. After several months of public and rule advisory committee meetings, the OWRD Commission adopted two basin rule changes to Umatilla Basin Rules OAR 690-507-0030 in May 2017. OAR 690-507-0030(4) requires installation of a totalizing flowmeter and water use reporting on all basalt wells with water rights through a Serious Water Management Problem Area designation (SWMPA per ORS 540.435). OAR 690-507-0030(3) classifies (per ORS 536.340) all new groundwater uses for exempt uses only (exempt as defined in ORS 537.545), meaning new groundwater rights are not available in the subbasin.

Water use reporting and classification of future groundwater allocation for exempt uses is not expected to be to prevent further groundwater decline. These changes allow analysis of

comprehensive CRBG aquifer water use and water level changes over time, and reserves the CRBG groundwater resources for current water right holders. In order to stabilize the groundwater levels in the area current groundwater users will need to reduce their water withdrawals or increase recharge. OWRD's Commission has two tools available for curtailment under current rules and statutes: the historically standard option of declaring the WWSB a Critical Groundwater Area (CGWA per ORS 537.730-537.742), or for the first time in Oregon negotiating Voluntary Agreements (ORS 537.745) between local well users that share the same aquifer. A CGWA would delineate a boundary within which the doctrine of prior appropriation would be guide curtailment; junior water right holders would be regulated off in order of increasing age of the permit until senior permit holders had enough water to fulfill their water rights. This does not withdraw the junior users' right, but only their ability to pump during a specified time period. The alternative, Voluntary Agreements, would require permit holders drawing from the same aquifer to collaborate to reduce groundwater decline (Woody & Gall, 2016). Artificially increasing groundwater recharge is possible under Aquifer Storage Recovery and Artificial Groundwater Recharge rules and statutes (OAR 690-350, ORS 537.531)

In either case the stabilization of aquifers depends on the assumption that the senior permit holders, junior permit holders, and signatories to a Voluntary Agreement are all actually drawing from the same interconnected aquifer. If they are drawing from different unconnected compartments of the aquifer then these management strategies will not accomplish their intentions.

To that end, this thesis work will provide an additional line of evidence for characterizing compartmentalization in WWSB basalt aquifers. Successful policy decisions in groundwater management depend on adequate knowledge of the reality of the physical environment in which they function.

Methods

Sample Collection Methods

Field work was carried out during three trips to the study area in the summer for 2018; it was supported by OWRD and supervised by an OWRD staff hydrogeologist, Jen Woody. Sample protocols and training were provided by the staff of the USGS Water Science Center in Portland, Oregon. This section will address site selection, field sampling processes, and the analytical procedures used by the laboratories which processed the samples.

Site selection was informed by both physical and practical concerns. Physical criteria included well construction, well location relative to faults, well depth, and pump test results. Practical criteria were the final constraining factor; sampling was not feasible if the well owner could not be contacted, the owner was contacted but did not allow access, or if the pump was not running. Physical well characteristics were research using OWRD's internal database of well logs. This study prioritized modern wells with known constructions that would minimize the likelihood of the well being open to alluvial aquifers or susceptible to contamination. OWRD had run pump tests in winter of 2013, 2017and 2018 to assess the impact of pumping a well on the water levels of nearby wells. These tests revealed certain patterns of strongly or minimally connected wells, and the study prioritized wells involved in those tests in order to see if distinct water chemistry might correspond to groups of wells with hydraulic connectivity. When possible, I tried to sample shallow and deep wells nearby each other, and wells on either side of the mapped faults. Once I had made a list of preferred wells based on those physical criteria, Jen Woody and I called the owners of the wells request access and inquire about projected dates when the wells would be pumping. The wells sampled in this study are illustrated in figure 6 below:

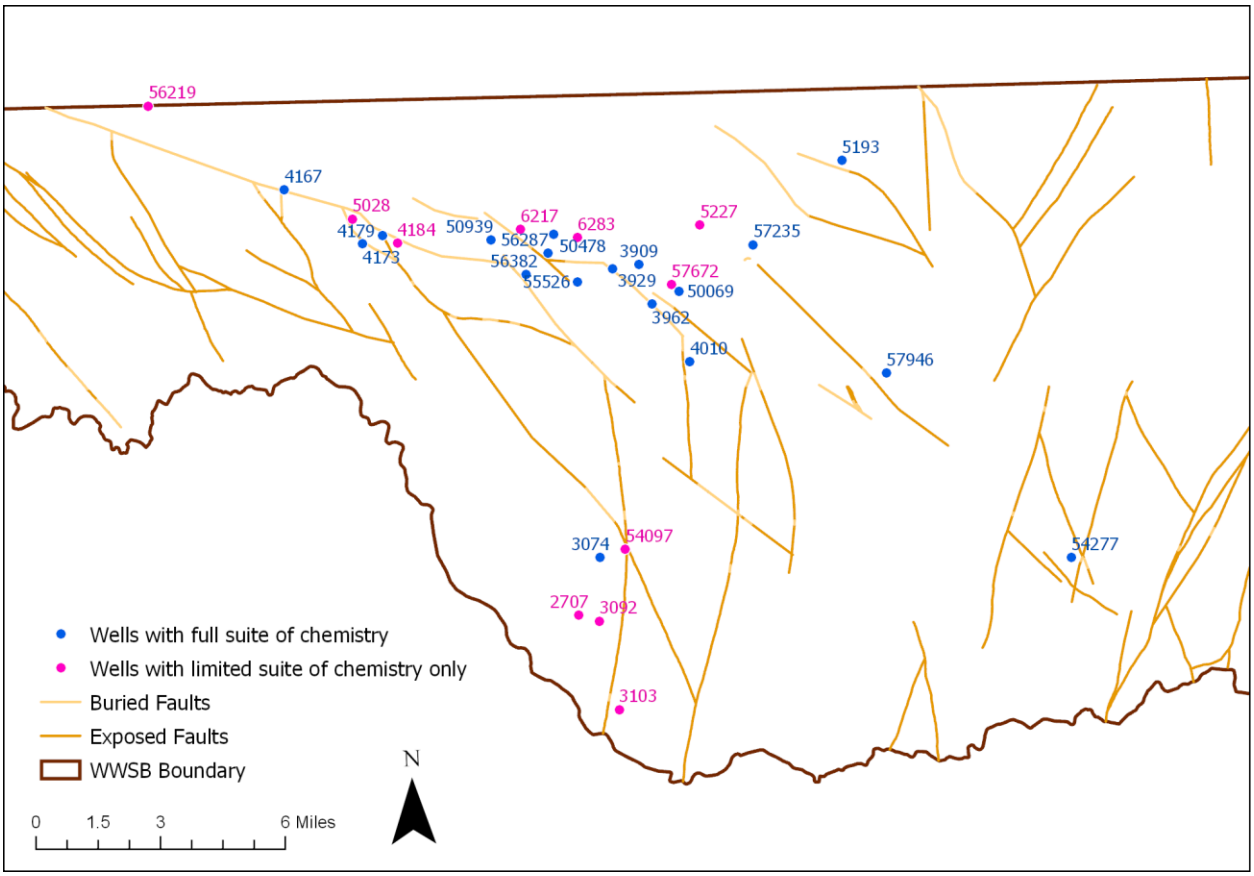

Figure 6: Map of wells sampled as part of this study in the summer of 2018

Once access had been arranged and we had travelled to the study area, the next task was to collect the samples. We collected pH, temperature, specific conductivity field parameters at each of the 31 sites, as well as filling 25 ml bottles for stable isotopes. A Hach multiparameter sensor and probe were used to take pH, temperature, and conductivity measurements. At the well, plumbing fittings were linked to the well's access point in order to enable the use of a ¾ inch hose splitter. A hose was attached to one side of the splitter, and a barb fitting was attached to the other side. The field parameters were measured by submerging the meter in a flow-through cell created by placing the free end of the hose into the beaker in which the multi-parameter meter's probe was submerged. Final measurements were noted once the readings had stabilized, and then the isotope sample was collected. At 18 of the sites we also collected samples for carbon-14,

tritium, cations, anions, and alkalinity. These samples were collected by attaching a length of ¼ ID tubing to the barb fitting. A fresh piece of acid-washed ¼ inch ID tubing was used for each well site. The sample bottles for cations, anions, and alkalinity were rinsed three times with well water before being filled and capped. The bottles for cations and anions were filled to the shoulder, while the bottle for alkalinity was filled with no head space. For tritium and carbon-14 the bottles were not field rinsed, the ¼ inch tubing was lowered to the bottom of the bottle to minimize aeration, and the bottles were filled with no head space.

A duplicate sample for well 56382 was submitted for QA/QC purposes. Two equipment blanks were prepared by running laboratory certified water through the two sections of fittings and hoses used to collect samples from the wells. These QA/QC samples were analyzed for pH, temperature, specific conductivity, major ions, and dissolved solids.

The following table contains sample IDs, date, analytes, formations, and well depths. For the analytical group type, “limited” group type samples were analyzed for pH, temperature, conductivity, oxygen isotope ratios, and hydrogen isotope ratios. Samples in the “full” group type were analyzed for all analytes in the “limited” group type plus carbon-14, tritium, and major ions.

OWRD Well ID*	Date sampled	Analytical Group Type	Well bottom depth (ft)**	Well bottom elevation (ft above sea level)*
UMAT0002707	8/15/2018	Limited	1215	589.06
UMAT0003074	6/22/2018	Full	542	1294
UMAT0003092	8/15/2018	Limited	1000	980
UMAT0003103	8/15/2018	Limited	1125	935
UMAT0003909	6/20/2018	Full	502	503
UMAT0003929	7/11/2018	Full	952	33
UMAT0003962	7/11/2018	Full	902	163
UMAT0004010	6/20/2018	Full	723	447
UMAT0004167	6/21/2018	Full	323	312
UMAT0004173	7/11/2018	Full	375	335
UMAT0004179	6/18/2018	Full	227	509
UMAT0004184	8/15/2018	Limited	300	448
UMAT0004864	7/11/2018	Limited	715	105
UMAT0005028	8/15/2018	Limited	383	287
UMAT0005193	7/12/2018	Full	760	480
UMAT0005227	8/15/2018	Limited	717	247.68
UMAT0005530	7/11/2018	Limited	1102	-92
UMAT0006217	8/14/2018	Limited	192	633
UMAT0006283	8/14/2018	Limited	1003	-93
UMAT0050069	6/21/2018	Full	706	474
UMAT0050478	6/19/2018	Full	475	402
UMAT0050939	6/19/2018	Full	1166	-311
UMAT0054097	8/16/2018	Limited	280	1370
UMAT0054277	6/19/2018	Full	400	1595
UMAT0055526	6/20/2018	Full	1040	108
UMAT0056219	7/11/2018	Limited	225	337
UMAT0056287	7/11/2018	Full	340	544.61
UMAT0056382	6/20/2019	Full	1055	35
UMAT0057235	6/19/2018	Full	905	165
UMAT0057672	8/16/2018	Limited	817	318
UMAT0057946	6/19/2018	Full	265	1285
** Source: well logs, accessed through OWRD Ground Water Information System (GWIS) *Source: OWRD data accessed through GWIS				

Table 1: Wells sampled in the summer of 2018

Laboratory Analysis Methods

Samples for this project were sent to USGS labs for analysis as part of a work order batch with samples from the USGS concurrent Umatilla Basin project.

The 18 samples for major ion analysis were sent to the USGS National Water Quality Lab in Lakewood, Colorado.

The 31 samples for stable isotope (d18O and d2H) analysis were sent to the USGS Reston Stable Isotope Laboratory in Reston, Virginia. Stable isotope ratios were measured using dual-inlet mass spectrometry. Vienna Standard Mean Ocean Water (VSMOW) was used as a standard for δ^2H and δ18O (Révész and Coplen, 2008a and 2008b).

The 18 samples for tritium analysis were sent to the USGS Menlo Park Tritium Laboratory in Menlo Park, California. The samples were prepared for analysis through distillation and electrolytic enrichment, and then the tritium in the concentrated samples was measured by liquid scintillation counters.

The 18 samples for carbon-14 analysis were sent to the National Ocean Sciences Accelerator Mass Spectrometry Lab at the Woods Hole Oceanographic Institution in Woods Hole, Massachusetts. Samples were acidified and purged before the C-14 atoms were counted using a continuous flow atomic mass spectrometry system.

Compilation of Physical Well Properties for Analysis

I used hydrometric and geological data available from previous studies to create a hydrogeologic block diagram of the area to inform interpretation of the geochemical results. The OWRD conducted interference tests in the winters of 2013, 2017, 2018 and 2019 in order to evaluate the response of wells in an area when one well is pumped. This kind of study provides valuable

evidence of both connection and compartmentalization which I will use to complement and refine my geochemistry-based compartmentalization models. These hydraulic tests are particularly useful in areas where the faults are buried and their exact location, magnitude of displacement, and orientation only estimated from previous studies. This hydraulic relationship between wells can then be used to control for differences in the isotopic and geochemical data at each well. I obtained geographic information for field-located wells from the OWRD database, and geographic information for faults and geological formations from Madin and Geitgey's (2007) compilation of geological quadrangle and study area maps in a unified geodatabase.

Statistical Methods: Principal Component Analysis

I used Principal Component Analysis (PCA) in order to effectively reduce the thirteen chemical parameters, four isotopic parameters, and multiple physical parameters for each well into a smaller number of principal components (PCs) that each explained a certain amount of variability within the data. I used the correlation matrix approach in R which scaled each parameter by its own variance to account for variables with different units (i.e. d2H measured in permil versus the unitless cation ratio) or ranges (bromide with values near 0.1 mg/L with bicarbonate with values closer to 200 mg/L). After evaluating the PCs produced by the PCA to explain relationships between the variable loadings, I could then use the PCs to map the effects of entire processes that create variability within the data instead of mapping distributions of individual parameters. PCA creates three primary outputs: the amount of variation in the data that each PC explains, the strength of each variable's effect on each PC (i.e. calcium's effect on PC1), and the strength of each individual's effect on each PC (i.e. UMAT0003074's effect on PC1).

Code in R was used to run and graphically visualize the PCA (Hayden 2018, Kassambara 2019). The results were then exported into ArcGIS Pro for geographic visualization. The results and discussion are included in the Results: Principle Component Analysis section of this document.

Statistical Analysis: Clustering Analysis of Limited Suite of Parameters

I was able to run clustering analysis for parameters that were recorded for the entire set of 31 wells, as 30 individuals are advised as the minimum for running this type of analysis in ArcGIS Pro. For each parameter I first ran Spatial Autocorrelation (Global Moran's I) in order to make sure that any clustering would have a statistically significant chance of not being due to random chance. If the p-value for that test was less than 0.05 the clustering pattern in the data had less than a 5% chance of being due to random chance, and I then ran the Spatial Correlation Clustering tool in order to highlight geographic clusters of similar values. I ran that second test several times in order to evaluate the optimal number of groups to minimize both outliers and single-well groups.

Results

Field-Measured Parameters: Temperature, pH, and Specific Conductance

A complete table of results for these parameters is presented in table A1 of Appendix A. Sampled pH values at the 31 values resulted in an average pH of 7.93, a median pH of 8.02, a minimum of 6.95, and a maximum of 8.9. The average specific conductance (SC) value was 293 microsiemens (ms), the median was 240 ms, the minimum was 114 ms, and the maximum was 774 ms. The average temperature value was 18.5º Celsius, the median was 19.3º C, the minimum was 12.2 º C, and the maximum was 23.5 º C. Figure C6 in Appendix C shows the observed ranges of groundwater sample pH values.

Well 54277 in the higher-elevation southeast corner of the study area had the highest pH value of the wells that were sampled, and wells 6217 and 56287 in the lowlands west of Milton-Freewater had the lowest values.

Wells 56219, 5028, and 56287 have elevated values of SC compared to the other sampled wells, which indicates elevated levels of dissolved solids in those wells. Wells 54277, 6217, and 6283 have the lowest values of SC. Figure C7 in Appendix C shows the observed ranges of groundwater sample SC values.

Geochemistry

Complete geochemical analysis for the 18 wells is provided in Appendix A. A summary table of statistics for chemical constituents is provided below in table 2. Percent analytical error for each constituent was calculated from the split sample taken at well 56382. Equipment blanks created by diverting laboratory water through the sampling equipment return ion values below detection limits in all cases.

Constituent	Minimum	Maximum	Mean	Median	Standard Deviation	Percent error
Calcium	8.98	83.4	23.84	19.9	18.27	0.01
Magnesium	1.2	27.9	8.37	7.38	6.17	0.01
Potassium	1.92	7.8	4.18	4.12	1.33	0.02
Sodium	8.39	27.8	18.75	19.8	5.32	0.01
Alkalinity	55.7	230	112.86	111	39.9	0
Bromide	0.013	0.094	0.04	0.043	0.02	0
Chloride	1.07	37.7	6.64	4.79	9.48	0
Fluoride	0.17	0.48	0.36	0.42	0.11	0
Silica	45.5	69.9	62.96	64.9	7.36	0.02
Sulfate	0.15	28.9	6	4.84	7.1	0
Iron	11.9	53.6	31.11	30.2	12.14	-0.02
Manganese	0.25	33.1	9.43	9.66	9.08	0.01
Total Dissolved Solids	106	507	201.46	188	96.1	-0.02

Table 2: Summary statistics for dissolved chemical constituents in mg/L.

Selected major ions can be visualized in a Stiff diagram, included as Figure C8 in Appendix C. The USGS smwrGraphs package in R was used to create the Stiff plots (Lorenz and Diekoff 2017). Two shapes of Stiff plots stand out on this diagram: a type of plot where sodium and calcium concentrations in meq/L are higher than magnesium concentrations (wells 4167, 4173, 4179, 50069, 50478, 50939, 54277, 55526, 56382, and 57235), and a second groups of plots where magnesium concentrations are greater than sodium concentrations and calcium conentrations are greater than magnesium concentrations (3074, 3909, 3962, 4010, 5193, 56287, and 57946). Bicarbonate dominates the anion composition at all wells.

Stable Isotopes

Thirty-one wells in this study have analytical results for the stable isotopes of oxygen and hydrogen. A full table of stable isotope results is presented in table A5 of Appendix A. The average d18O value was -14.24, the median value was -14.3, the minimum value was -15.54, and the maximum value was 12.93. The average d2H value was -110, the median value was -109.5,

the minimum value was -122, and the maximum value was -102. Figure 7 below shows the relationship between d18 and d2H at each well coded by the aquifer formations to which it is open.

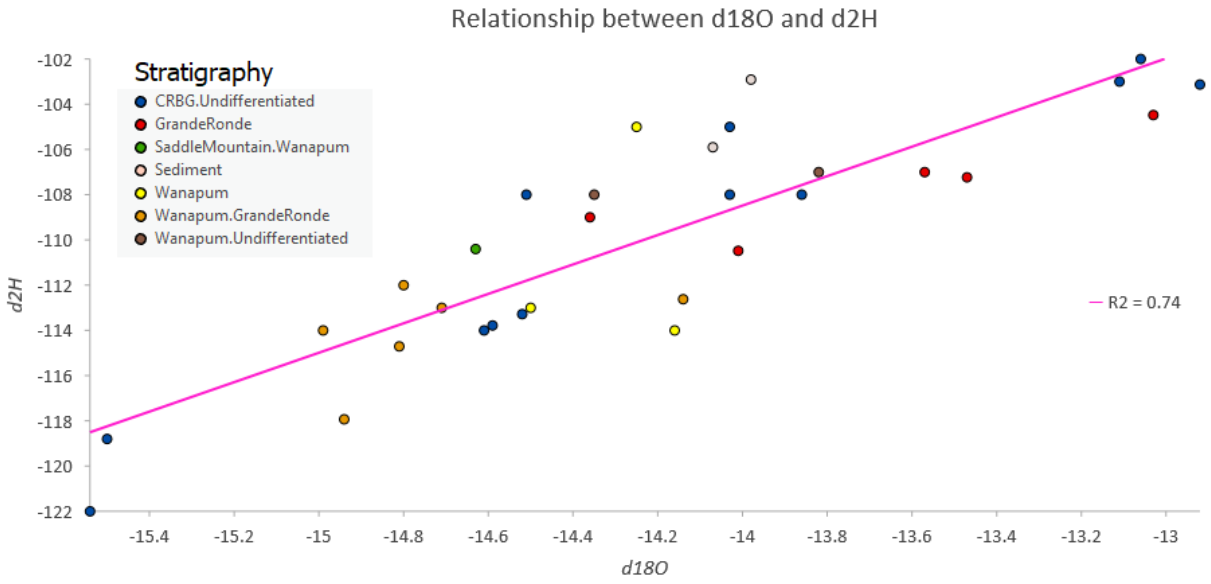

Figure 7: Relationship between d18O and d2H, with stratigraphy.

The wells open to both the Grande Ronde and the Wanapum formations had more negative d18O values (-14.7 to -15) than wells open to only the Wanapum formation (-14.5 to -14.15). However, the wells open to both the Grande Ronde formation and the Wanapum formation also had more negative stable isotope values than the wells open to only the Grande Ronde, or ranges of values that overlapped. The two sedimentary wells tested as part of this study, wells 6217 and 56219, had d18O values of -13.98 and -14.07 respectively. The Grande Ronde well with the most positive stable isotope valley was 3092 in Weston west of the Thorn Hollow fault, followed by wells 3909 and 50069 further down into the valley in Milton-Freewater. 3103, another well open to only the Grande Ronde formation near Weston, is located on the eastern side of the Thorn Hollow fault from the other Weston wells. The Grande Ronde well with the most negative

d18O value is 55526, located south of the Barrett-County Road fault west of Milton-Freewater. Its d18O and d2H values overlap with wells marked as only open to the Wanapum formation.

Radioactive Isotopes

Carbon-14 values in the study results ranged between 109 pmC and 15 pmC, with a mean of 43 pmC and a median of 38 pmC. This translates to a mean uncalibrated calculated groundwater age of 8,462 years, a median of 7,730 years, a maximum of 15,290 years, and a minimum of -620 years (interpreted as modern). Of the eighteen samples for tritium (excluding the one duplicate), seven samples came back below the detection limits, five were below the 4TU guideline that suggest pre-bomb recharge and/or significant dilution with older water, and seven samples had values larger than 4TU which suggested modern recharge with some possible dilution. Modern recharge is defined as post-1950

A table with the complete radioactive isotope results for each well is presented in table A4 of Appendix A.

Principal Component Analysis

This section contains results and interpretation for Principle Component Analysis of the chemical and physical information for the eighteen wells with the complete suite of chemical analyses. The parameters were divided into two subgroups as per Taylor and Gazis 2014 to maintain fewer variables than individuals in the PCA. The first group contain ion concentration results for wells, and the second included d18O, d2H, temperature, pH, specific conductivity, the depth to the end of the well, and the cation ratio.

For the parameter subgroup including ion concentrations, the first two out of the 11 principle components explained about 80% of the variation in my data. The first one, PCI, explained 55% of the variation in the data set and is shown on the X axis of the graph below. It is strongly influenced by concentrations of calcium, magnesium, chloride, alkalinity, sulfate, bromide, and sodium, which all have eigenvalues on the X axis greater than |1|. Comparing the scree plot to the loading plot, wells 56287, 3074, 4179, and 4167 are the primary individual drivers of PC1. PC2 explains another 25% of the variance in my data, and is shown on the Y axis. Fluoride, silicon, and manganese are the primary variable drivers of variation between the individuals in PC2. Variable coordinates of ion parameters in PC1 and PC2 are provided in figure C19 in Appendix C.

Next, I present the PCA results for the non-ion parameters. This PCA grouping contains different types of chemical and physical properties of water. These include pH, temperature, and specific conductivity which were measured in the field, the analyzed values of hydrogen and oxygen isotopes as well as tritium, the elevation of the bottom of the well, and the cation ratio. The cation ratio is a standard calculated parameter for groundwater chemistry which is equal to ([Na] + [K]) / ([Ca] + [Mg]). As water spends more time in contact with the rock, the exchange of monovalent for divalent ions with the rock leads to a larger cation ratio value. PCA biplots from this analysis are presented as figures C22a and C22b in appendix C. The first biplot graphs PC1 (~40% of variation) on the X axis against PC2 (22% of variation) on the Y axis, and the second biplot graphs PC1 on the X axis versus PC3 (~18% of variation) on the Y axis.

The PC1 grouping explains variance among the samples by inversely correlating tritium, deuterium (d2H) and oxygen-18 (d18O) with pH and the cation ratio. More positive PC1 values

show that the individual has high d18O and d2H values, and low cation ratio and pH values. All d18O and d2H values are negative; values that are closer to 0 (larger, for the purposes of this plot) are more enriched in the heavier isotope. PC2 is predominantly driven by an inverse correlation between well bottom elevation and temperature. PC3 inversely correlates tritium, specific conductance, and well bottom elevation with temperature, d2H, and d18O. Variable coordinates for non-ion PCA PC1, PC2, and PC3 are provided as figure C23 in Appendix C.

OWRD_ID	ions PC1	ions PC2	non-ions PC1	non-ions PC2	non-ions PC3
UMAT0056287	-6.79	-3.23	3.78	-1.15	-2.68
UMAT0003929	-0.05	-2.09	1.80	-0.34	-0.03
UMAT0003909	1.96	-1.96	0.50	0.66	0.16
UMAT0050478	2.38	-1.17	1.21	0.04	-0.71
UMAT0057946	1.87	-1.16	2.68	2.21	0.69
UMAT0003962	1.00	-1.15	-0.07	0.16	0.83
UMAT0003074	-2.60	-1.07	0.32	1.25	-1.54
UMAT0054277	3.43	-0.88	-3.11	3.66	-1.09
UMAT0005193	0.87	0.21	1.46	0.48	1.68
UMAT0055526	1.16	0.52	-0.99	-0.62	1.02
UMAT0004010	1.24	0.57	0.54	-0.30	0.84
UMAT0050069	0.80	0.74	-0.18	0.27	1.44
UMAT0004173	0.04	1.12	-1.17	-0.28	-0.03
UMAT0057235	0.21	1.24	0.15	-1.23	1.41
UMAT0056382	0.33	1.44	-1.86	-1.16	0.44
UMAT0050939	0.45	1.82	-1.76	-1.27	-0.06
UMAT0004179	-3.65	2.18	-0.75	-1.12	-0.47
UMAT0004167	-2.65	2.85	-2.52	-1.26	-1.90

Table 3: Principle component individual coordinates for wells for first two ion principle components which contributed to over 80% of variance in the ion PCA, and for the three non-ion principal components which contributed to over 80% of the variance in non-ion PCA. Interpretation of these coordinate is presented in the table on the following page.

more negative:	more influenced by greater conc of all ions (more concentrated)	more influenced by Ca/MG (less evolved)	more influenced by high ph/high cation ration (more evolved)	lower elevation, higher temperature	higher SC, tritium	
more positive:	lower concentration of all ions (less concentrated)	More influenced by NA/FI/SIO2 (more evolved)	more influnced by higher tritium and stable isotopes (younger)	higher elevation, lower temperature	higher temperature, stable isotopes	
OWRD_ID	ions PC1 (55.7%)	ions PC2 (24.9%)	non-ionsPC1 (40.1%)	non-ions PC2 (22.0%)	non-ions PC3 (18.4%)	PC interpretations agree?
UMAT0056287	**more concentrated**	**less evolved**	**younger**	**lower elev, higher temp.**	**higher SC, tritium**	yes, but low elevation and higher temperature don't match hypotheses
UMAT0003929	weakly influenced by PC1	**less evolved**	**younger**	weakly influenced by PC2	weakly influenced by PC3	Yes
UMAT0003909	**less concentrated**	**less evolved**	weakly influenced by PC1	weakly influenced by PC2	weakly influenced by PC3	Yes
UMAT0050478	**less concentrated**	**less evolved**	**younger**	weakly influenced by PC2	weakly influenced by PC3	Yes
UMAT0057946	**less concentrated**	**less evolved**	**younger**	**higher elev, lower temp**	weakly influenced by PC3	Yes
UMAT0003962	weakly influenced by PC1	**less evolved**	weakly influenced by PC1	weakly influenced by PC2	weakly influenced by PC3	Only influenced by ion PC2
UMAT0003074	**more concentrated**	**less evolved**	weakly influenced by PC1	**higher elev, lower temp**	**higher SC, tritium**	Yes
UMAT0054277	**less concentrated**	weakly influenced by PC2	**more evolved**	**higher elev, lower temp**	**higher SC, tritium**	high elevation/lower temperature/higher SC/Higher tritum is unusual for a sample with a high non-ion PC1 value
UMAT0005193	weakly influenced by PC1	weakly influenced by PC2	**younger**	weakly influenced by PC2	**higher temp., stable isotopes**	Yes, but unusual higher temperature for a "younger" sample
UMAT0055526	**less concentrated**	weakly influenced by PC2	**more evolved**	weakly influenced by PC2	**higher temp., stable isotopes**	Yes, but higher stable isotopes for a "more evolved" sample
UMAT0004010	**less concentrated**	weakly influenced by PC2	weakly influenced by PC1	weakly influenced by PC2	weakly influenced by PC3	Only influenced by ions PC1
UMAT0050069	weakly influenced by PC1	weakly influenced by PC2	weakly influenced by PC1	weakly influenced by PC2	**higher temp., stable isotopes**	Only influenced by non-ions PC3
UMAT0004173	weakly influenced by PC1	**more evolved**	**more evolved**	weakly influenced by PC2	weakly influenced by PC3	Yes
UMAT0057235	weakly influenced by PC1	**more evolved**	weakly influenced by PC1	**lower elev, higher temp.**	**higher temp., stable isotopes**	Yes, but higher stable isotopes for a "more evolved" sample
UMAT0056382	weakly influenced by PC1	**more evolved**	**more evolved**	**lower elev, higher temp.**	weakly influenced by PC3	Yes
UMAT0050939	weakly influenced by PC1	**more evolved**	**more evolved**	**lower elev, higher temp.**	weakly influenced by PC3	Yes
UMAT0004179	**more concentrated**	**more evolved**	weakly influenced by PC1	**lower elev, higher temp.**	weakly influenced by PC3	Yes
UMAT0004167	**more concentrated**	**more evolved**	**more evolved**	**lower elev, higher temp.**	**higher SC, tritium**	Yes, but higher tritum for a "more evolved" sample

Table 4: comparison of PCA group interpretations

Spatial Analysis of PCA

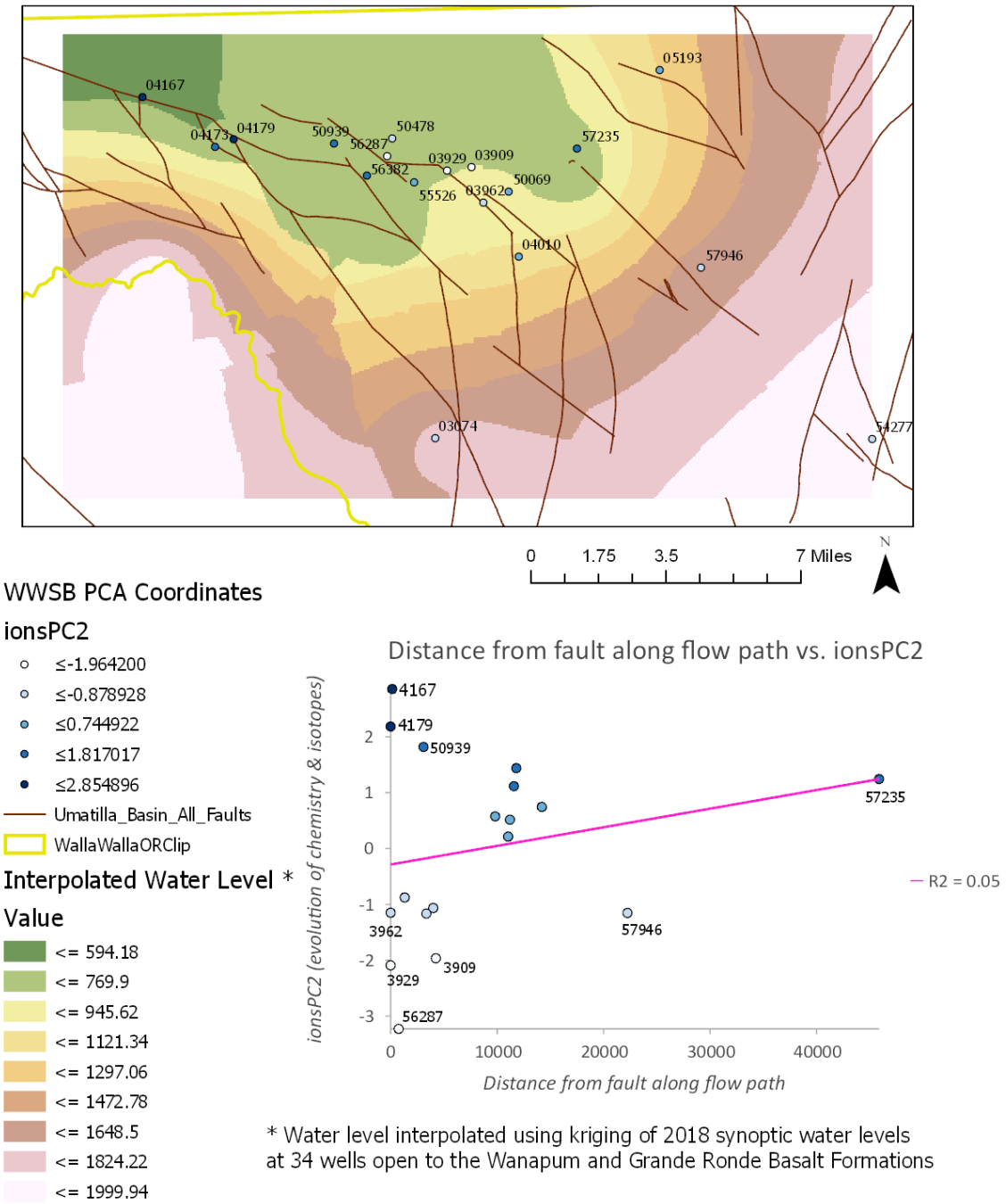

Figure 8a (top): Map of ion PC2 individual values at wells compared to interpolated potentiometric surface and faults. Figure 8b (bottom right): Graph of distance from fault along flow path versus ion PC2 score.

Clustering Analysis of Limited Suite of Parameters

I ran Spatial Autocorrelation (Global Moran's I) in ArcGIS on the distribution of d2H in order to determine whether the data were clustered. This statistical test returned a Moran's Index of 0.087, and z-score of 2.01, and a p-value of 0.044. This indicates that the spatial distribution of d2H values is clustered, and that there is less than a 5% chance of the clustering being the result of random chance. As the data was found to be clustered, I subsequently ran the Spatially Constrained Multivariate Clustering tool on the d2H data to evaluate the geographical distribution of clusters. See figures C26a and C26b in Appendix C for the map and boxplots of these clustered groups.

The distribution of d18O values had a Moran's Index of 0.258, and z-score of 4.07, and a p-value of 0.00005. As this value was also clustered, I ran the Spatially Constrained Multivariate Clustering tool using both d2H and d18O. The mapped output and graph are provided as figures C27a and C27b in Appendix C.

Comparison of Interference Tests and Chemical Data

OWRD performed well pumping interference tests in select areas of the WWSB during the early spring seasons of 2018 and 2019. During these tests, one well was turned on while water levels in nearby wells were monitored for changes in response to that pumping. Twenty-nine wells were tested over the two years, of which twelve were also sampled for geochemistry and ions in the summer of 2018 for this project. These twelve wells were divided into seven groups based on communication type (a well did or did not respond to pumping at another), and chemical and physical properties were compared between the groups. These wells, groups, and communication relationships are mapped in Figure 9 on the following page.

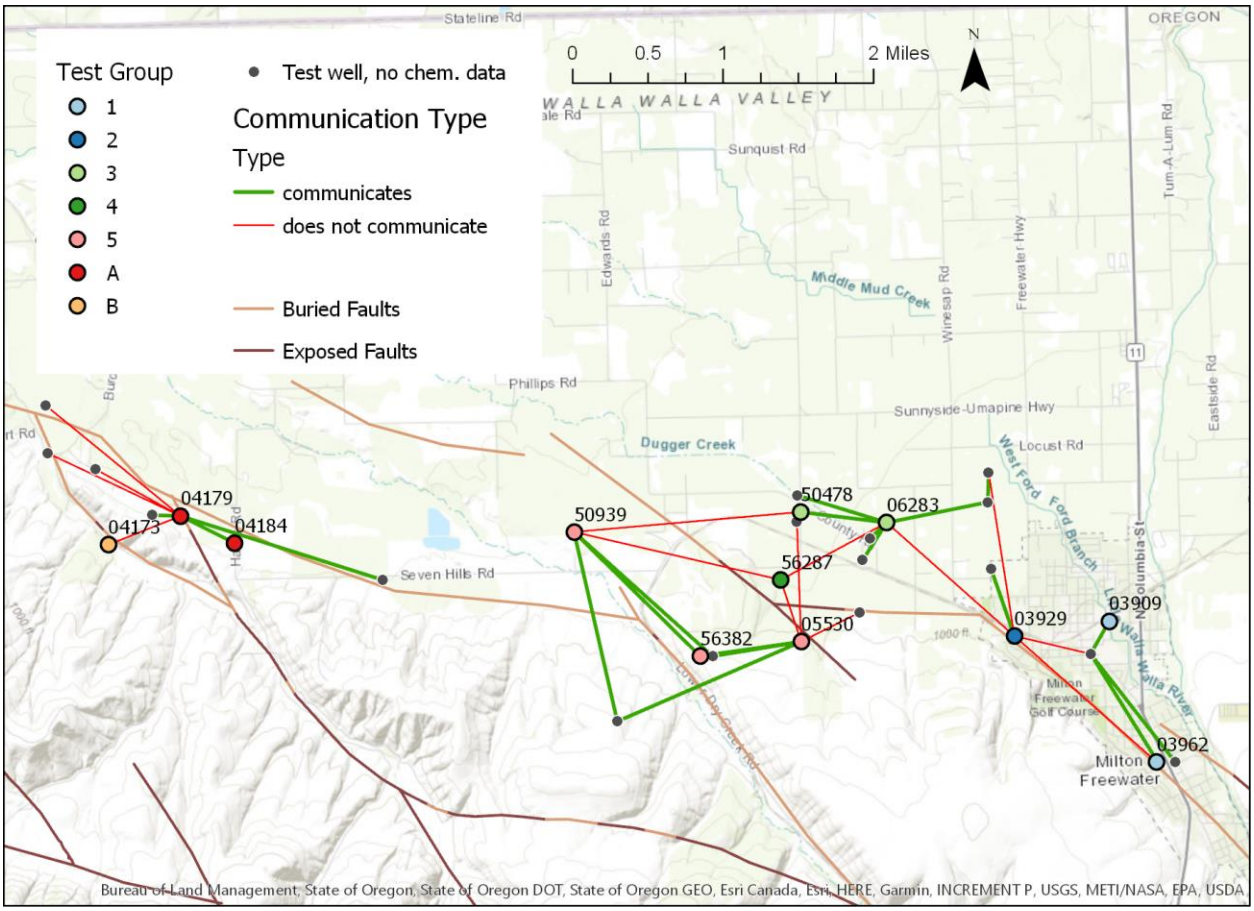

Figure 9: Map of pumping interference test results

Groups A and B could be differentiated by pH, specific conductivity (SC), temperature, and well bottom elevation. Groups 1 and 2 differ in d2H, SC, and well bottom elevation. Groups 2 and 3 differ in d2H, SC, and temperature. Groups 3 and 4 differ in d2H, pH, SC, temperature, and well bottom elevation. Groups 4 and 5 differ in d2H, pH, SC, temperature and well elevation. Overall, specific conductivity was the only parameter that effectively distinguished between all five possible pairings of groups based in interference test relationships. Figures C30a through C30e in Appendix C show boxplots of each parameter for the test groups.

ANOVA f-tests were run on this data set in order to assess variation of each parameter within and between the groups. The indicated that variation between groups was not more significant

than variation within groups for pH (f-statistic of 0.3265) and temperature (f-statistics of 0.1095). However, variation between groups of wells that did not communicate was more significant than variation within groups of communicating wells for specific conductivity (f-statistics of 2.192e-6), d2H (f-statistic of 0.001423) and d18O (f-statistics of 0.02668).

Discussion

Field-Measured Parameters: Temperature, pH, and Specific Conductivity

It has been speculated that faults which act as barrier would dam up-gradient flow, forcing groundwater to rise along the fault until it either reaches the surface or flows around the barrier, and that this phenomenon could be traced by measuring the deviation of groundwater temperature from the expected gradient based on depth (Newcomb 1965). Newcomb proposes that the groundwater gradient could be defined as 1.8 degrees Fahrenheit for each hundred feet of depth beyond the first 100 feet below the surface and that the water temperature between 0 and 100 feet would be 53.5 degrees Fahrenheit, which is the average yearly temperature in the WWSB. Newcomb considered differences greater than two degrees Fahrenheit from the expected value to be significant. I calculated the expected temperature based on the gradient equation and well depth for each well, and then compared that value to the temperature that was measured in the field during sample collection. The mapped values are shown in figure 10 on the following page.

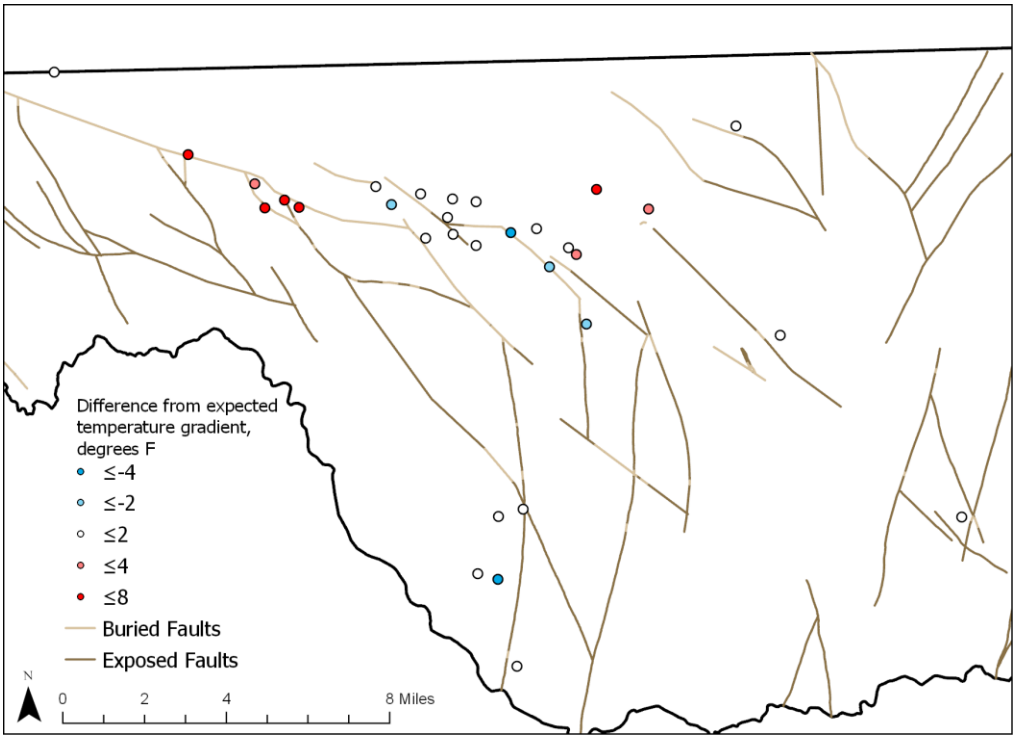

Figure 10: Difference between measured water temperature and expected geothermal gradient

This analysis shown insignificant variation of deviance from the expected temperature gradient at the sampled locations, with the exception of a cluster of wells in the western part of the study area. These five wells are in close vicinity to the mapped buried Wallula fault zone and show an elevated observed temperature compared to the expected temperature based on the geothermal gradient. However, elevated temperatures relative to the expected gradient also were evident in wells 5227, 57235, and 3962 in the eastern part of the basin, which are not near a fault likely to act as a groundwater barrier. It is possible that processes other than faulting effect the well temperatures relative to the geothermal gradient, such as a greater head at increasing depths that leads to deeper, warmer water rising into the well. Significant negative temperature anomalies are also noticeable at three wells near Milton-Freewater, one well in Weston, and one well in the lowland area west of Milton-Freewater. This indicates cooler water than expected entering the well, either from shallower water bearing units or from a fault creating a vertical permeability

anomaly allowing colder water to flow deeper into the aquifer before it equilibrates to a higher temperature.

pH was directly correlated with the cation ratio (r = 0.45) and inversely correlated with percent modern carbon-14 (r = 0.36).

Geochemistry

The cation ratio is a standard calculated parameter for groundwater chemistry which is equal to ([Na] + [K]) / ([Ca] + [Mg]). As water spends more time in contact with the rock, the exchange of monovalent for divalent ions with the rock leads to a larger cation ratio value. A map of cation ratio values for the sampled wells is presented in figure C9 in Appendix C.

In an uninterrupted groundwater flow system, this ratio would be expected to increase along the flow path. Two uninterrupted models of groundwater flow have been hypothesized for the CRBG. The first describe a scenario where water flows through strongly anisotropic interflow zones with lateral hydraulic conductivity from upland areas where the layer is exposed at the surface. In this region the upland areas have significantly more precipitation than the lowland areas and are the primary sources of recharge (OSU PRISM, 2014). In that first model, the cation ratio would be hypothesized to increase with decreasing surface elevation of the well as less chemically evolved water is recharged in the higher elevation and flows through the interflow zones to wells at lower elevations further from the recharge zone.

Conversely if the aquifers were recharged by water that infiltrated vertically, the cation ratio would be expected to increase with increasing well depth, as the flow path length would increase with increasing depth instead of with increasing distance from the recharge zone. Figures C10

through C12 in appendix C illustrate the relationships between the cation ratio, well bottom elevation, well depth, and land surface elevation.

Land surface elevation at the well and cation ratio are weakly correlated. The regression line for the data points actually shows the opposite relationship than expected: increasing cation ratio with elevation. This is influenced by a high-elevation outlier with a high cation ratio. The other high elevation wells have lower cation ratios than most of the lower elevation wells, although several low elevation wells also have very low cation ratios.

There is no correlation between cation ratio and well depth, and the regression line has a slope of 0. This shows that there are varieties of cation ratios at well depth, and vertical groundwater movement in the vicinity of the well is likely not a factor in groundwater residence time.

While well depth represents the distance that a well was drilled to reach water, well bottom elevation represents the well's absolute depth in the geologic system independent of the position of the land surface. Well bottom elevation and cation ratio are also very poorly correlated, indicating that flow paths at the scale of the entire aquifer are not the sole influence on the chemical evolution of groundwater.

Cation ratios for the sampled wells reveal little to no correlation with well depth, well surface elevation, or well bottom elevation. This contradicts both the hypothesis of unimpeded flow laterally from recharge zones at higher elevation and the hypothesis of unimpeded flow vertically from local recharge. Therefore, it is likely that more local conditions such as fault compartmentalization, recharge along faults, or well construction are influencing flow paths on a local scale as represented by the groundwater sample's chemical evolution.

Stable Isotopes

Graphs showing the relationships between d18O, land surface elevation, well bottom elevation, and well depth are presented as figures C13 through C15 in appendix C. In general, for the basalt wells, d18O value increase with the increasing elevation of the land surface at the well. The exceptions to this relationship are the higher-elevation wells 3074, 2707, 3103, and 54277, as well as the sedimentary wells 6217 and 56219. Well 54277, located in the southeastern side of the study area has the most negative d18O value of the higher-elevation wells. This may be related to the fact that this well is located in a documented fault zone, where geochemistry of well cuttings shows that the well document a layer of the Wanapum Basalt that has become sandwiched between two layers of Grande Ronde Basalt. This well also has the highest cation ratio of any of the wells sampled in this study, which indicates longer groundwater residences times at that well.

The positive trend of the regression line is the opposite of what would be expected if elevation fractionation was assumed, in which case the heaviest (least negative) of the values would be at the lower elevations and the precipitation stable isotope values would become more negative with increasing elevation as water molecule with heavier isotopes were preferentially precipitated. However, this positive regression would support the hypothesis of progressively younger packets of water closer to a higher-elevation recharge zone, which then age with increasing distance from the recharge zone. Holocene precipitation occurred in a gradually warmer, wetter climate than Pleistocene precipitation, causing a trend of increasing stable isotope values with decreasing age (Larson et al 2000). In their study of aquifers in the Grande Ronde and Wanapum Basalt formations Pullman, WA, Larson et al found that some water samples from the Grande Ronde had significantly more depleted d18O values between -16.5 and

-17.5, which are more negative than any values found in samples from this study. This could indicate that the wells in my study area either were recharge slightly more recently, or that there has been mixing in the aquifer of older water with significantly more recent recharge.

Regression shows no relationship between d18O and well depth.

I compared the stable isotope results for the groundwater samples with stable isotope values for precipitation for the Blue Mountains in the Upper Umatilla Basin compiled in McCarthy 1989, as well as the local meteoric water line of d2H = 6.9d18O -18.5 proposed by Larson et al. 2000 (Figure C16 in appendix C). McCarthy's measured stable isotope values for snow fell almost exactly along the global meteoric water line (GMWL), while the precipitation values plotted below the GMWL. Larson et al.'s local meteoric water line is depleted in d2H compared to the GMWL. The groundwater samples had d18O values very similar to the d18O values of the 1987 snow, although their d2H values were up to 10 permil more negative than the snow samples with equal values of d18O. The groundwater samples had both d18O and d2H values more negative than all but one precipitation sample.

Certain intriguing comparisons suggest themselves within the sampled wells. Well 56287 (west of Milton-Freewater) and 3929(near downtown Milton-Freewater) show similar d2H values of 105, despite having significantly different well construction. While both wells are drilled through Post-CRB sediments into unclassified Columbia River Basalts, well 56287 is unsealed while 3929 is sealed to a depth of 220 feet. Well 3929's well log mentions that it is completed in "basalt fault gouge". Well 56287 is completed in the first basalt flow top that the drillers reached. Because of well 56287's construction and stratigraphy, it is very likely that this well contains significant amounts of modern recharge. This juxtaposition suggests that Well 3929 might get an

increased amount of modern recharge similar to well 56287 that enters it through the fault's damage zone.

Mapped values of deuterium excess at the sampled wells are presented as figure C17 in Appendix C. Deuterium excess is a metric for evaluating temperature at the time of precipitation that compares d2H value with the idealized value compared to d18O as described by the global meteoric water line, where d2H = 10 + 8d18O (Pfahl and Sodemann 2014). Calculated deuterium excess for each well is presented in table A5 of Appendix A. Larger values of deuterium excess indicate a colder environment when the water that later fell onto the landscape was evaporated from its source, resulting the preferential evaporation of lighter isotopes including ^{2}H, ^{1}H, and ^{16}O in the water molecules, and the exclusion of ^{18}O. Modern winter precipitation in the Pacific Northwest has deuterium excess values between 3 and 12 permil, while modern summer precipitation in the Pacific Northwest has deuterium excess values between 0 and 3 permil (Pfahl and Sodemann 2014). Deuterium excess values in the groundwater sampled as part of this study range between -0.72 and 9 permil, a mean value of 3.9 permil, and a median value of 3.3 permil.

Larger values of deuterium excess (between 5 and 9 permil) are present in wells in Milton-Freewater, the lower elevation irrigation wells directly west of the town, the lower elevation sedimentary well in the northwestern corner of the study area, and the higher elevation basalt well in the southeastern side of the WWSB. Low to moderate values of deuterium excess, between 1and 3 permil, are present in the lower elevation wells east of Milton-Freewater, medium-elevation wells further west of Milton-Freewater, and in one isolated higher-elevation well south of Weston. The lowest values of deuterium excess, between 0 and 1 permil, are

present at four higher-elevation wells near Weston in the southern part of the study area and in well 3092 in Milton Freewater.

Radioactive Isotopes

A comparison of 14C values in pmC with tritium values indicates that even water samples with the oldest average ages contain traces of modern recharge. Tritium concentrations have larger values and a larger range of values as measured percent modern carbon increases. This is illustrated in figure 11 below.

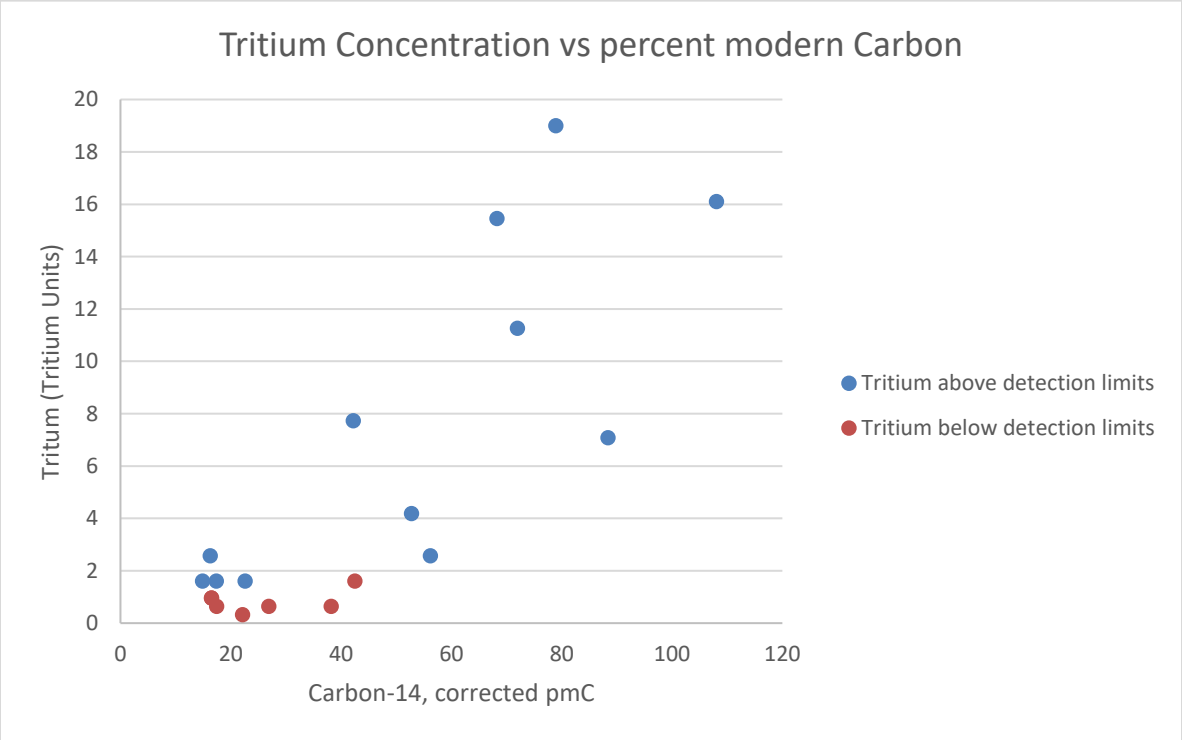

Figure 11: Tritium concentration versus percent modern carbon.

Calculating age using tritium has the weakness that the tritium concentration of the recharge water must be assumed, based on a hypothesis of whether the water is likely pre-bomb-tests. Often a pre-bomb tritium concentration of 4TU is assumed (Kazemi 2006). For the purposes of this thesis, I have not undertaken estimation of tritium age or estimation of mixing along

different groundwater recharge paths. Instead, I have used tritium values as an indicator of modern recharge.

A linear regression of ^{14}C values with d2H values reveals a correlation value of 0.67 and a trend of enrichment in ^{2}H with increasing percent modern carbon, shown in figure 12 below.

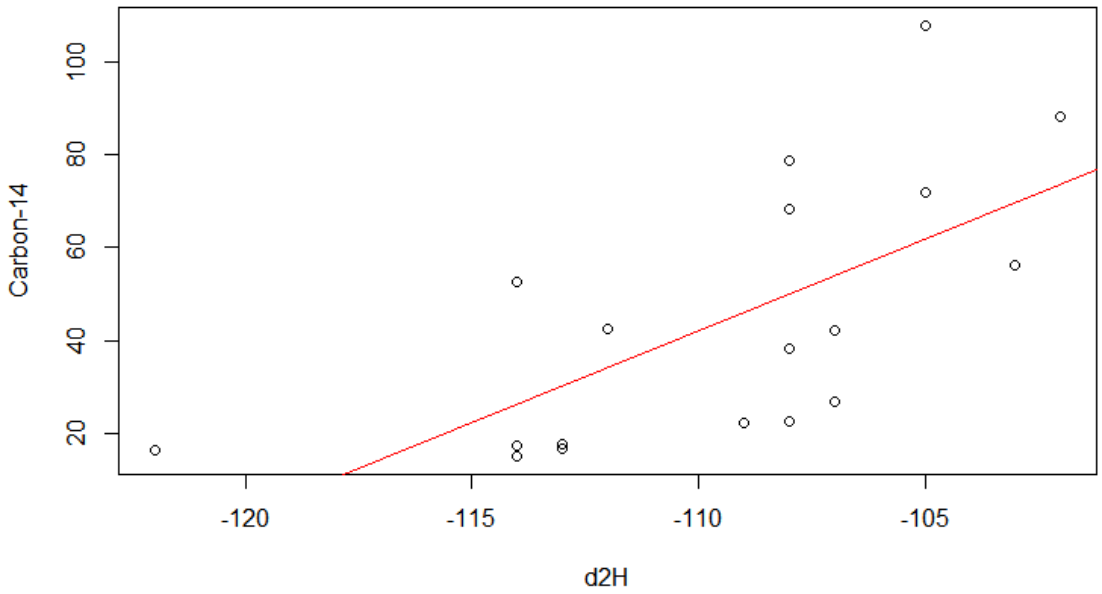

Figure 12: Graph of d2H versus ^{14}C

Principal Component Analyses

Based on the coordinate information for the variables, the variation explained by Ion PC1 is due to increased levels of calcium, magnesium, potassium, sodium, alkalinity, bromide, chloride, and sulfate at four wells. These similar loadings for most variables in the model suggest a system with increased concentrations of ions in certain individual wells compared to other individuals. In an undisturbed basalt setting though time, calcium and magnesium tend to decrease as sodium and potassium increase. The fact that these four parameters vary together in PCI indicates that a process other than ion replacement is driving ion concentration. The variation in PC2 is

predominantly explained by fluoride, dissolved silica, and manganese. Elevated concentrations of these three variables in comparison to the other variables indicates that the groundwater has spent more time in the basalt. In PC2, calcium and magnesium are inversely related to sodium,

Ion PC1 is heavily driven by four wells on the western side of the basin, both in the lowlands and near Weston (Figure C20 in Appendix C). These wells have higher concentrations of all ions than the other wells.

The spatial distribution of Ion PC2 values shows interesting results along the hypothesized flow path between the recharge zone and the valley (Figure C21 in Appendix C). More negative values indicate samples which were less influenced by the ion replacement and dissolution processes of groundwater traveling through the basalt. Negative values are present both at the higher elevations and at lower-elevation wells near Milton-Freewater which are downgradient of certain faults. This could indicate that those PC2 negative downgradient wells are cut off from the longer flow paths of groundwater by faults that act as barriers to groundwater flow. Wells with more positive PC2 values indicate samples that were more influenced by the along-flow-path ion reactions. These results confirm multiple recharge mechanisms into the aquifer, both from the higher-elevation areas that receive much of the regional precipitation and from recharge at lower elevations from vertical infiltration and fault conduits.

Figure C24 in Appendix C shows a map of Non-Ion PC1 coordinates for individual wells. Yellow/orange points on the figure above have more positive Non-Ion PC1 loadings. They have higher d18O, d2H, and tritium values, and lower cation ratio and pH values. The lower cation ratio and pH values indicate that the sample is less chemically evolved based on the expected ion exchange reactions in the basalt. The inverse relationship between tritium and the cation ratio

was expected, because tritium has a short half-life and indicates modern recharge. PC1 indicated that samples with low cation ratio values were more likely to be enriched in the heavier isotopes of hydrogen and oxygen.

Figure C25 in Appendix C shows a map of Non-Ion PC2 coordinates for individual wells. Points with positive PC2 loadings have variance that can be partially explained by higher well bottom elevations and lower temperatures. This PC is consistent with observations of increasing temperature with depth in the Columbia River basalt group due to geothermal activity (Newcomb 1965). The model is strongly driven by the three highest-elevation wells: 54277, 3074, and 57946.

A comparison of interpretations of PCs from both Ion and Non-Ion PCAs for each well was presented in table 3 on page 38. The two PCs interpreted to indicate aspects of groundwater residence time, Ion PC2 and Non-Ion PC1, do not contradict each other at any of the wells although some wells are more strongly influence by Ion PC2 than Non-Ion PC1 or vice versa. Two wells are weakly influenced by four of the five PC models analyzed including Ion PC2 and Non-Ion pC2, indicating that PCs should be supplemented by other information when classifying wells. Non-Ion PC1 scores (interpreted to indicate total concentration of ions) do not appear to be correlated to Ion PC2 or Non-Ion PC1 scores. Three out of four of the wells with the significantly negative scores for Ion PC1 (indicating greater total ion concentration) also had significantly negative scores for Non-Ion PC2 (indicating lower well bottom elevation and higher temperature). Five out of the six wells with significantly negative scores for Non-Ion PC2 had significantly positive values for Ion PC2 (indicating water that was more chemicaly evolved).

Spatial Analysis of Principal Component Analysis

I hypothesized that ion PC2 would increase with decreasing potentiometric surface elevation. An increased score in ionPC2 indicates an elevation sodium concentrations and pH and a decrease in calcium and magnesium caused by a progressive ion exchange reaction between the groundwater and the basalt. Because water flows from higher potentiometric elevations to lower potentiometric elevations, I would expect water samples from lower potentiometric elevations to show chemical evidence of increased interaction with the basalt. If this process of down-gradient groundwater flow were the only process influencing the ion exchange reactions, the well symbols on the map below would become progressively darker as the interpolated well level surface elevation decreased and the wells were further from the up-gradient recharge zone.

However, upon examining a map of ion PC2 values this is not the case - there are anomalously low values of PC2 in the valley, where one would expect to see increased values if groundwater flowed uninterrupted from the up-gradient recharge zones. In this method I introduced the variable of distance from faults in order to test another hypothesis: that faults compartmentalized groundwater flow, promoting vertical permeability and modern recharge into the down-gradient aquifer. I also hypothesized that if a fault was a barrier, PC2 values up-gradient of the fault would be elevated as the fault trapped water behind it. This would result in more chemically evolved groundwater behind the fault, and less chemically evolved groundwater down-gradient of the fault.

The results of this study tentatively support the conceptual model of fault compartmentalization. In particular, water samples from wells in the valley down-gradient of the fault zones have evidence of less exposure to the basalt than wells further towards the recharge zones. 15 of the

18 wells sampled show a positive correlation between distance from a fault along a flow path and ion PC2 score, especially when graphed points are compared to their up-gradient and down-gradient neighbors (i.e. 57946 is up-gradient from 57235 and down-gradient from 54277).

Because of the width of the raster cells indicating faults and their flow direction in this model, four wells ended up have a distance from faults of 0. This does not seem unreasonable, because examination of exposed fault zones in the area indicated that many are up to a couple hundred meters wide. Additionally, while geological studies of the area indicate that the faults are close to vertical, their exact dip angles are unknown and this introduces a certain amount of uncertainty about their location at depth. Ion PC2 values of wells with dist_from_fault = 0 show an interesting dichotomy of either very high (4167, 4179) or very low (3929, 3962) values. I believe this indicates that wells 4167 and 4179 are up-gradient of faults that could possibly act as barriers, while 3929 and 3962 are slightly down-gradient or a fault that is acting as a recharge zone or are within the fault damage zone itself. These relationships are illustrated in Figure 8B on page 40.

Clustering Analysis of Limited Suite of Parameters

Two Spatially Constrained Multivariate Clustering (SCMC) analyses of d18O and d2H were performed in ArcGIS Pro as part of this study: the first with five groups in order to view broader patterns in the dataset and minimize groups containing only one well, and a second with twelve groups for comparison with the OWRD grouping scheme that grouped the sampled wells into twelve categories. Maps showing well values for the 5-cluster and 12-cluster analyses are shown as figure C27A and C28 in Appendix C. A map of the sampled wells with their OWRD classification groups is presented as figure C29 in Appendix C.

The 5-group analysis grouped the points into three main clusters; group 1 in the west with low-to-moderate d18O values and low d2H values, group 2 in the central and southern area with moderate d18O values and higher d2H values, and group 3 in the eastern and southern area higher values of both d18O and d2H. In the Weston area, there is an interesting juxtaposition of groups 1 and 3. Wells open to the Wanapum formation fall into group 1, while wells open to the Grande Ronde formation are in group 3. The sedimentary well in the northwesternmost corner of the study area has values similar to group 2, and the high-elevation well 54277 which is drilled into a fault zone has values similar to group 1. Group 4 contained only one well, the high-elevation well in the southeastern corner of the study area, and have stable isotope values similar to cluster 1. Group 5 contained one well, the sedimentary well 56219 in the northwestern corner of the study area, and has stable isotope values similar to cluster 2.

Comparison of the twelve-group Spatially Constrained Multivariate Clustering analysis with the OWRD classification groups based on water level reveal patterns of similarities as well as opportunities for the isotope information both to support grouping when well construction does not allow for water level measurement and to refine the elevation classifications (Table 5).

OWRD groups classified by water level elevation	Corresponding SCMC d2H-D18O group	Suggestions for change to OWRD water level elevation classification
525-575	6	Add OWRD unclassed well 4864 to this group based on d2H/d18O clustering.
575-675	9	
650-700	1	Although it shares similar isotopic properties with the other wells, well 4173 should be removed from this management group due to lack of communication with the other wells in the pumping interference test.
700-750	2, 10, 12	Well 56287 was grouped with the nearby sedimentary well 6217 in the d2H/d18O clustering analysis (group 10). Well 3929 was grouped with nearby wells 3909 and 3962 (group 12).
750-800	2	Combine OWRD group 750-800 with OWRD group 700-750 based on similarities of d2H/d18O clustering at well 55526
800-850	3, 12	d2H/d18O clustering split this OWRD group into two groups and suggest the addition of two unclassed wells. Group 3 includes wells 57672 and 50069 and suggests the addition of unclassed wells 4010 and 57235. Group 12 includes wells 3929, 3909, and 3962.
800-900	8	While the two wells in these two OWRD groups have similar isotopic composition, their differences in water levels and stratigraphy suggest that they remain in two different groups for management purposes.
1450-1500	8	
1550-1600	8	The proximity of the two wells in these OWRD water elevation groups, their similar isotopic properties, and their similar stratigraphy (both are open to the Grande Ronde formation) and water levels suggest grouping them together for management purposes.
1620-1640	8	
1680-1720	11	d2H/d18O clustering analysis and similar stratigraphy (both are open to both the Wanapum and Grande Ronde formations) suggests the addition of well 2707 to this group.
1950-2000	4	

Table 5: Comparison of manual well clustering based on water level elevation with SCMC analysis based on d2H and d18O values, stratigraphic information, and pumping test information.

Comparison of Interference Tests with Chemical and Isotopic Data

There is sufficient evidence for a difference in means between disconnected wells/groups of wells for the parameters of specific conductivity and stable isotopes, but not for pH or temperature. However, this analysis might contain error because of the small sample sizes and the fact that within these groupings there are differences in well construction.

Conclusion

Cation ratio values at measured wells are not consistent with the flow paths that would be hypothesized if this WWSB system behaved like unfaulted systems elsewhere in the CRBG (i.e. increasing cation ratio with depth and with distance from recharge zone). Comparison of a principal component with variation explained by the cation ratio and stable isotope values with measured distances of the wells from faults shows a trend of increasing groundwater evolution and decreasing stable isotope values with increased distance from the nearest fault along hypothesized flow paths.

Stable isotope values do not show a correlation with well depth, and show tentative negative correlations with well land surface elevation and well bottom elevation. Because springs or surface bodies of water were not tested as part of this study, it is not possible to confirm whether precipitation elevation, also known as the “rain-out” effect, has influenced groundwater stable isotope values. However, a much stronger correlation of d2H with carbon-14 age suggests that changing atmospheric and precipitation patterns during the transition from the last glacial maximum to modern climatic conditions may have contributed to variability in groundwater stable isotope values.

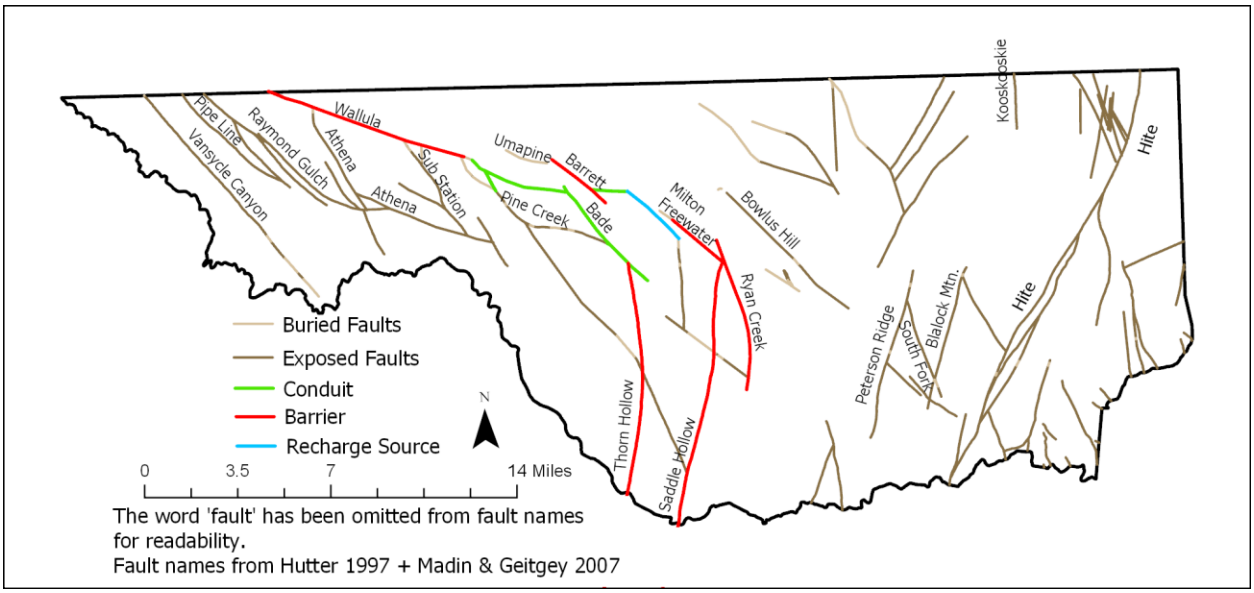

Figure 13: Mapped conclusions for fault properties.

The Wallula Fault is likely a barrier to groundwater flow based on its wide, highly deformed fault core (Hutter 1997), large amount of vertical offset (~250m) and strike-slip offset (~2km) (Kienle et al 1979), and the high temperature anomaly on south side of fault (this study).

The Barrett Fault is likely a barrier based on interference test results (OWRD 2018). Additionally, there is likely groundwater recharge along this fault based on chemistry differences on down-gradient side including lower cation ratios, heavier stable isotopes, and younger C-14 ages compared to up-gradient wells. In a spatially constrained multivariate clustering analysis, this fault separated groups 1 and 2 based on d2H and d18O values. The Barrett-County Road fault did not separate groups in the clustering analysis of d2H and d18O, and as of the publication of this paper does not have OWRD interference test data available for wells on either side of it. The Bade Fault is not a barrier based on interference test results (OWRD 2018). This fault is not testable with geochemical and isotope data in this study because of lack of sampled wells on either side of the fault. The Milton-Freewater Fault is likely a barrier based on

interference test results (OWRD 2018), in addition to Newcomb's 1965 observations and pumping test.

The Thorn Hollow Fault is likely a barrier because of strong hydrogen sulfide smell at upgradient wells, springs and seeps along the fault to the south of the study area. The Saddle Hollow fault is a barrier to groundwater flow based on springs, seeps, and moisture-loving vegetation along fault trace that point to upward flow along the fault (Kienle et al 1979). This fault is not testable with geochemical and isotope data in this study because of lack of sampled wells on either side of the fault.

The Bowlus Hill fault is not testable with geochemical and isotope data in this study because of lack of sampled wells on either side of the fault. The fault strike is close to parallel to groundwater flow direction, so it may not significantly block or compartmentalize flow (this study).

Carbon-14 values in the study results ranged between 109 pmC and 15 pmC, with a mean of 43 pmC and a median of 38 pmC. This translates to an approximate mean uncalibrated calculated age of 8,462 years, an approximate median of 7,730 years, an approximate maximum of 15,290 years, and an approximate minimum of -620 years (interpreted as modern). The well with the minimum age has a shallow seal depth compared to the others (the top is open to a sedimentary unit) and so was more likely to have modern recharge. These carbon-14 ages are interpreted as the average age of water that contains a certain distribution of mixed ages. While calibration to correct for subsurface interaction with organic material was not performed on these results and so the true ages might be slightly younger, these carbon-14 results suggest large amounts of old water in the WWSB basalt groundwater system with much smaller inputs of modern recharge.

Measured tritium values at the same wells show that of the twelve of the eighteen wells that had detectable tritium, the median value was 5.6 tritium units. This indicates a small amount of modern recharge into the system.

This study collected a significant amount of data on groundwater isotopic and chemical composition in the Walla Walla Subbasin that could provide input for future research to better understand its groundwater system. In particular, a partial mixing model using carbon-14 and tritium concentrations would allow for estimates of recharge volumes along different flow paths and timescales in the subbasin. One statistical weakness of this study was the small number of wells with the full suite of chemical and isotopic parameters used in the principal component analyses. This issue could be solved by including more data points from wells that are being sampled as part of a planned USGS and Washington Department of Ecology study in the Washington portion of the Walla Walla River Basin that will take place in 2019 and 2020.

References

Bense, V. F., et al. "Fault zone hydrogeology." *Earth-Science Reviews*, vol. 127, 10 Oct. 2013, pp. 171-92.

Brown, B. H. "The State-line earthquake at Milton and Walla Walla." *Bulletin of the Seismological Society of America*, vol. 27, 1937, pp. 205-09.

Burns, E.R., Morgan, D.S., Peavler, R.S., and Kahle, S.C., 2011, Three-dimensional model of the geologic framework for the Columbia Plateau Regional Aquifer System, Idaho, Oregon, and Washington: U.S. Geological Survey Scientific Investigations Report 2010-5246, 44 p.

Brown KB, McIntosh JC, Baker VR, Gosch D, 2010. Isotopically depleted late Pleistocene groundwater in Columbia River basalt aquifers: evidence for recharge of glacial Lake Missoula floodwaters? Geophys Res Lett 37:L21402. doi:10.1029/2010GL044992

Douglas, A.A., Winter, G., Baldwin, J., Brackney, K., Mann, H., 2005. Isotopic Age Dating of Municipal water wells in the Lewiston basin, Idaho. Ground Water Quality Technical Report No. 24, Idaho Department of Environmental Quality, Lewiston, Idaho.

Douglas, Alyssa A, et al. *Carbon-14 Dating of ground water in the Palouse Basin of the Columbia river basalts*. 2006. Journal of Hydrology 334, 502-512

INTERNATIONAL ATOMIC ENERGY AGENCY, Isotope Methods for Dating Old Groundwater, IAEA, Vienna (2013).

Golder Associates, Inc. City of Walla Walla Extended Area Aquifer Storage and Recovered Groundwater Flow Model. Golder Associates and City of Walla Walla, 2007.

Gollini et al. (2014). GWmodel: an R package for exploring spatial heterogeneity using geographically weighted models. *arXiv, 1306.0413v2 [stat.AP]*. https://arxiv.org/pdf/1306.0413.pdf

Paul P. Hearn, William C. Steinkampf, Duane G. Horton, G. Cleve Solomon, L. Doug White, John R. Evans; Oxygen-isotope composition of ground water and secondary minerals in Columbia Plateau basalts: Implications for the paleohydrology of the Pasco Basin. *Geology* ; 17 (7): 606–610.

Pfahl, S, and H Sodemann. "What controls deuterium excess in global precipitation?" *Climate of the Past*, vol. 10, Apr., pp. 771-81, doi:10.5194/cp-10-771-2014.

Hayden, Luke. Principal Component Analysis in R, DataCamp, 9 Aug. 2018, www.datacamp.com/community/tutorials/pca-analysis-r.

Hutter, Ingrid L. February 1997. The Wallula Fault Zone: A Study of the Structure and Tectonic History of a Portion of the Olympic-Wallowa Lineament. MS Thesis. Western Washington University.

Jasechko, S. (2018, May). *Groundwater Age Dating*. Presented at the Isotope Tracers in Catchment Hydrology, University of Saskachewan.

Jombart, T. (2015, June 23). A tutorial for the spatial Analysis of Principal Components (sPCA) using adegenet 2.0.0, Imperial College London, 50.

Kassambara, Alboukadel. get_pca: Extract the results for individuals/variables in Principal Component Analysis - R software and data mining , STHDA, www.sthda.com/english/wiki/get-pca-extract-the-results-for-individuals-variables-in-principal-component-analysis-r-software-and-data-mining. Accessed 6 May 2019.

Kendall, C., and J.J. McDonell, ed. 1998. *Isotope Tracers in Catchment Hydrology*. Amsterdam: Elsevier.

Khazemi, Gholam A., et al. *Groundwater Age*. John Wiley & Sons, Inc., 2006.

Kienle, Clive F., et al. *Geologic Reconnaissance of the Wallula Gap, Washington - Blue Mountains - LaGrande, Oregon Region*. Shannon & Wilson, Inc, 1979.

Lane, R. C., and K. J. Whiteman. *Ground-Water Levels Spring 1985, and Ground-Water Level Changes Spring 1983 to Spring 1985, in Three Basalt Units Underlying the Columbia Plateau, Washington and Oregon*. USGS Numbered Series, 88–4018, 1989. *pubs.er.usgs.gov*, http://pubs.er.usgs.gov/publication/wri884018.

Larson, Kathryn R., Keller, C. Kent, Larson, Peter B., & Allen-King, Richelle M. (2000). Water Resource Implications of [O.sup.18] and [H.sup.2] Distributions in a Basalt Aquifer System. *Ground Water, 38*(6), 947-950.

Lorenz, David L., and Aliesha L. Diekoff. "SmwrGraphs—An R package for graphing hydrologic data, version 1.1.2." USGS Open-File Report, vol. 2016, no. 1188, 2017, p. 17, doi:https://doi.org/10.3133/ofr20161188, pubs.usgs.gov/of/2016/1188/ofr20161188.pdf.

Madin, Ian P., and Ronald P. Geitgey. *Preliminary Geologic Map of the Umatilla Basin, Morrow and Umatilla Counties, Oregon*. O-07-15 ed., State of oregon Department of Geology and Mineral Industries, 2007.

McMahon, P.B., Plummer, L.N., Bohlke, J.K., Shapiro, S.D., and Hinkle, S.R., 2011, *A comparison of recharge rates in aquifers of the United States based on groundwater-age data*: Hydrogeology Journal, DOI 10.1007/s10040-011-0722-5

Newcomb, R. C. (1965). *Geology and ground-water resources of the Walla Walla River basin Washington-Oregon* (Report No. 21). Olympia, WA. Retrieved from https://pubs.usgs.gov/wsp/1999n/report.pdf

Newcomb, R. C. (1972). *Quality of the Ground Water in Basalt of the Columbia River Group, Washington, Oregon, and Idaho* (Report No. 1999). Washington, DC. Retrieved from http://pubs.er.usgs.gov/publication/70047774

OAR 690-507-0030 Umatilla Basin Program, Oregon Secretary of State, 19 Jan. 2018, secure.sos.state.or.us/oard/view.action?ruleNumber=690-507-0030.

ORS 536.340 Classification of water as to highest and best use and quantity of use, oregonlaws.org, 2017, www.oregonlaws.org/ors/536.340.

ORS 540.435 Installation of totalizing measuring device, oregonlaws.org, 2017, www.oregonlaws.org/ors/540.435.

Packard, F.A., Hansen, A.J., Jr., and Bauer, H.H., 1996, *Hydrology and simulation of flow and the effects of development alternatives on the basalt aquifers of the Horse Heaven Hills, south-central Washington*: U.S. Geological Survey Water-Resources Investigations Report 94-4068.

Reidel, Stephen P. "Emplacement of Columbia River Flood Basalt." Journal of Geophysical Research, vol. 103, no. B11, 10 Nov. 1998, pp. 393-410.

Révész, Kinga, and Coplen, T.B., 2008a, *Determination of the δ($^{2}H/^{1}H$) of water: RSIL lab code 1574, chap. C1 of Révész, Kinga, and Coplen, T.B., eds., Methods of the Reston Stable Isotope Laboratory*: U.S. Geological Survey Techniques and Methods 10–C1, 27 p.

Révész, Kinga, and Coplen, T.B., 2008b, *Determination of the δ($^{18}O/^{16}O$) of water: RSIL lab code 489, chap. C2 of Révész, Kinga, and Coplen, Tyler B., eds., Methods of the Reston Stable Isotope Laboratory*: U.S. Geological Survey Techniques and Methods, 10–C2, 28 p.

Steinkampf, W. C. *Water-Quality Characteristics of the Columbia Plateau Regional Aquifer System in Parts of Washington, Oregon, and Idaho*. USGS Numbered Series, 87–4242, Dept. of the Interior, U.S. Geological Survey ; Books and Open-File Reports Section [distributor], 1989. *pubs.er.usgs.gov*, http://pubs.er.usgs.gov/publication/wri874242.

Taylor, Sarah A., and Carey Gazis. "A geochemical study of the impact of irrigation and aquifer lithology on groundwater in the Upper yakima River basin, Washington, USA."

Environmental Earth Science, vol. 72, 11 Feb. 2014, pp. 1569-87, doi:10.1007/s12665-014-3062-7. Accessed 18 May 2018.

Thane, Lindsay. Walla Walla Subbasin Closed to New Groundwater Permits. (2017, July 5). Retrieved May 8, 2018, from https://www.water-law.com/walla-walla-subbasin-closed-new-groundwater-permits/

Tolan, Terry L., et al. "An Introduction to the stratigraphy, structural geology, and hydrogeology of the Columbia River Flood Basalt Province." *GSAPUBS Field Guides*, vol. 15, 2009, pp. 599-643, doi:10.1130/2009.fld015(28), www.geology.cwu.edu/facstaff/nick/g351/2009_Tolan_CRB_Primer.pdf.

USGS Umatilla Basin Ground-Water Study. (n.d.). Retrieved May 8, 2018, from https://or.water.usgs.gov/proj/umatilla_gw/background.html

USGS Oregon Center for Water Science, Methods for Alkalinity Calculator. (n.d.). Retrieved May 22, 2018, from https://or.water.usgs.gov/alk/methods.html

Vlassopoulos D, Goin J, Zeliff M, Porcello J, Tolan T, Lindsey K (2009) *Groundwater geochemistry of the Columbia River Basalt Group aquifer system: Columbia Basin ground water management area of Adams, Franklin, Grant, and Lincoln Counties June 2009. Columbia basin ground water management area groundwater geochemistry report*. http://www.cbgwma.org/. Accessed 16 Feb 2012

Woody, J. (2016, December 3). Basalt Groundwater of the Walla Walla Subbasin. Oregon Water Resources Department. Retrieved from http://www.oregon.gov/owrd/docs/Place/Walla_Walla_Subbasin/WWSB_Hydrogeology_Dec2016.pdf

Woody, J., & Gall, I. (2016, September). Walla Walla Subbasin Groundwater Management Options. OWRD. Retrieved from http://www.oregon.gov/owrd/docs/Place/Walla_Walla_Subbasin/MIltonFreewater_Area_GW_Management_Final_Sept2016_Community_Presentation.pdf

Appendix A: Tables of Analytical Results

OWRD ID	pH	Specific conductance, microsiemens per centimeter at 25 degrees Celsius	Temperature, degrees Celsius	Hydrogen Sulfide Odor
UMAT0003074	8	383	14.7	No
UMAT0003909	7.7	194	14.4	No
UMAT0003929	7.8	312	16.2	No
UMAT0003962	8.2	236	17	No
UMAT0004010	8.1	225	19.4	No
UMAT0004167	8.1	333	19.5	No
UMAT0004173	8.2	243	18.9	Yes
UMAT0004179	7.9	364	21.5	No
UMAT0005193	7.8	258	18.7	No
UMAT0050069	8.1	232	20.5	No
UMAT0050478	7.4	155	16.8	No
UMAT0050939	8.1	225	19.3	No
UMAT0054277	8.9	114	14.1	No
UMAT0055526	8.2	219	21	No
UMAT0056287	7.1	774	15.4	No
UMAT0056382	8.2	243	22.3	No
UMAT0057235	7.3	239	23.2	No
UMAT0057946	7.5	203	14.4	No
UMAT0002707	7.92	291	21.2	No
UMAT0003092	7.48	310	13.6	No
UMAT0003103	8.04	250	22.8	Yes
UMAT0004184	7.96	378	21.4	No
UMAT0004864	8.17	216	20	No
UMAT0005028	7.81	755	17.1	No
UMAT0005227	8.41	238	23.5	No
UMAT0005530	8.21	241	23.4	No
UMAT0006217	6.95	143.2	12.2	No
UMAT0006283	8.31	162.7	20.6	No
UMAT0054097	NULL	NULL	14.2	Yes
UMAT0056219	7.78	611	14.5	No
UMAT0057672	8.23	232	20.9	No

Table A1: Field-Measured Parameters

OWRD ID	TDS	Ca	Mg	K	Na	Chloride	HCO3*	CO3*	Sulfate
UMAT0003074	237	34	17	7.5	23	10.2	203.1	0.9	14.8
UMAT0003909	153	19	7.8	3.9	8.7	4.91	96.4	0.2	9.32
UMAT0003929	236	30	13	4.2	13	15.5	137.1	0.4	17.9
UMAT0003962	185	22	8.5	3.6	13	8.2	117.5	0.9	11.3
UMAT0004010	165	21	8.5	2.6	15	4.9	131.4	0.8	2.63
UMAT0004167	246	27	9.3	5.3	30	15.5	150.7	0.9	21.8
UMAT0004173	193	24	9	3.9	22	5.98	132.2	1	7.73
UMAT0004179	271	33	13	4.6	27	21.3	147.7	0.5	35.7
UMAT0005193	209	25	9.2	3.3	15	3.1	143.1	0.4	6.75
UMAT0050069	185	20	7.6	3.3	19	7.53	133.8	0.8	0.15
UMAT0050478	128	14	4.8	4.4	11	1.83	91.9	0.1	2.46
UMAT0050939	190	19	6.9	4.6	20	3.68	131.4	0.8	4.06
UMAT0054277	106	9	1.2	1.9	15	1.07	63.3	2.3	2.43
UMAT0055526	173	19	7.5	3.4	17	4.29	127.4	0.9	3.27
UMAT0056287	507	83	28	7.8	28	37.7	280	0.2	28.9
UMAT0056382	191	20	7.3	4.1	22	4.79	139.5	1	4.84
UMAT0057235	194	21	6.9	4.9	20	5.5	132.7	0.1	6.66
UMAT0057946	169	20	7.6	4.1	8.4	2.4	108.3	0.2	4.01
*Values calculated from pH and alkalinity									

Table A2: Major Ions, in mg/L

OWRD ID	Alkalinity	Bromide	Fluoride	Silica	Iron	Manganese
UMAT0003074	168	0.135	0.47	44.1	<10.0	1.36
UMAT0003909	79.4	0.019	0.14	50.8	<10.0	0.94
UMAT0003929	113	0.022	0.2	53.1	<10.0	0.48
UMAT0003962	97.7	0.056	0.22	55.3	<10.0	2
UMAT0004010	109	0.038	0.4	60.4	11.5	15.8
UMAT0004167	125	0.148	0.45	71.2	71.4	40.1
UMAT0004173	110	0.06	0.37	67.9	27.1	17
UMAT0004179	122	0.198	0.4	69.3	20.6	36.5
UMAT0005193	118	0.039	0.46	62.9	<10.0	0.25
UMAT0050069	111	0.054	0.38	64.9	11.9	10.2
UMAT0050478	75.5	0.013	0.23	53	<10.0	0.97
UMAT0050939	109	0.035	0.42	66.6	53.6	33.1
UMAT0054277	55.7	<0.010	0.21	45.5	<10.0	3.9
UMAT0055526	106	0.032	0.37	62.8	32.7	11.9
UMAT0056287	230	0.094	0.17	59.8	<10.0	2.27
UMAT0056382	116	0.043	0.44	68.8	30.2	14.7
UMAT0056382	116	0.043	0.44	68.8	30.2	14.7
UMAT0056382	116	0.043	0.44	69.9	29.6	14.8
UMAT0057235	109	0.056	0.48	68	<10.0	9.12
UMAT0057946	89	0.034	0.24	57.6	<10.0	<0.20

Table A3: Secondary ion analytes, in mg/L

OWRD ID	Carbon-14 counting error, filtered, percent modern	Carbon-14, filtered, percent modern	delta carbon-13/carbon-12, unfiltered, per mil	Uncalibrated Carbon-14 Age	Tritium, picocuries per liter	Tritium, Tritium units
UMAT0050939	0.12	15.07	-14.13	15,290	0.5	1.61
UMAT0057235	0.11	22.85	-15.05	11,940	0.5	1.61
UMAT0004179	0.12	17.55	-15.04	14,060	0.5	1.61
UMAT0004167	0.09	16.47	-14.17	14,580	0.8	2.576
UMAT0005193	0.14	56.81	-14.35	4,630	0.8	2.576
UMAT0003074	0.13	53.44	-12.86	5,130	1.3	4.186
UMAT0057946	0.19	89.3	-14.81	990	2.2	7.084
UMAT0004010	0.12	42.58	-16.32	6,930	2.4	7.728
UMAT0003929	0.14	72.58	-17	2,640	3.5	11.27
UMAT0050478	0.16	68.89	-16.08	3,070	4.8	15.456
UMAT0056287	0.2	108.9	-17.56	-620	5	16.1
UMAT0003909	0.17	79.53	-17.9	1,900	5.9	18.998
UMAT0055526	0.12	22.37	-15.22	12,110	R0.1	<0.322
UMAT0003962	0.11	38.55	-16.52	7,730	R0.2	<0.644
UMAT0004173	0.09	17.62	-15.36	14,030	R0.2	<0.644
UMAT0050069	0.09	27.13	-16.62	10,550	R-0.2	<0.644
UMAT0056382	0.11	16.69	-14.5	14,470	R0.3	<0.966
UMAT0056382	0.11	16.69	-14.5	14,470	R0.3	<0.966
UMAT0054277	0.25	42.78	-18.24	6,880	R0.5	<1.61

Table A4: Radioactive isotopes

OWRD ID	d18O	d2H	Calculated d2H excess
UMAT0050069	-13.57	-107	1.56
UMAT0003074	-14.16	-114	-0.72
UMAT0004167	-15.54	-122	2.32
UMAT0050478	-14.51	-108	8.08
UMAT0050939	-14.99	-114	5.92
UMAT0055526	-14.36	-109	5.88
UMAT0056382	-14.71	-113	4.68
UMAT0003909	-14.35	-108	6.8
UMAT0004010	-13.82	-107	3.56
UMAT0057946	-13.06	-102	2.48
UMAT0057235	-13.86	-108	2.88
UMAT0054277	-14.8	-112	6.4
UMAT0004179	-14.61	-114	2.88
UMAT0005193	-13.11	-103	1.88
UMAT0003962	-14.03	-108	4.24
UMAT0056287	-14.25	-105	9
UMAT0003929	-14.03	-105	7.24
UMAT0004173	-14.5	-113	3
UMAT0003103	-14.01	-110	2.08
UMAT0003092	-13.03	-104	0.24
UMAT0002707	-14.14	-113	0.12
UMAT0054097	-12.92	-103	0.36
UMAT0057672	-13.47	-107	0.76
UMAT0005530	-14.81	-115	3.48
UMAT0004184	-14.52	-113	3.16
UMAT0006283	-14.63	-110	7.04
UMAT0005227	-14.59	-114	2.72
UMAT0006217	-13.98	-103	8.84
UMAT0004864	-15.5	-119	5
UMAT0005028	-14.94	-118	1.52
UMAT0056219	-14.07	-106	6.56

Table A5: Stable Isotope Results, in permil

Appendix B: Well Physical Characteristics

OWRD ID*	Stratigraphy Source * **	Well bottom detailed stratigraphy	Well bottom formation	All formations open to the well column	Depth of seal*	Well bottom elevation*	Altitude of land surface*	Depth of well, feet below land surface*
UMAT0002707	OWRD	Crbg Grb N2 Sentinel Bluffs	Grande Ronde	Wanapum, Grande Ronde	Not recorded	589	1804	1215
UMAT0003103	Burns	Crbg Grb	Grande Ronde	Wanapum, Grande Ronde	Not recorded	935	2060	1125
UMAT0006217	OWRD	PostCrbSediments	PostCrbSediments	PostCrbSediments	Not recorded	633	825	192
UMAT0056219	OWRD	PostCrbSediments	PostCrbSediments	PostCrbSediments	Not recorded	337	562	225
UMAT0050478	Burns	Crbg Smb	SaddleMountain	Saddle Mountain	270	405	880	475
UMAT0004864	Burns	Crbg Wb	Wanapum	Saddle Mountain, Wanapum	100	105	820	715
UMAT0006283	OWRD	Crbg Wb FrenchmanSprings SilverFalls	Wanapum	Saddle Mountain, Wanapum	470	-93	910	1003
UMAT0003909	Burns	Crbg Grb	Grande Ronde	Saddle Mountain, Wanapum, Grande Ronde	0	503	1005	502
UMAT0003929	Burns	Crbg Grb	Grande Ronde	Saddle Mountain, Wanapum, Grande Ronde	0	33	985	952
UMAT0003962	Burns	Crbg Grb	Grande Ronde	Saddle Mountain, Wanapum, Grande Ronde	0	163	1065	902
UMAT0004167	Burns	Crbg Grb	Grande Ronde	Saddle Mountain, Wanapum, Grande Ronde	0	312	635	323
UMAT0005193	Burns	Crbg Grb	Grande Ronde	Saddle Mountain, Wanapum, Grande Ronde	50	475	1235	760

OWRD ID*	Stratigraphy Source * **	Well bottom detailed stratigraphy	Well bottom formation	All formations open to the well column	Depth of seal*	Well bottom elevation*	Altitude of land surface*	Depth of well, feet below land surface*
UMAT0003074	OWRD	Crbg Wb FrenchmanSprings Sentinel Gap	Wanapum	Wanapum	30	1285	1836	551
UMAT0004173	OWRD	Crbg Wb Frenchman Springs Gingko	Wanapum	Wanapum	19	331	706	375
UMAT0004179	Burns	Crbg Wb	Wanapum	Wanapum	0	513	740	227
UMAT0056287	OWRD	Crbg Wb FrenchmanSprings	Wanapum	Wanapum	0	550	890	340
UMAT0003092	OWRD	Crbg Grb N2 Sentinel Bluffs	Grande Ronde	Wanapum, Grande Ronde	0	980	1980	1000
UMAT0004184	Burns	Crbg Grb	Grande Ronde	Wanapum, Grande Ronde	0	448	748	300
UMAT0005028	OWRD	Crbg Grb N2 Sentinel Bluffs	Grande Ronde	Wanapum, Grande Ronde	39	287	670	383
UMAT0005227	Burns	Crbg Grb	Grande Ronde	Wanapum, Grande Ronde	36	247	964	717
UMAT0005530	OWRD	Crbg Grb N2 Sentinel Bluffs	Grande Ronde	Wanapum, Grande Ronde	502	-92	1010	1102
UMAT0050939	OWRD	Crbg Grb N2 Sentinel Bluffs	Grande Ronde	Wanapum, Grande Ronde	360	-307	859	1166
UMAT0054277	OWRD	Crbg Grb N1 DowneyGulch	Grande Ronde	Wanapum, Grande Ronde	90	1590	1990	400
UMAT0055526	OWRD	Crbg Grb N2 Sentinel Bluffs	Grande Ronde	Wanapum, Grande Ronde	495	112	1152	1040
UMAT0056382	OWRD	Crbg Grb N2 Sentinel Bluffs	Grande Ronde	Wanapum, Grande Ronde	460	32	1088	1056
UMAT0056382	OWRD	Crbg Grb N2 Sentinel Bluffs	Grande Ronde	Wanapum, Grande Ronde	460	32	1088	1056
UMAT0056382	OWRD	Crbg Grb N2 Sentinel Bluffs	Grande Ronde	Wanapum, Grande Ronde	460	32	1088	1056
UMAT0004010	OWRD	Crbg Grb	Grande Ronde	Wanapum, Grande Ronde	78	119	1170	1051

OWRD ID*	Stratigraphy Source * **	Well bottom detailed stratigraphy	Well bottom formation	All formations open to the well column	Depth of seal*	Well bottom elevation*	Altitude of land surface*	Depth of well, feet below land surface*
UMAT0050069	OWRD	Crbg Grb N2 Sentinel Bluffs	Grande Ronde	Grande Ronde	630	481	1187	706
UMAT0057235	Burns	Crbg Grb	Grande Ronde	Grande Ronde	475	168	1073	905
UMAT0057672	OWRD	Crbg Grb N2 WinterWater	Grande Ronde	Grande Ronde	556	319	1136	817
UMAT0057946	Burns	Crbg Grb	Grande Ronde	Grande Ronde		1289	1554	265
UMAT0054097	Burns	Crbg Grb	Grande Ronde	Grande Ronde	0	1370	1650	280

Table B1: Well stratigraphy and construction. * marks information from OWRD Groundwater Information System Database. ** indicates data from Burns et al 2011.

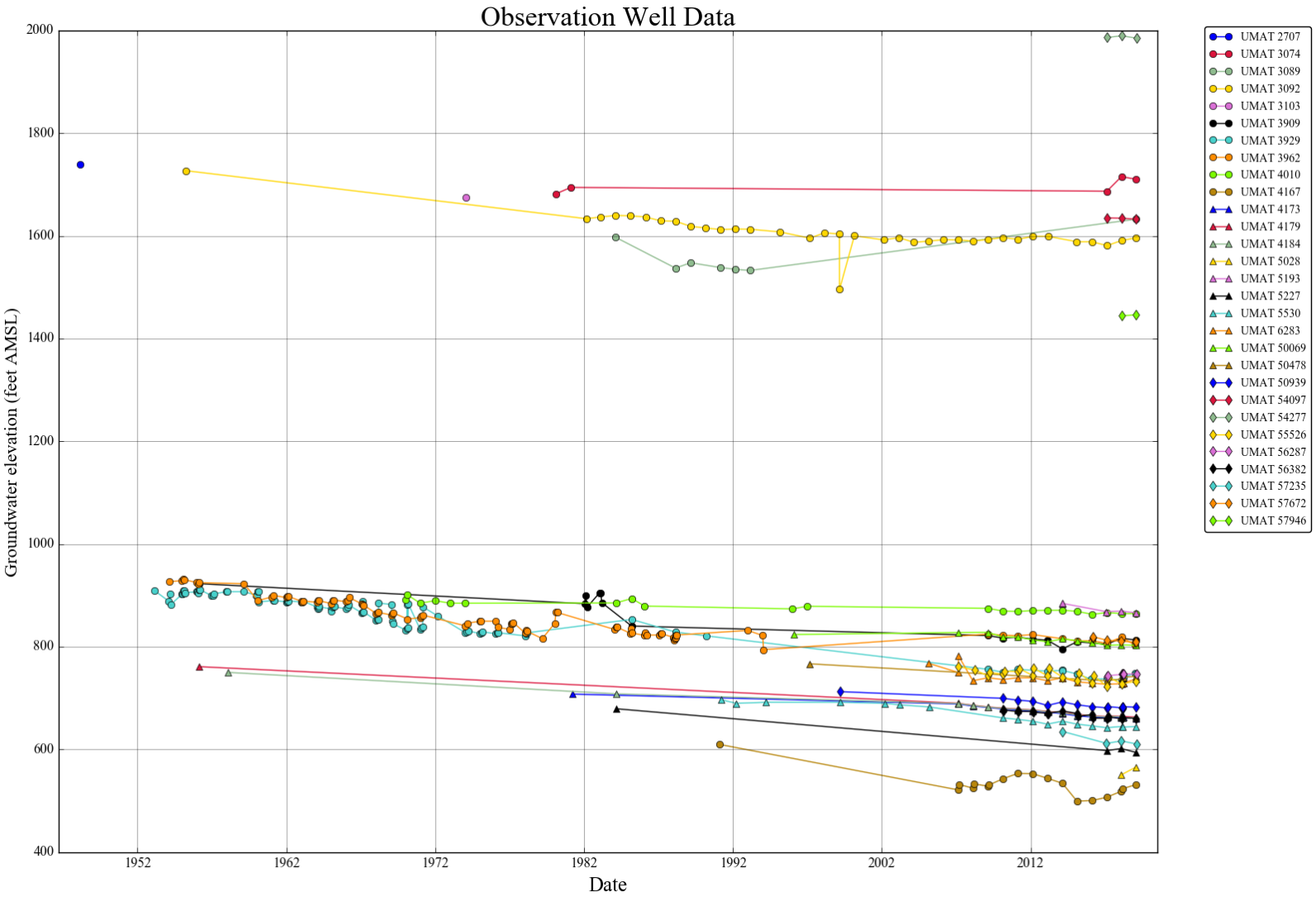

Figure B1: Historical winter hydrograph data for wells sampled in this study.

Appendix C: Figures

Series		Group	Subgroup	Formation	Member	Isotopic Age (m.y.)	Magnetic Polarity
Miocene	Upper	Columbia River Basalt Group	Yakima Basalt Subgroup	Saddle Mountains Basalt	Lower Monumental Member	6	N
					Ice Harbor Member	8.5	
					Basalt of Goose Island		N
					Basalt of Martindale		R
					Basalt of Basin City		N
					Buford Member		R
					Elephant Mountain Member	10.5	N , T
					Pomona Member	12	R
					Esquatzel Member		N
					Weissenfels Member		
					Basalt of Slippery Creek		N
					Basalt of Tenmile Creek		N
					Basalt of Lewiston Orchards		N
					Basalt of Cloverland		N
					Asotin Member	13	
					Basalt of Huntzinger		N
					Wilbur Creek Member		
					Basalt of Lapwai		N
					Basalt of Wahluke		N
					Umatilla Member		
					Basalt of Sillusi		N
					Basalt of Umatilla		N
	Middle			Wanapum Basalt	Priest Rapids Member	14.5	
					Basalt of Lolo		R
					Basalt of Rosalia		R
					Roza Member		T , R
					Shumaker Creek Member		N
					Frenchman Springs Member		
					Basalt of Lyons Ferry		N
					Basalt of Sentinel Gap		N
					Basalt of Sand Hollow	15.3	N
					Basalt of Silver Falls		N , E
					Basalt of Ginkgo	15.6	E
					Basalt of Palouse Falls		E
					Eckler Mountain Member		
					Basalt of Dodge		N
					Basalt of Robinette Mountain		N
					Vantage Horizon		
				Grande Ronde Basalt	Sentinel Bluffs Member	15.6	
					Slack Canyon member		
					Fields Springs member		
					Winter Water member		N_2
				Prineville Basalt	Umtanum member		
					Ortley member		
					Armstrong Canyon member		
					Meyer Ridge member		
					Grouse Creek member		
					Wapshilla Ridge member		R_2
					Mt. Horrible member		
				Picture Gorge Basalt	China Creek member		
					Downy Gulch member		N_1
					Center Creek member		
					Rogersburg member		
					Teepee Butte Member		R_1
					Buckhorn Springs member	16.5	
	Lower			Imnaha Basalt			R_1
							T
							N_1
						17.5	R_0

Figure C1: CRBG Stratigraphy from Reidel et al 2002.

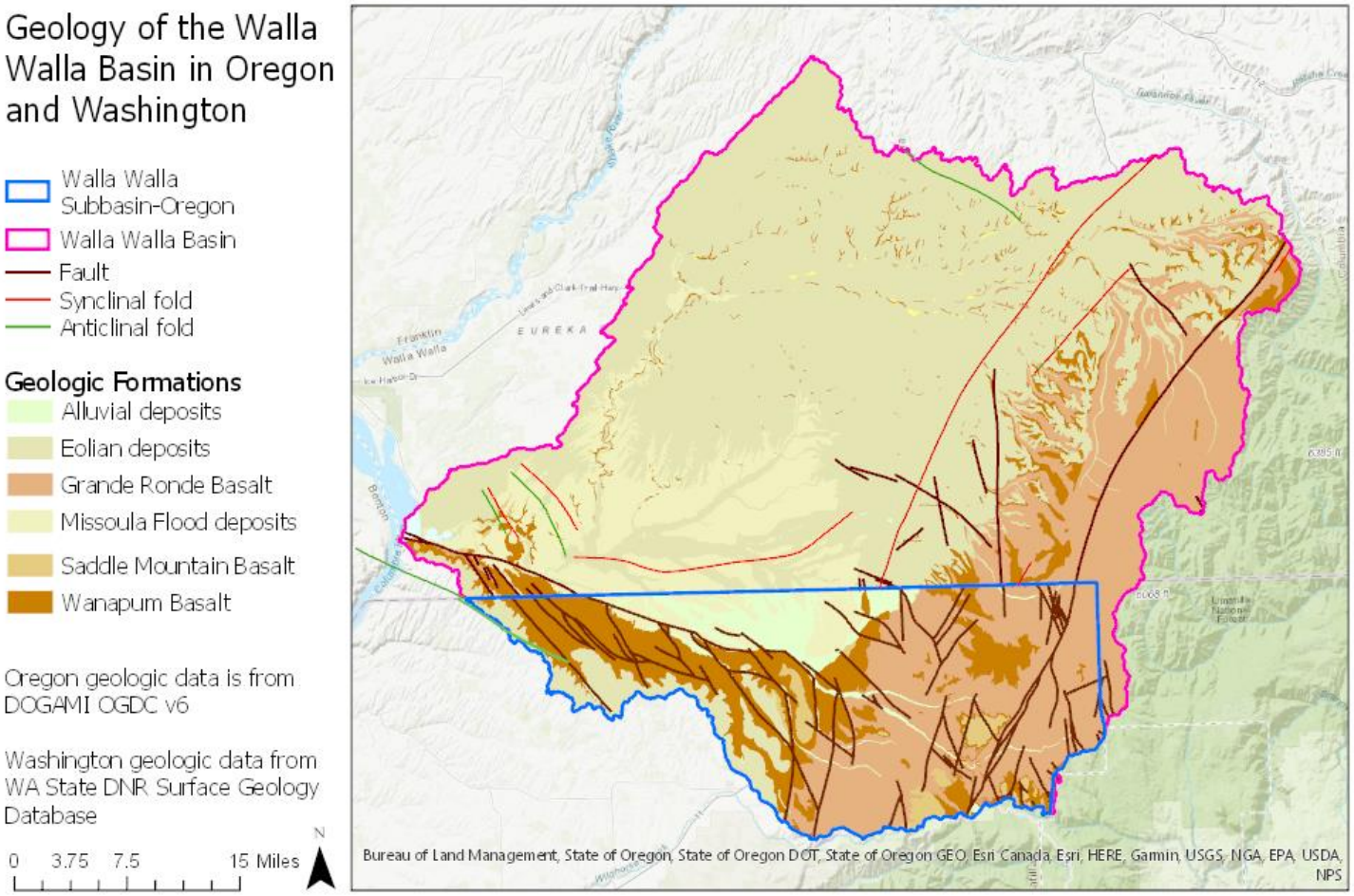

Figure C2: Geology of Walla Walla Basin and Subbasin. Map created by author.

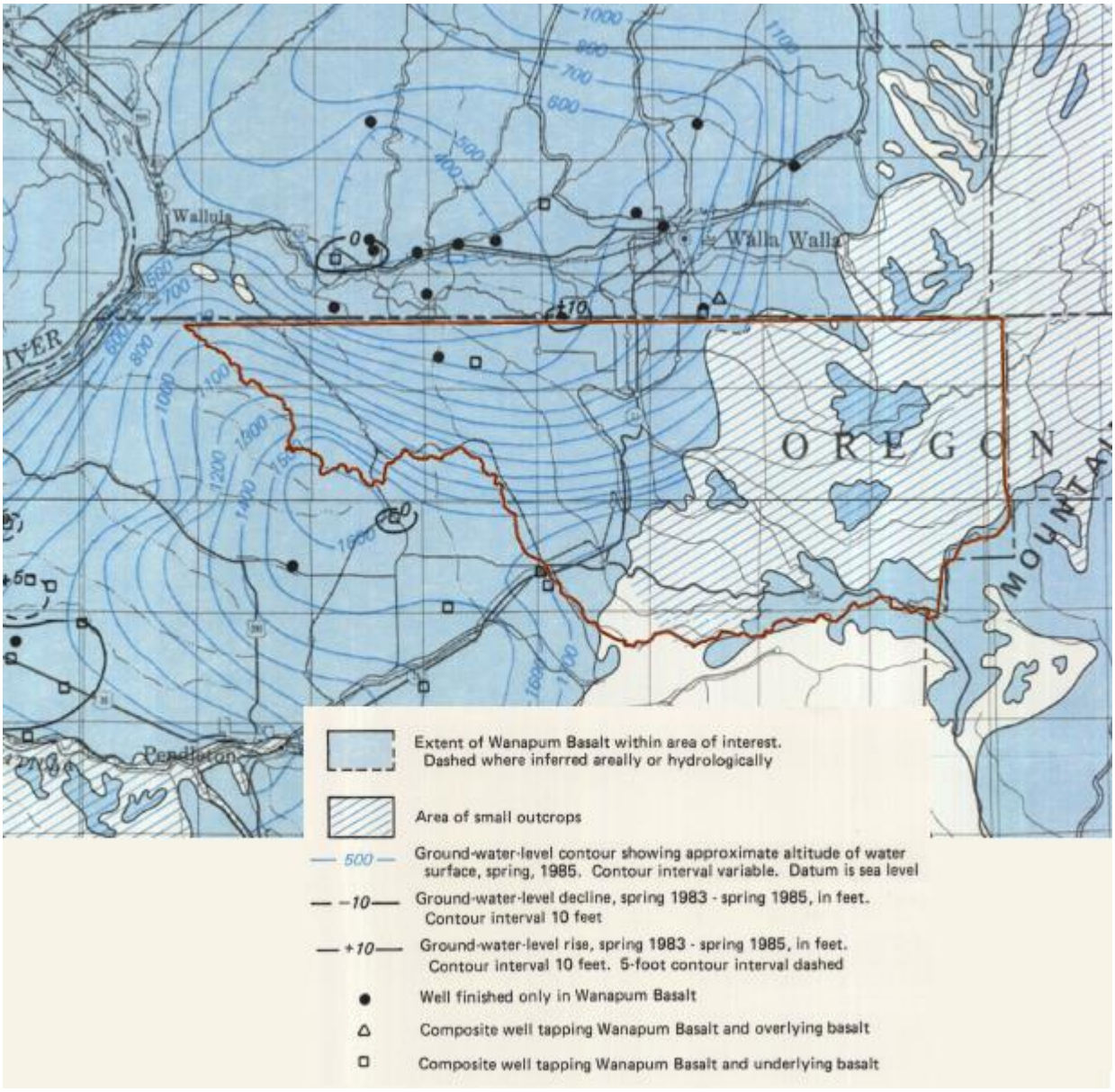

Figure C3: 1985 interpolated potentiometric surface in the Wanapum Basalt, WWSB outlined in brown, map modified from Lane and Whitman 1989.

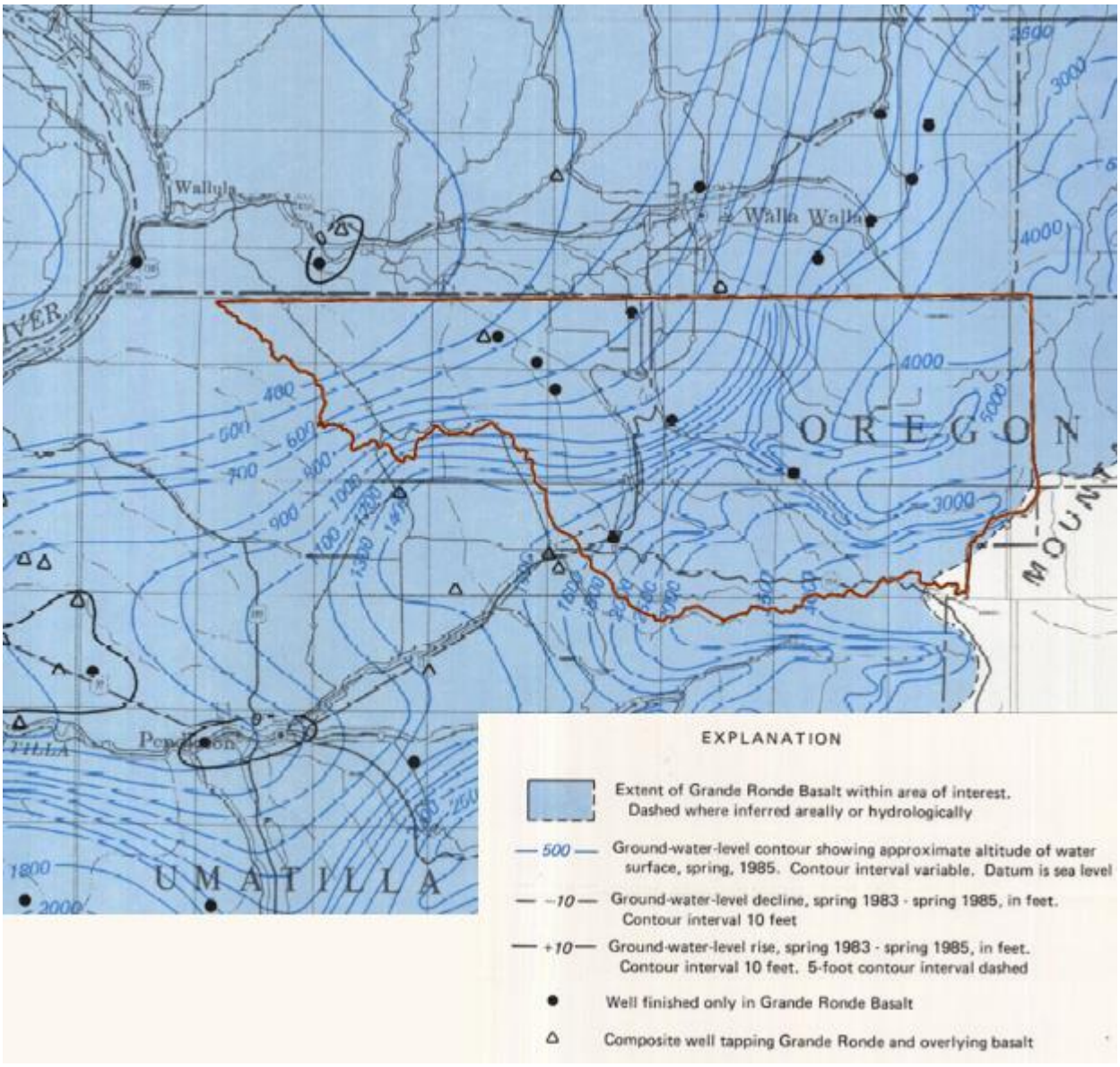

Figure C4: 1985 interpolated potentiometric surface in the Grande Ronde Basalt, WWSB outlined in brown, map modified from Lane and Whitman 1989.

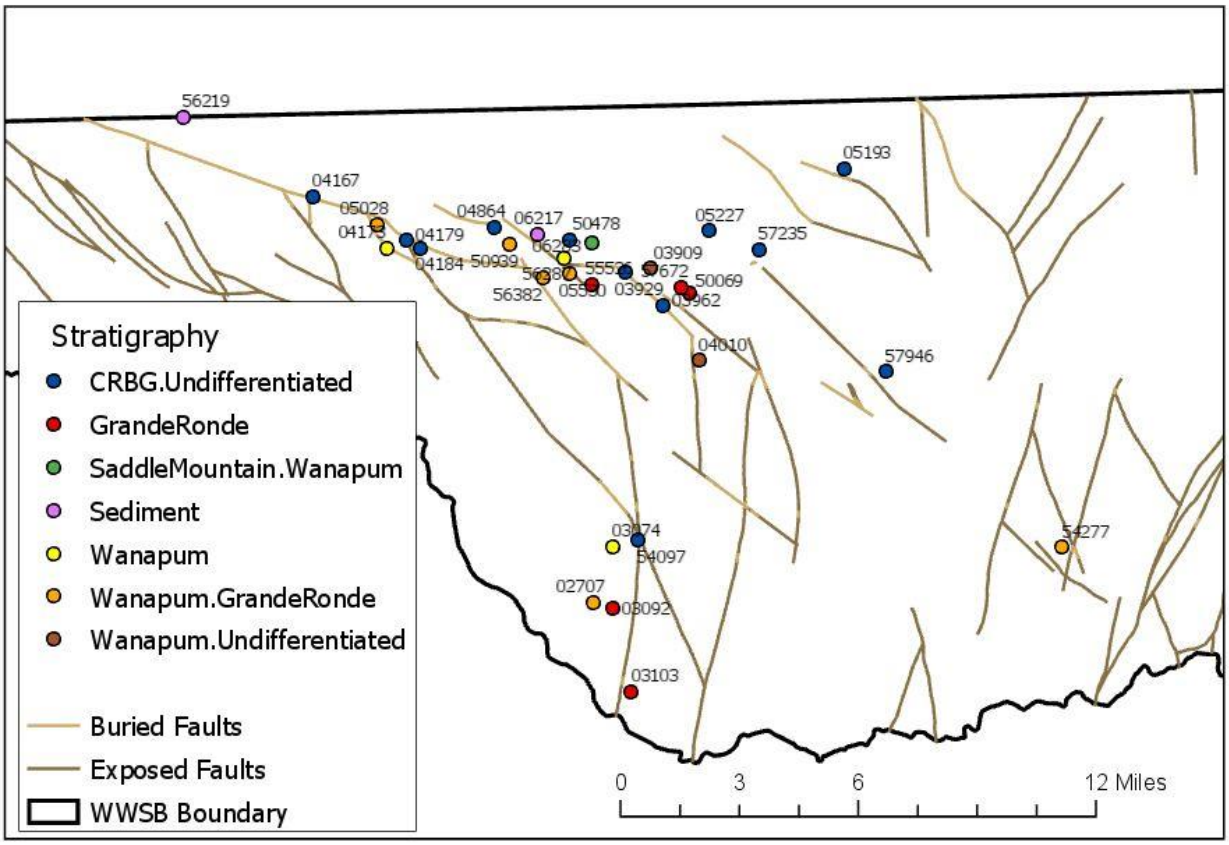

Figure C5: Sampled wells with stratigraphy from OWRD database

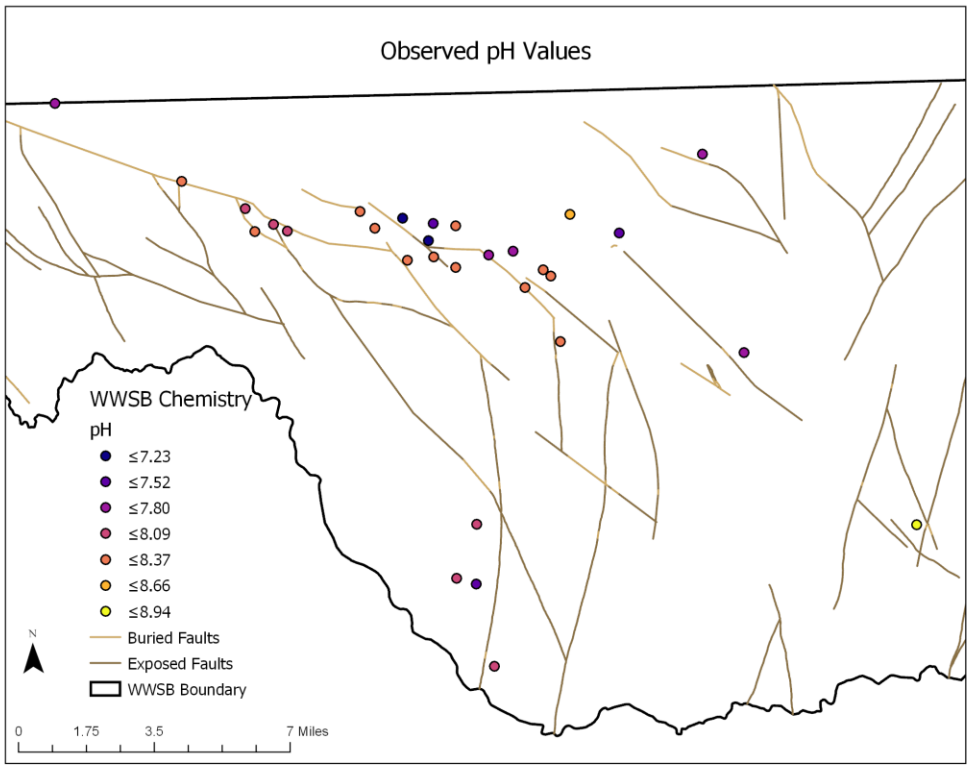

Figure C6: map observed ranges of pH values

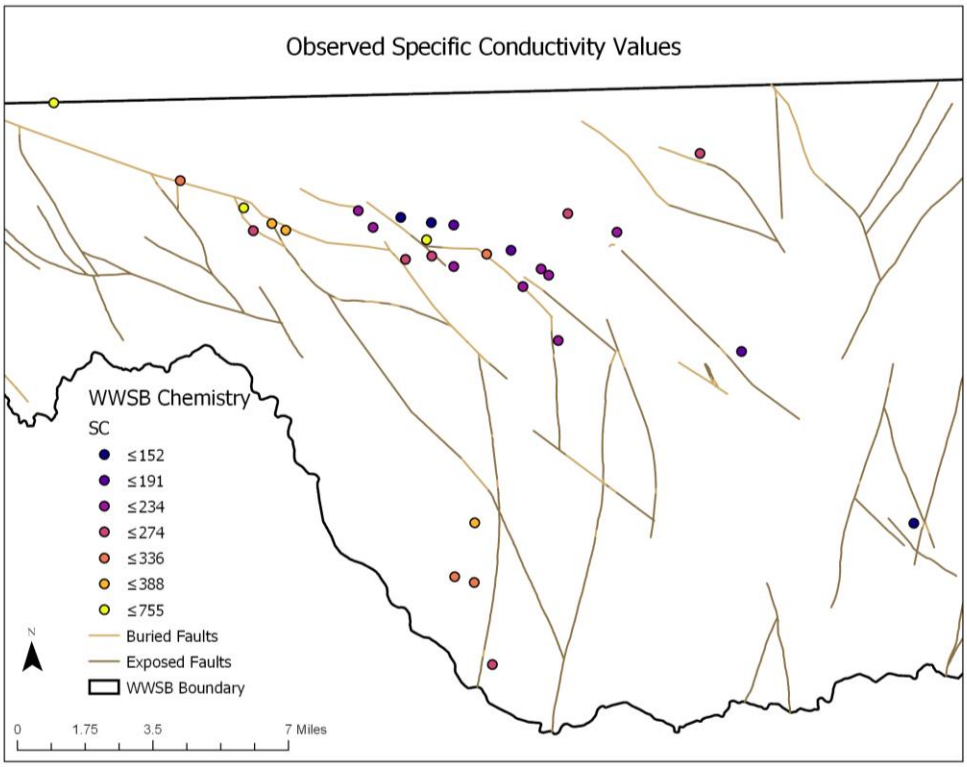

Figure C7: observed ranges of SC values

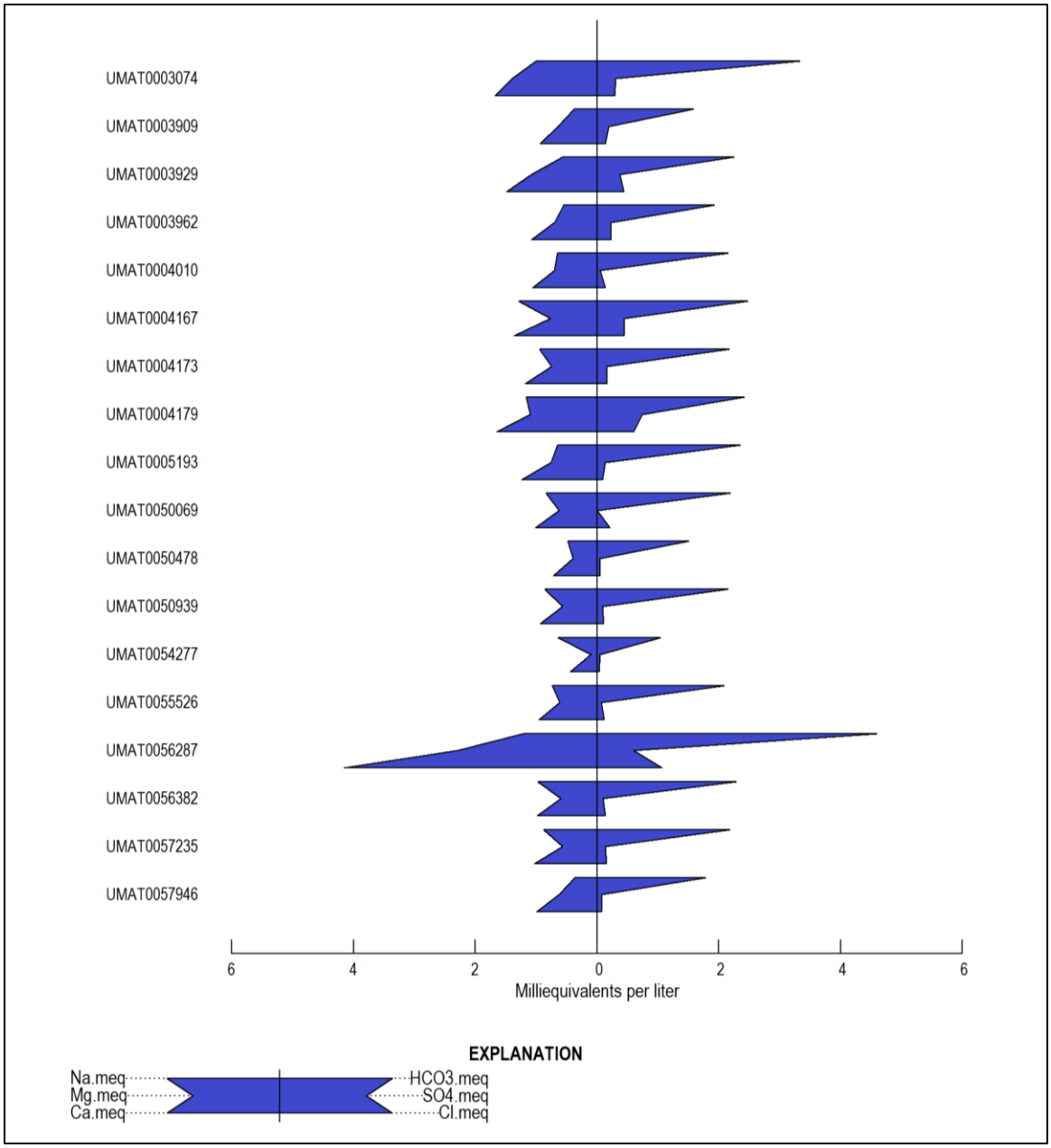

Figure C8: Stiff diagrams for groundwater samples

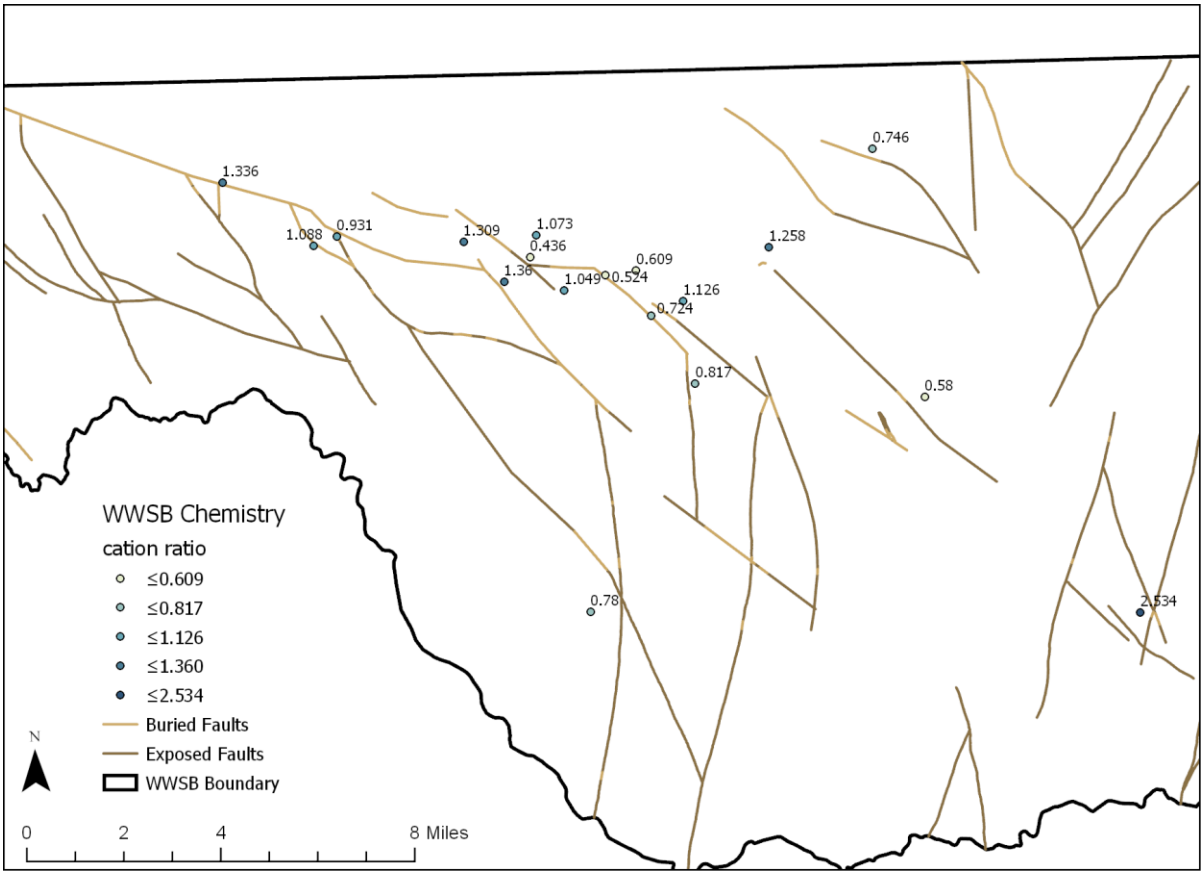

Figure C9: map of cation ratio values

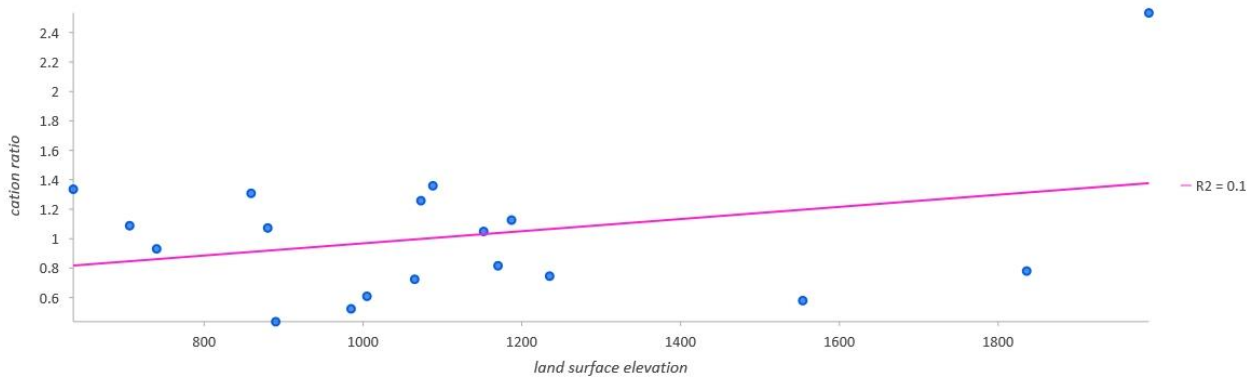

Figure C10: relationship between land surface elevation and cation ratio.

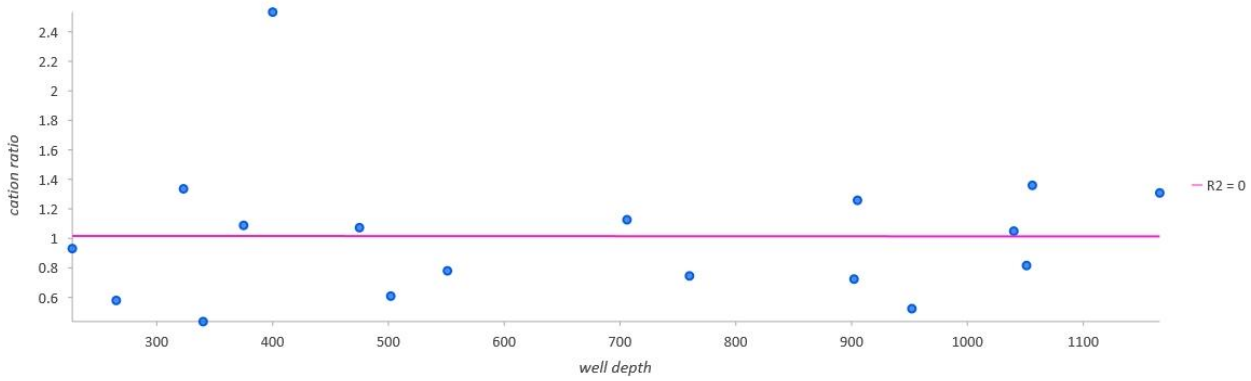

Figure C11: Relationship between well depth and cation ratio

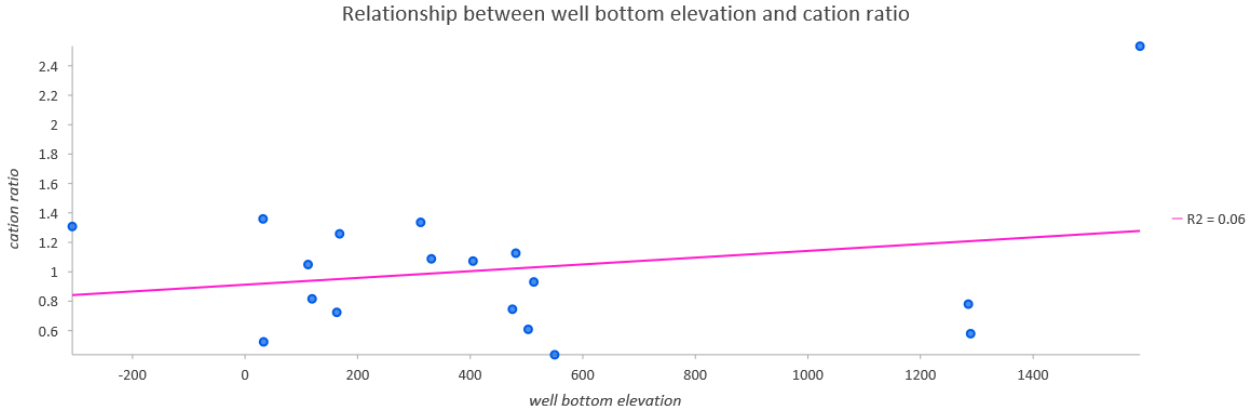

Figure C12: Graph of the relationship between well bottom elevation and cation ratio

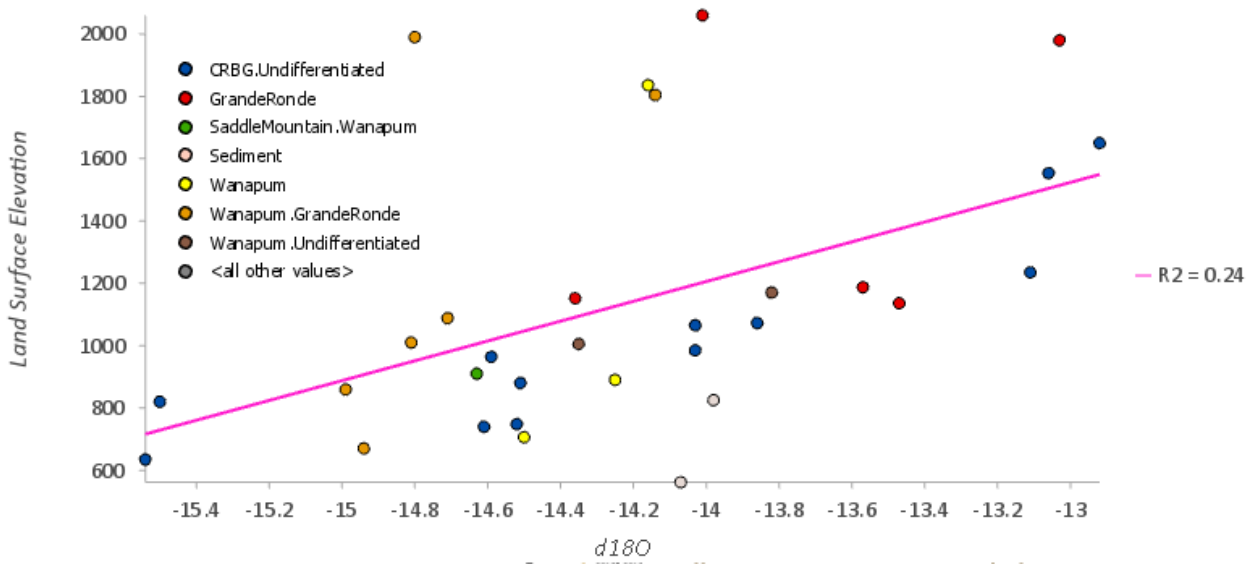

Figure C13: Relationship between d18O and land surface elevation

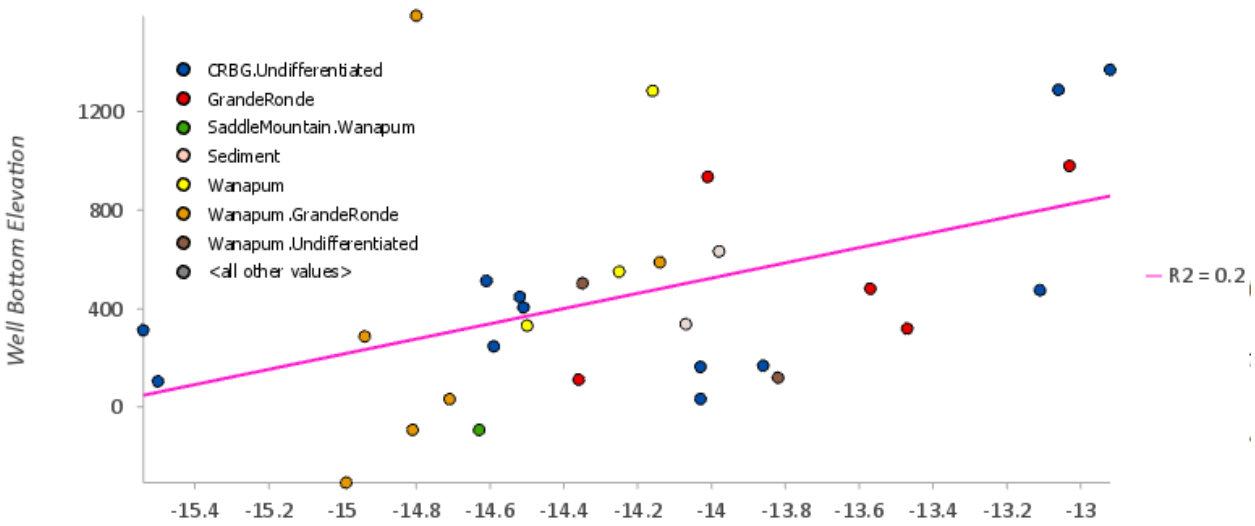

Figure C14: Graph of the relationship between d18O and well bottom elevation

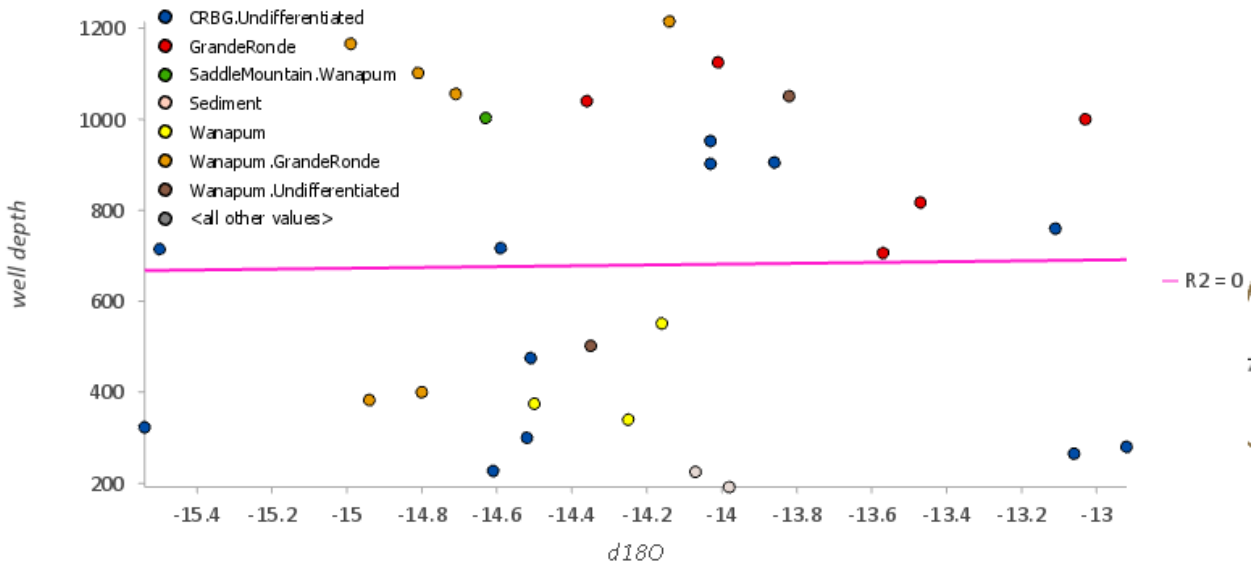

Figure C15: Graph of the relationship between d18O and well depth

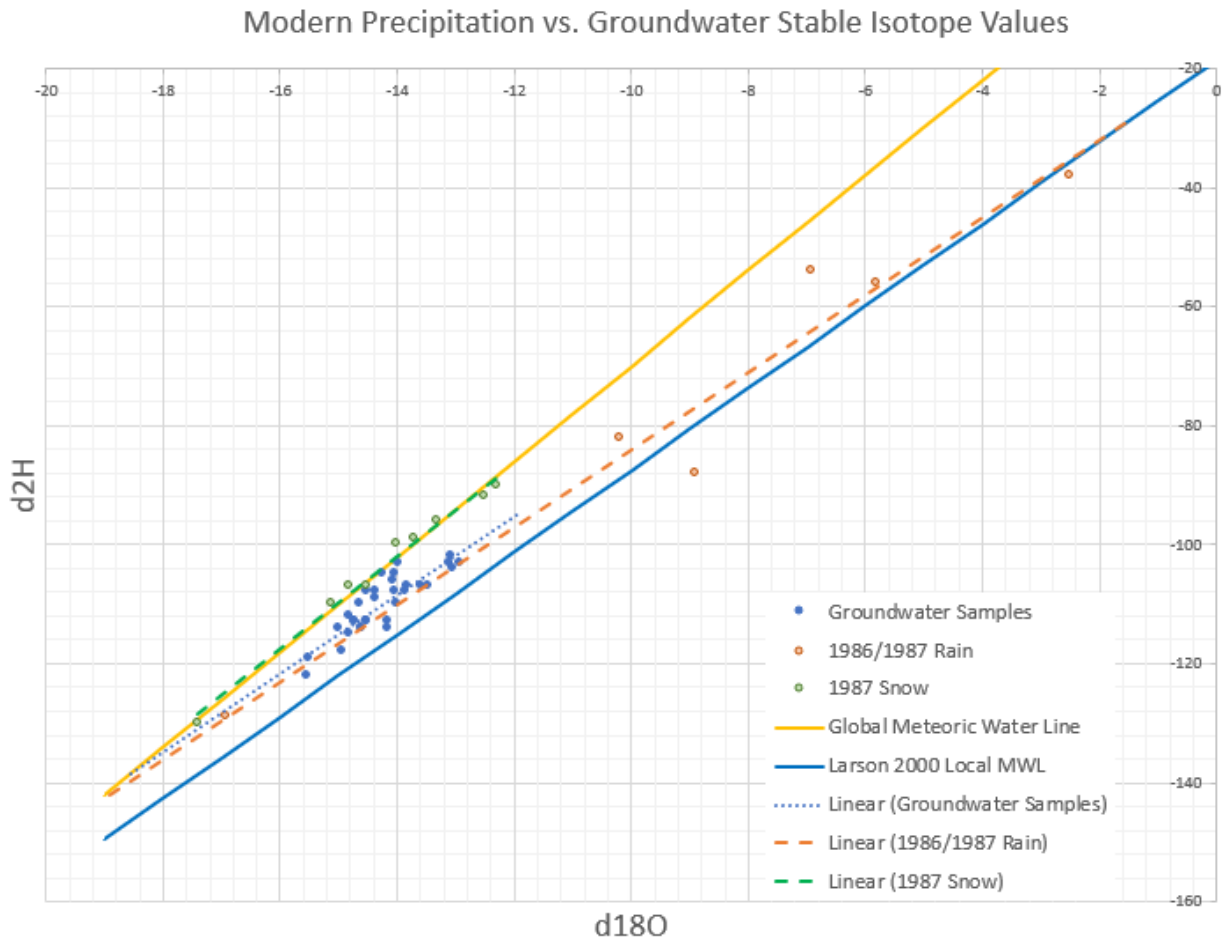

Figure C16: Graph of modern precipitation and groundwater stable isotope values

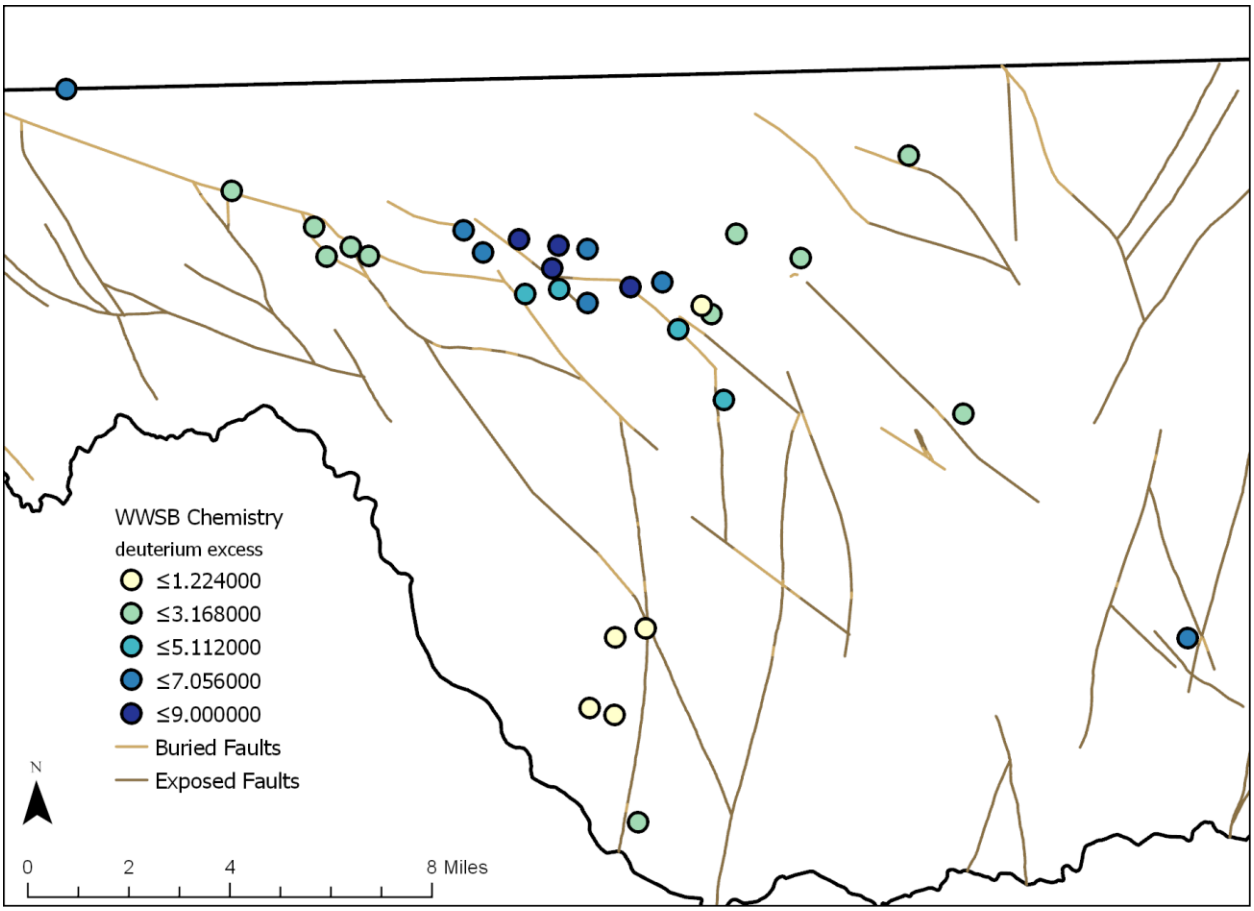

Figure C17: Mapped ranges of deuterium excess values

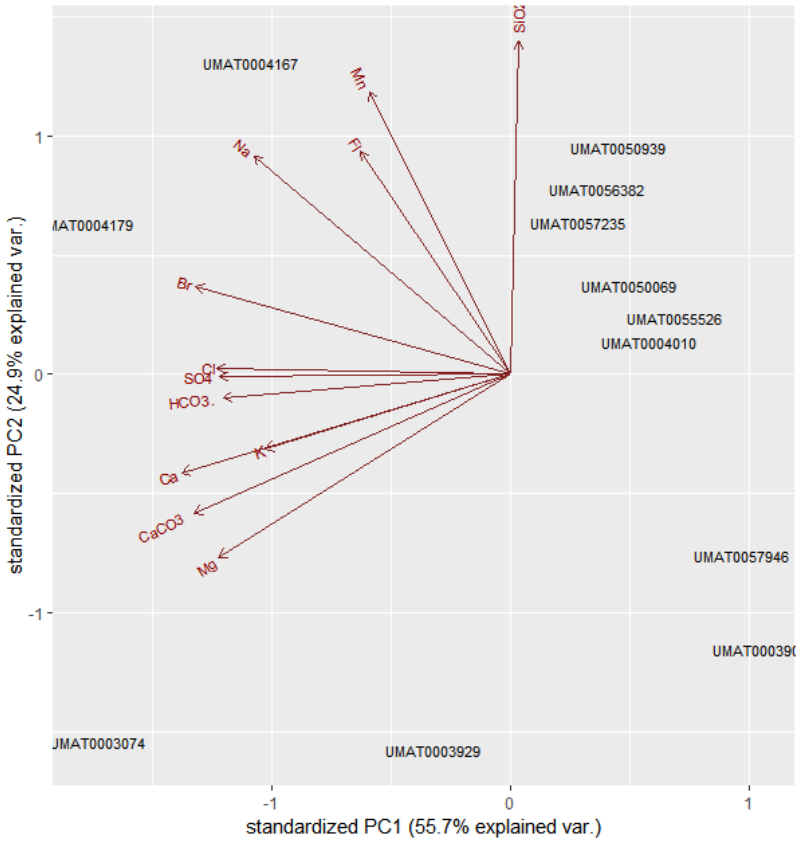

Figure C18: PCA biplot of ion PC1 versus ion PC2

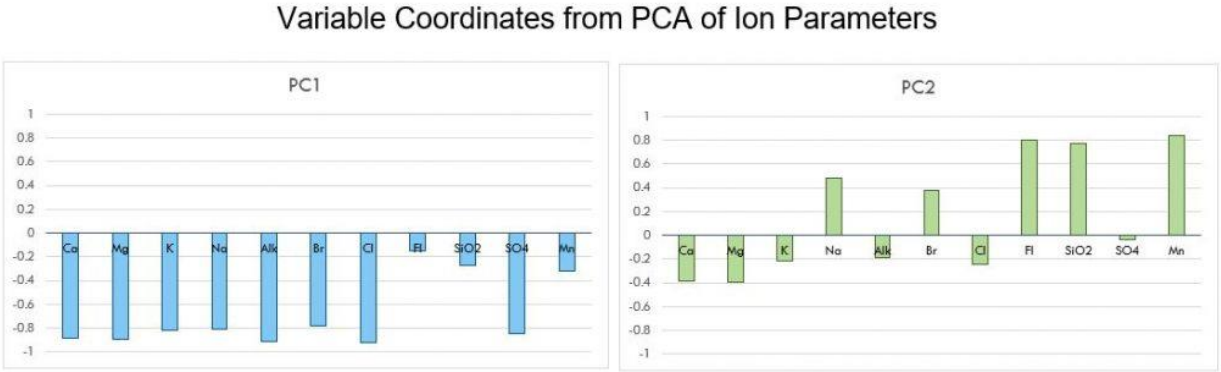

Figure C19: variable coordinates of ion parameters in PC1 and PC2

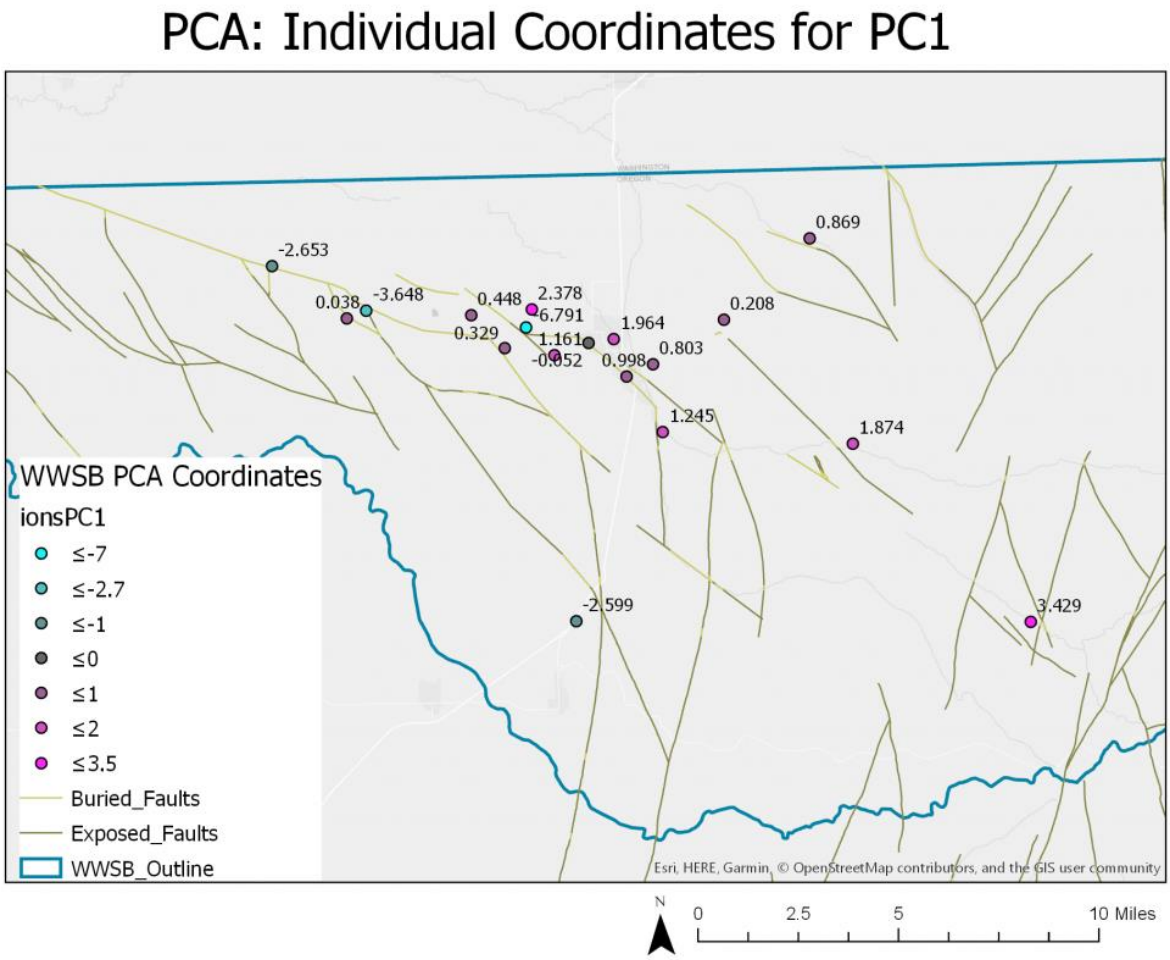

Figure C20: Map of individual coordinate values for ion PC1

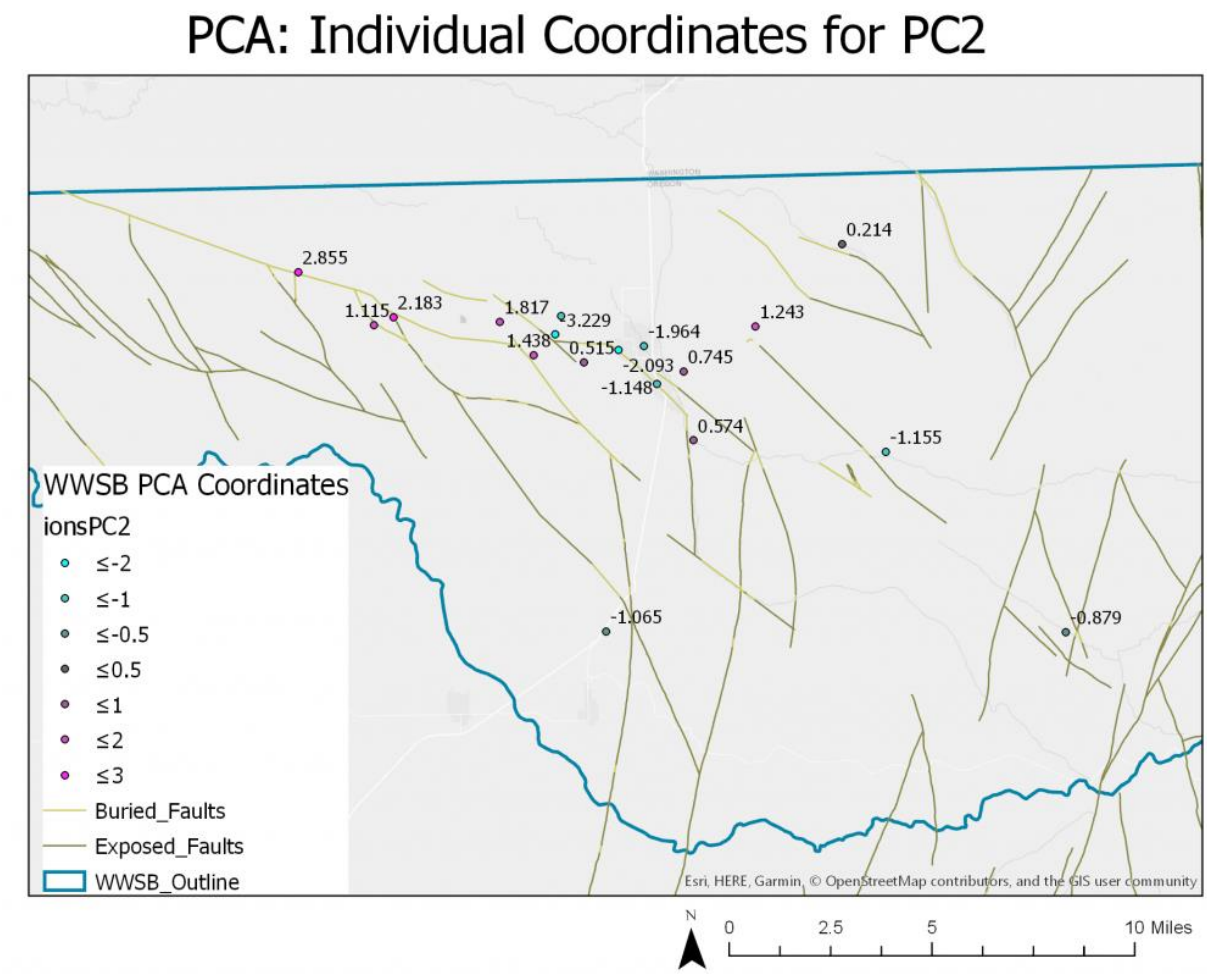

Figure C21. Map of individual coordinate values for ion PC2

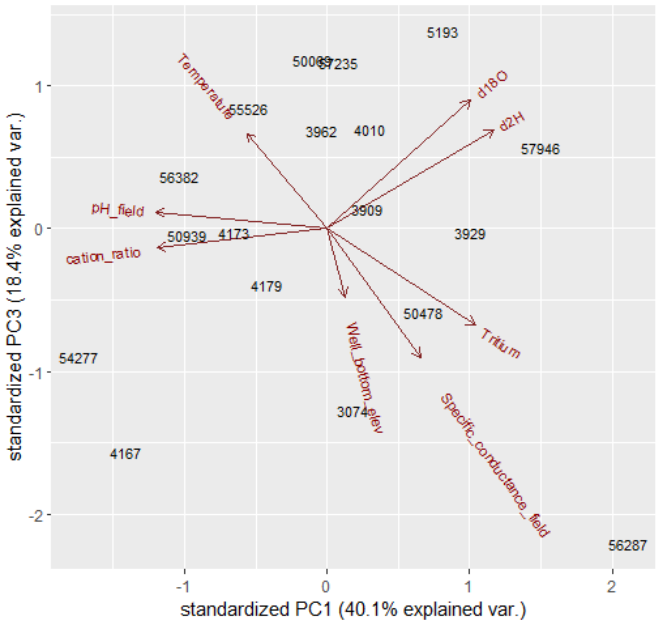

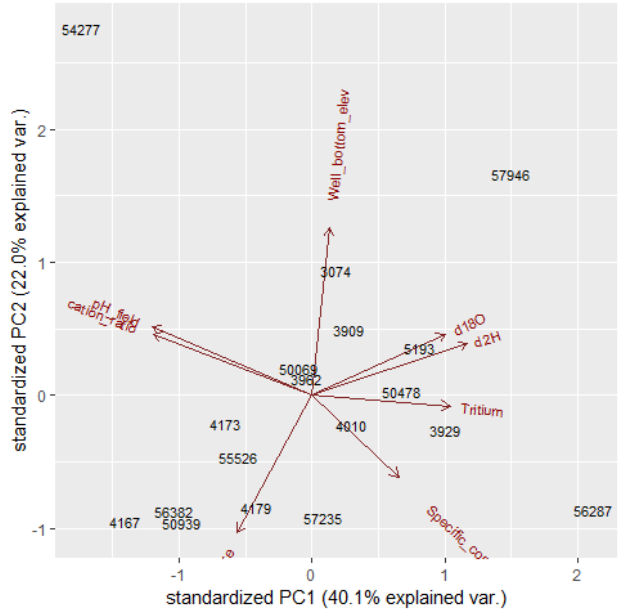

Figures C22a (left): PCA biplot of non-ion PC1 vs non-ion PC2. Figure C22b (right) PCA biplot of non-ion PC2 vs non-ion PC3

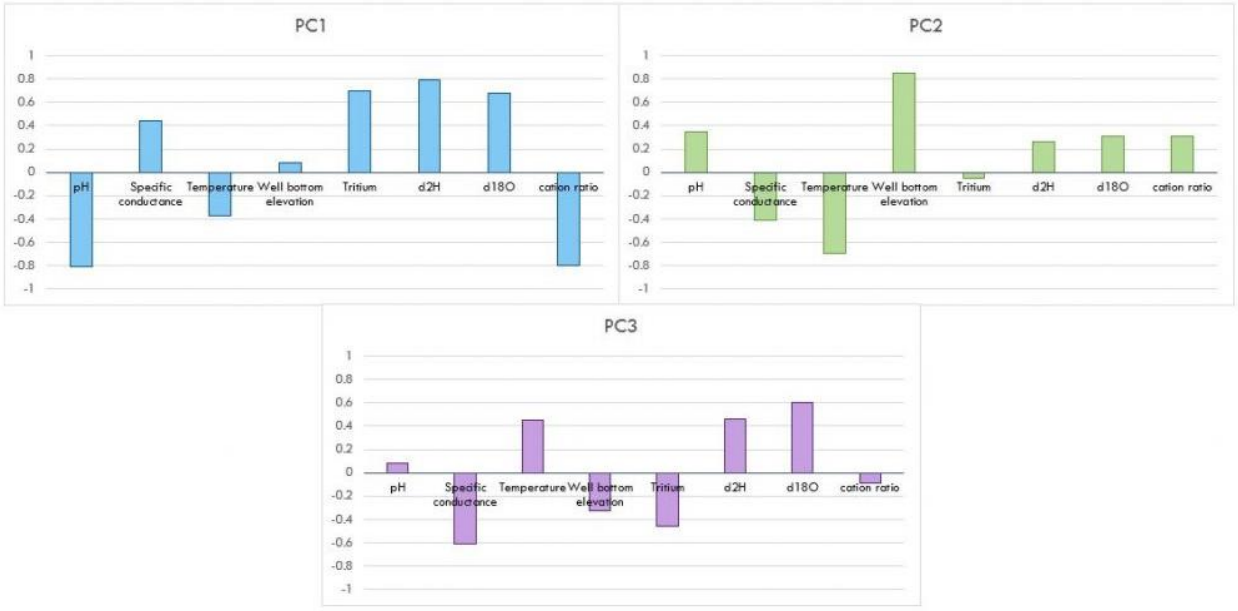

Figure C23: Variable coordinates from PCA of non-ion parameters

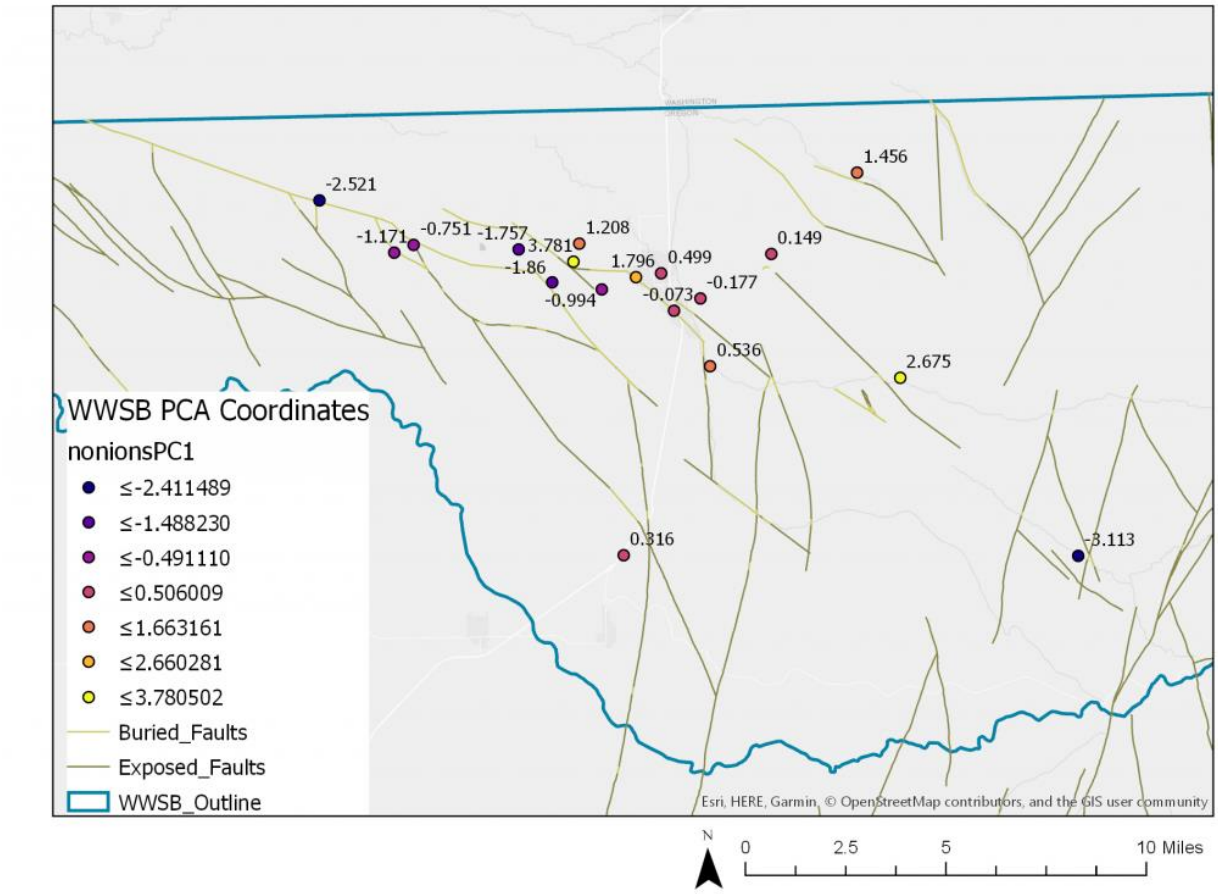

Figure C24: Individual non-ion coordinates for PC1

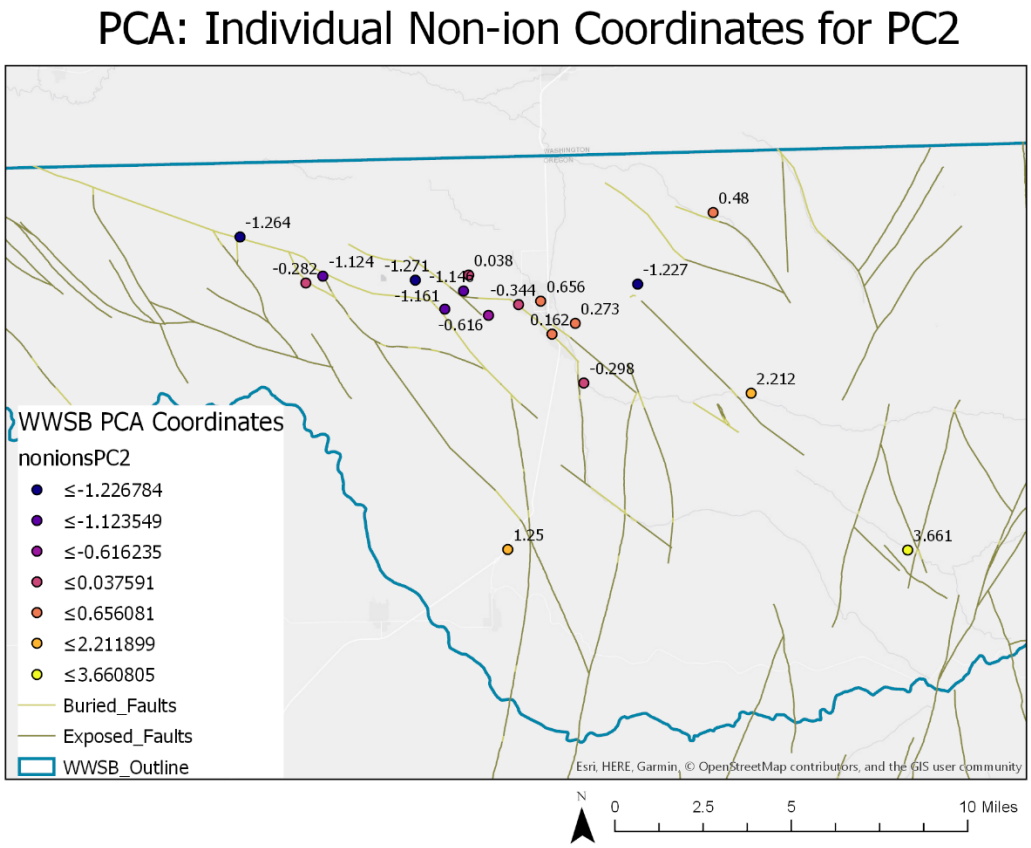

Figure C25: Individual coordinates for non-ion PC2.

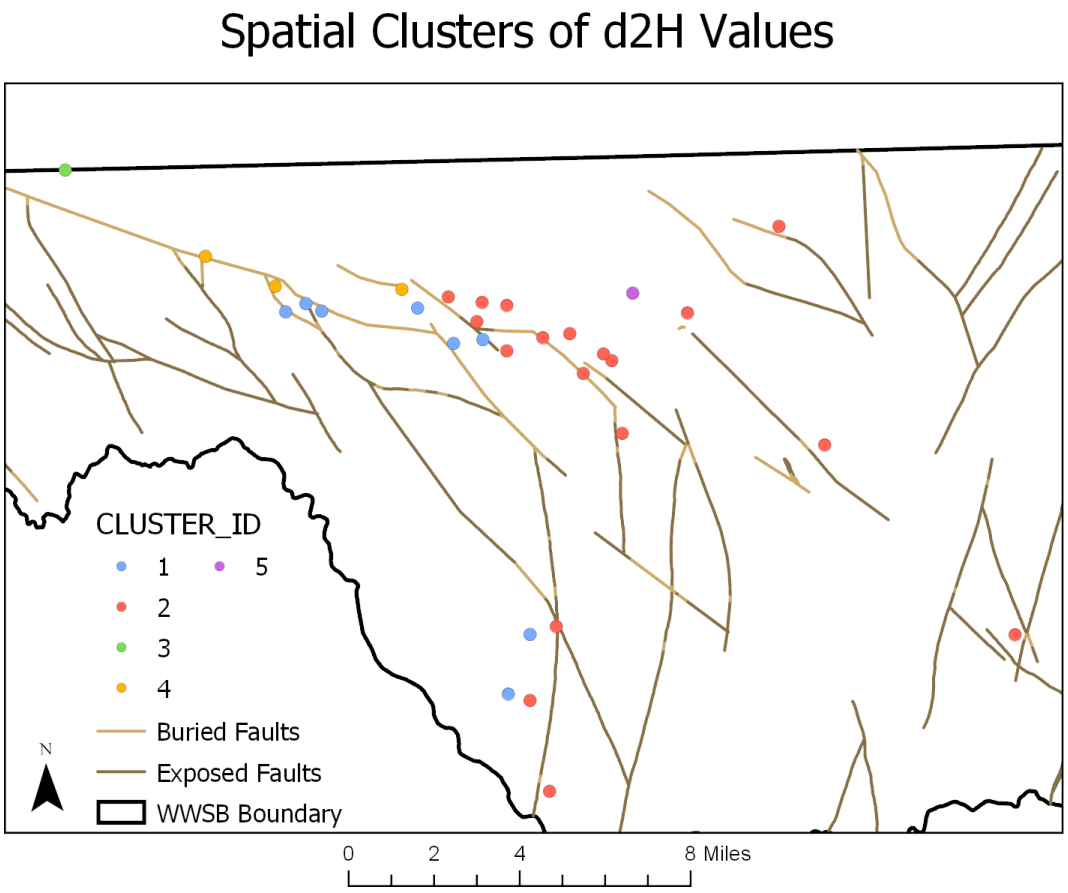

Figure C26a: Map of spatial clusters of d2H values

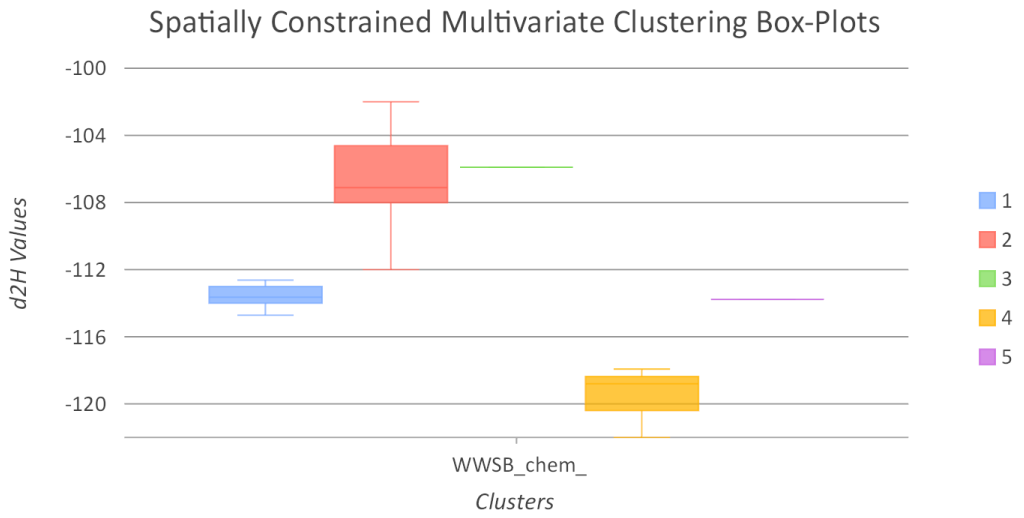

Figure C26b: Spatially constrained multivariate clustering box plots for d2H

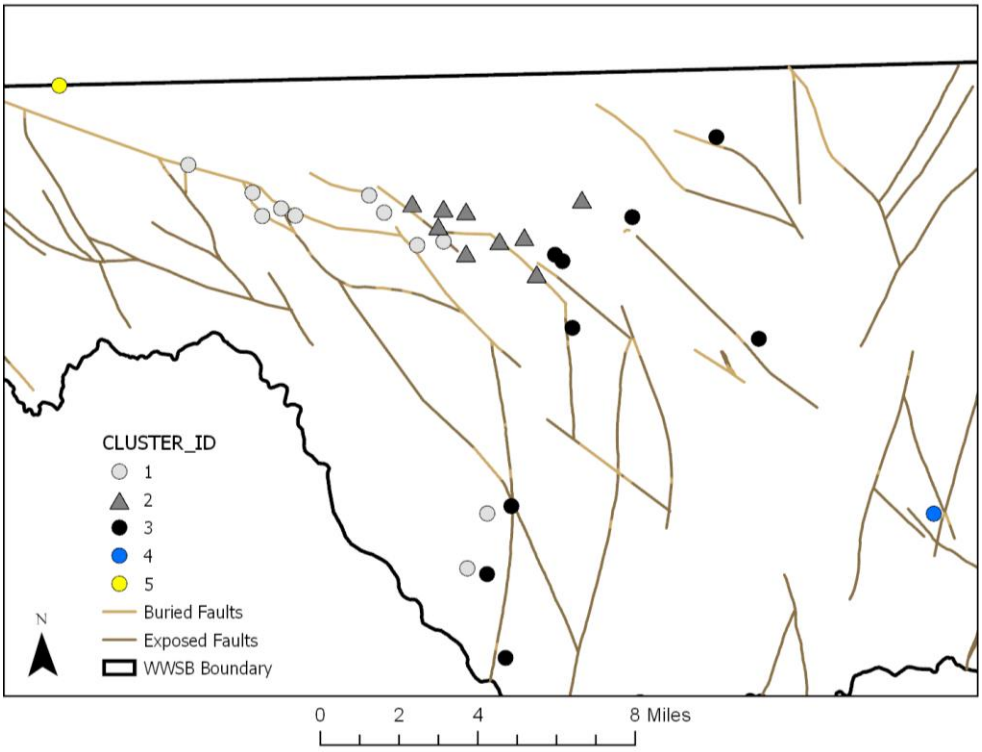

Figure C27a: Map of spatial clusters of d2H and d18O values

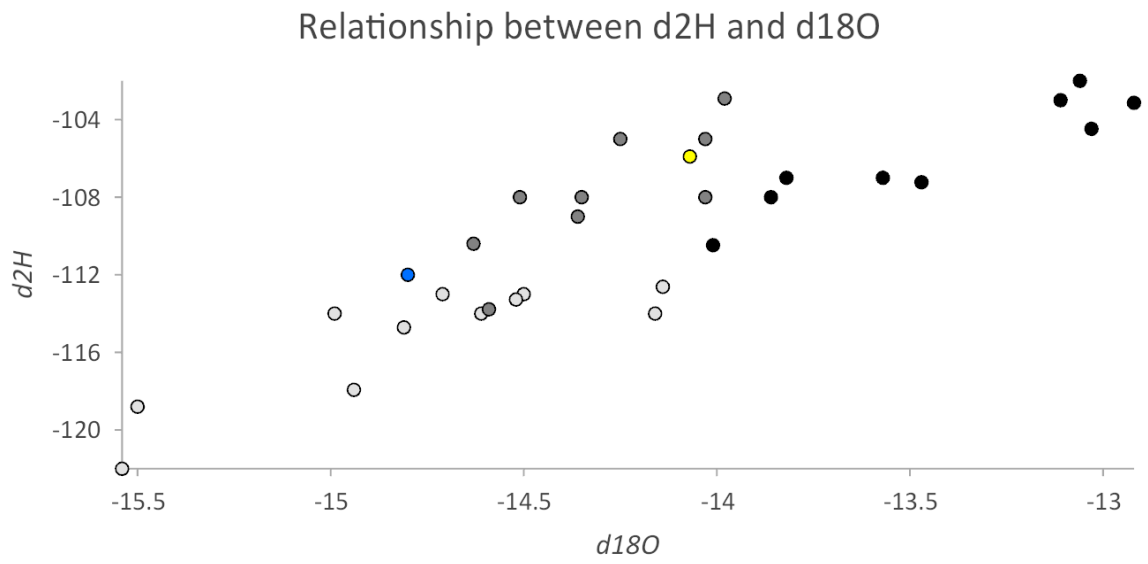

Figure C27b: graph of spatial clusters and d2H versus d18O

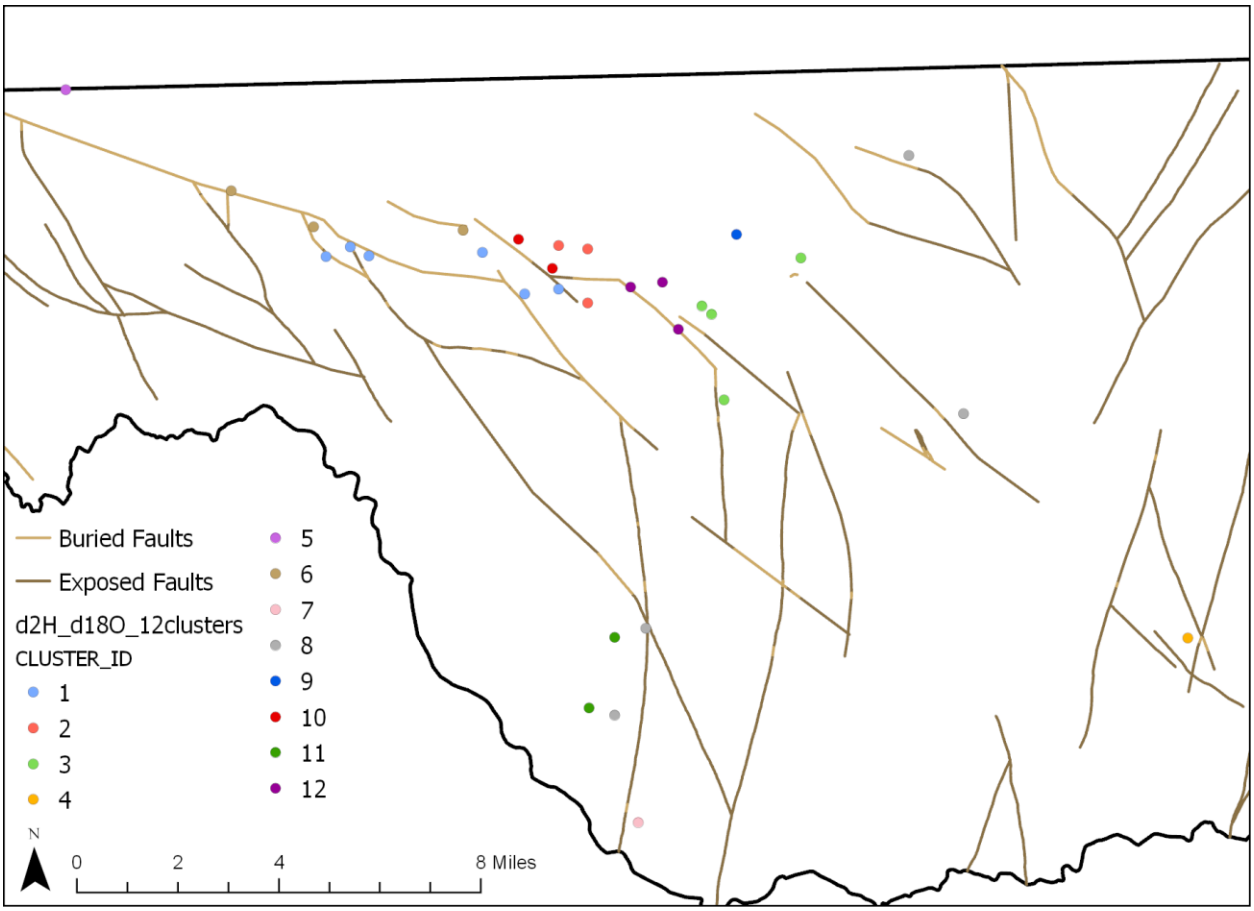

Figure C28: Map of 12-cluster Spatially Constrained Multivariate Clustering analysis of d2H and d18O.

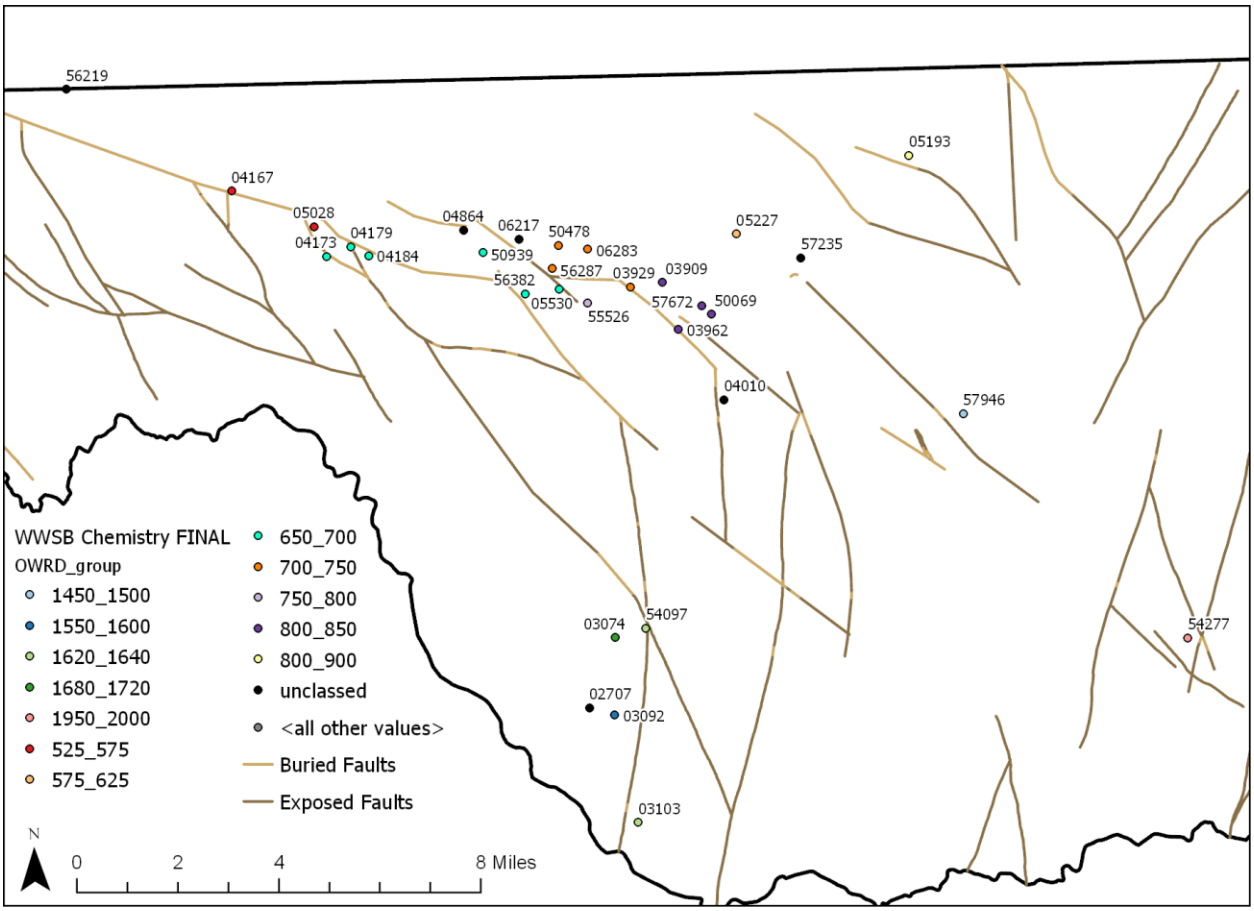

Figure C29: Sampled wells classified by the OWRD by water level elevation.

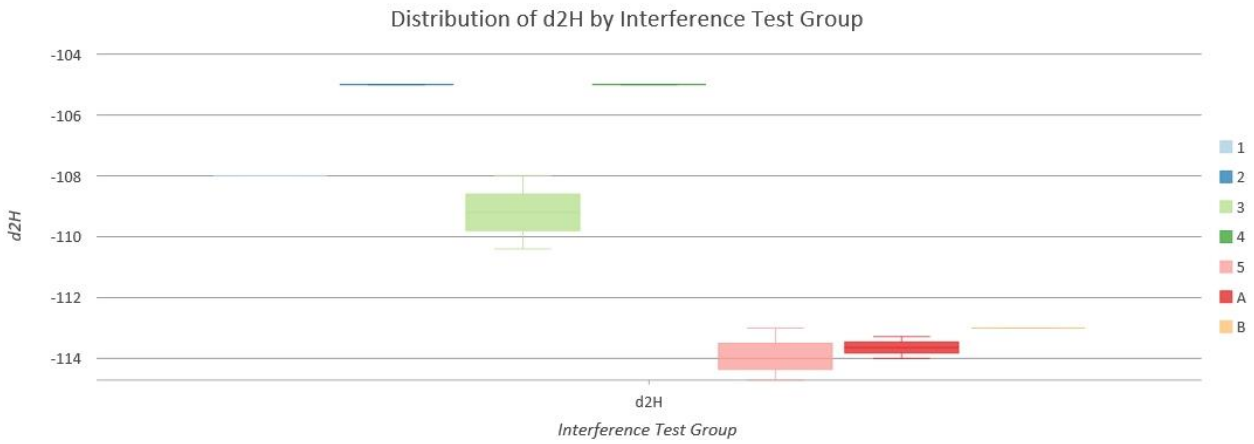

Figure C30a: Boxplots of d2H by interference test group

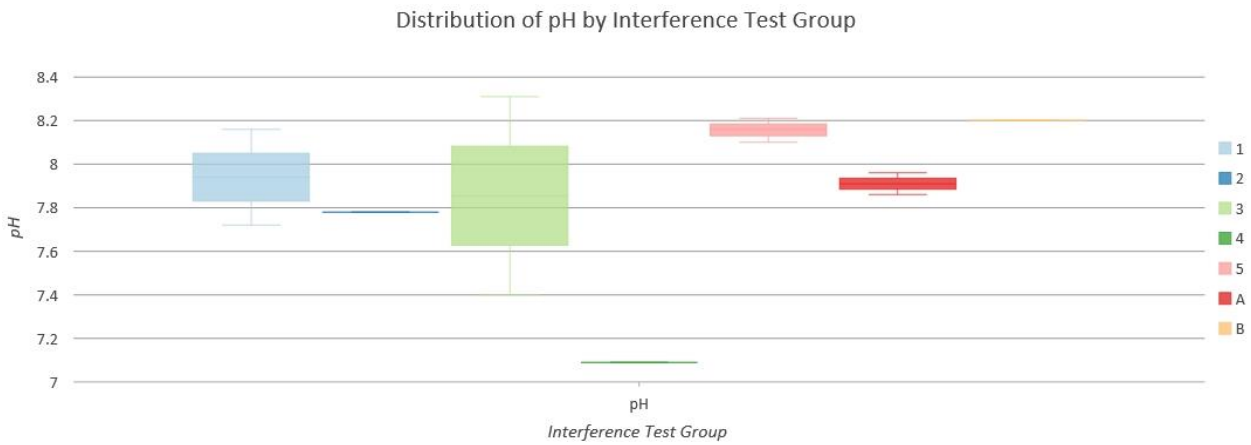

Figure C30b: Boxplots of pH by intereference test group

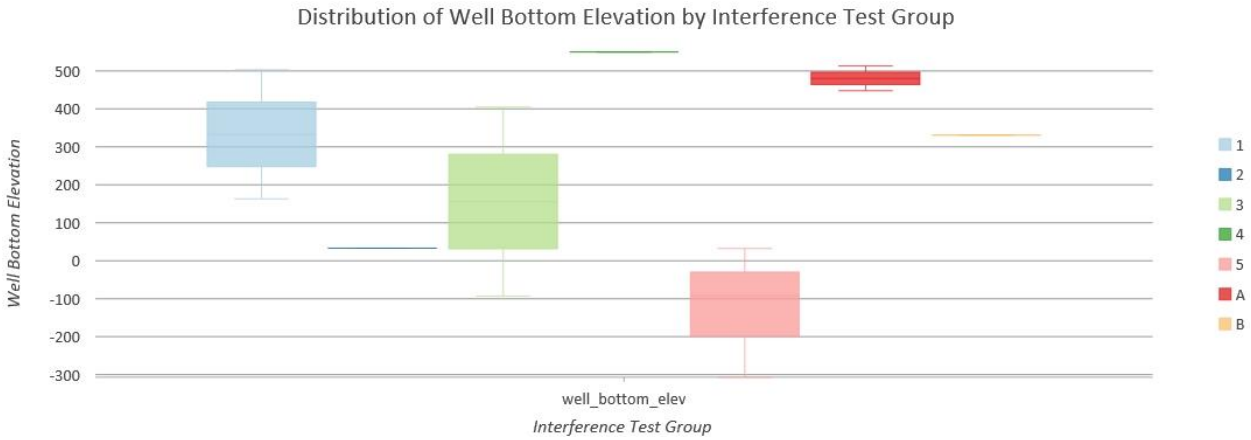

Figure C30c: Boxplots of well bottom elevation by interference test group

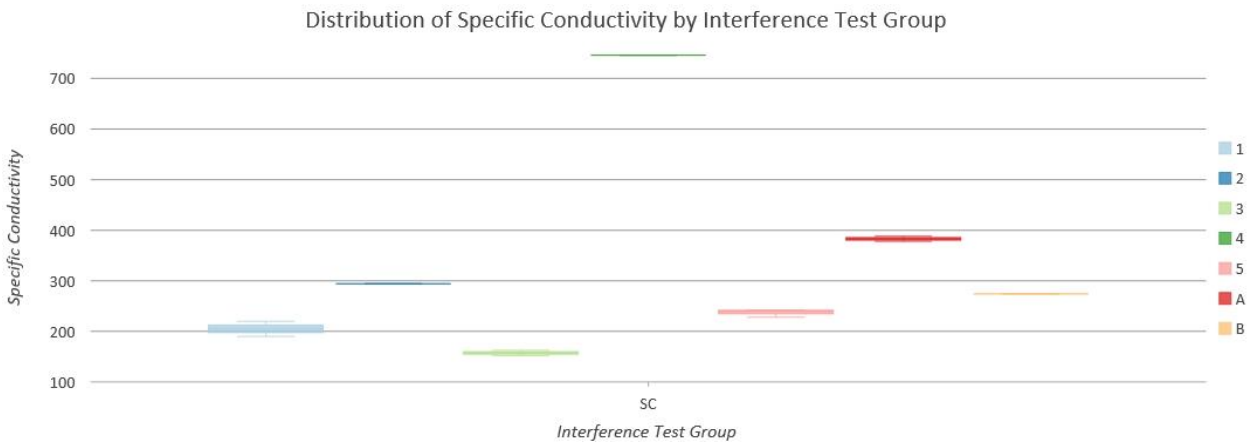

Figure C30d: Boxplots of specific conductivity by interference test group

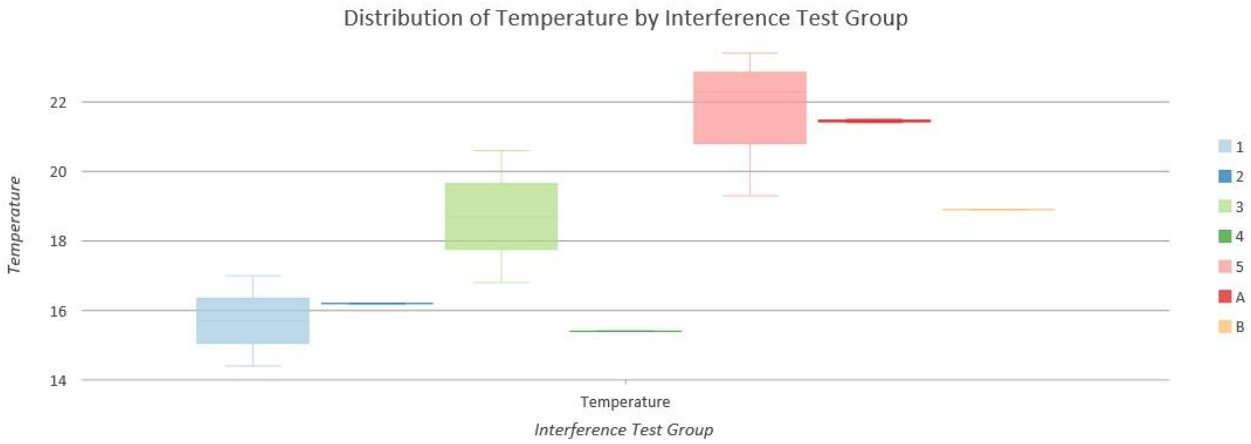

Figure C30e: Boxplots of temperature by interference test group